# Charge Fluctuations in Lattice QCD with Domain-Wall Fermions

A Dissertation Presented

by

**Prasad S. Hegde**

to

The Graduate School

in Partial Fulfillment of the Requirements

for the Degree of

**Doctor of Philosophy**

in

**Physics**

Stony Brook University

August 2010

**Stony Brook University**

The Graduate School

## Prasad S. Hegde

We, the dissertation committee for the above candidate for the Doctor of Philosophy degree, hereby recommend acceptance of this dissertation.

Frithjof Karsch – Dissertation Advisor
Senior Scientist, Brookhaven National Laboratory

Abhay Deshpande – Chairperson of Defense
Associate Professor, Department of Physics and Astronomy

Jacobus Verbaarschot– Co-Advisor
Professor, Department of Physics and Astronomy

Dominik Schneble
Assistant Professor, Department of Physics and Astronomy

Robert D. Pisarski
Senior Scientist, Brookhaven National Laboratory

This dissertation is accepted by the Graduate School.

Lawrence Martin
Dean of the Graduate School

Abstract of the Dissertation

# Charge Fluctuations in Lattice QCD with Domain-Wall Fermions

by

**Prasad S. Hegde**

**Doctor of Philosophy**

in

**Physics**

Stony Brook University

2010

In this work, we undertook an exploratory study of QCD thermodynamics with domain-wall fermions. This had been studied before but with much smaller lattices and a heavier pion. In this new study, we report on results obtained on much larger volumes and discuss what needs to be done to go even closer to the chiral limit. A second new aspect of our study was the introduction of a chemical potential for the first time in the domain-wall formalism. We measured the lowest-order quark number susceptibilities and found a well-defined, smooth transition in some of these susceptibilities.

We also carried out several analytic calculations in the free-field case. One motivation was to understand how these fermions worked, especially with respect to thermodynamic simulations. However another motivation was to understand cutoff effects, which had not been studied before for these fermions.

We found that these effects were significant for the free operator.

We therefore implemented and tested an improved version of the operator with much smaller discretization errors. In this work, we also present some preliminary results of simulations that show that observables measured using this operator show much smaller cutoff errors.

# Contents

# Acknowledgements

It is a pleasure to remember everyone who helped and advised me during the last three years during which this work was done. First of all, I would like to thank my advisor Prof. Frithjof Karsch for his guidance and for all that he has taught me. I have learned a lot about Lattice QCD as well as about QCD thermodynamics in general from him, and I was very fortunate to have an advisor as patient and approachable as him.

Next, I would like to thank everyone at Brookhaven Laboratory for providing such a wonderful atmosphere for study, as well as the exposure to exciting research. I am fortunate to have had the opportunity to interact with its faculty and attend the various seminars and workshops that took place from time to time. I have benefited greatly from this opportunity.

I have also benefited from interactions with Prof. Norman Christ and Prof. Bob Mawhinney and more generally the Lattice group at Columbia University. The work that we did with the Columbia group forms a large part of this thesis. Equally, I would like to express my thanks to Prof. Edwin Laermann of Bielefeld University and Prof. Christian Schmidt for getting me started in this field and for their guidance at several stages during the last three years.

My thesis might not have materialized without the BlueGene/L machine, which belongs to the New York Center for Computational Sciences (NYCSS) and on which I performed all the simulations described in this work. The BlueGene/L machine is one of the best of its kind in the world today, and I am grateful for the access I was provided to it.

I would like to thank Peter Petreczky and Swagato Mukherjee for their encouragement and for several stimulating discussions, Chulwoo Jung for helping me out whenever I was stuck during the implementation of the domain-wall operator in the Columbia Physics System (CPS) code and for teaching me many things about the CPS and programming in general, and Stratos Efstathiadis for his help in getting my code to run on BlueGene/L.

Lastly, I would like to thank my parents and sister for their constant encouragement and love over the last five years. I would also like to remember my aunt Prof. Vasanti Bhat-Nayak who always encouraged me to pursue physics

before she passed away last year. I couldn't have made it this far without them.

# Chapter 1

# Synopsis

A combination of increased computing power and algorithmic breakthroughs has made dynamical domain-wall (DW) simulations feasible in the last few years. Domain-wall fermions are interesting because they are invariant under a modified form of chiral symmetry, known as the Ginsparg-Wilson equation. The Ginsparg-Wilson equation reduces to the statement of chiral symmetry, $\{\gamma_5, D\} = 0$, as the lattice spacing is sent to zero. Its advantage lies in the fact that it protects operators from additive renormalization on the lattice in much the same way as chiral symmetry protects operators in the continuum. The presence of a symmetry also prevents certain classes of operators from mixing and this simplifies the analysis of results.

Domain-wall fermions also do not suffer from the doubling problem that afflicts staggered fermions. This makes their continuum limit non-controversial. Furthermore the absence of doublers means that their spectrum resembles the QCD spectrum. In thermodynamic studies too, these fermions belong to the same universality class as continuum QCD. The downside is that domain-wall fermions are much more time-consuming than either staggered or Wilson fermions, the two most widely used fermion actions. That is why domain-wall simulations have become practical only in the last few years.

The nature of the phase diagram governing the chiral phase transition is one of the important questions in finite-temperature QCD. As is well-known, the QCD ground state breaks chiral symmetry so that instead of hadron multiplets one has light mesons with the quantum numbers of the broken symmetries. However it is known, from lattice simulations for example, that chiral symmetry is restored at high temperatures. Depending on the number of light flavors $N_f$ and their masses, this transition can be first-order, second-order or merely a crossover. Thus for instance, for $N_f = 2$ the transition is second-order belonging to the $O(4)$ universality class while for $N_f = 3$ one has a first-order transition that terminates on a critical line belonging to the $Z(2)$ universality

class [1].

## Scope of this Work

The Columbia group had studied the thermodynamics of domain-wall fermions earlier [2]. Those studies were on coarse lattices and the pion too was rather heavy ($\sim 400$ MeV). Due to the computational and algorithmic advances since then, we were able to revisit this question using finer lattices, larger volumes and somewhat lighter pions. In this thesis we shall present our results of those simulations.

We also expanded the scope of our work to include observables related to the chemical potential $\mu$. Since this was the first time that a chemical potential had been introduced in domain-wall simulations, we studied the behavior of the free action analytically. The chemical potential was introduced as the imaginary part of the gauge links in the time direction viz. $U_4(x) \to \mathrm{e}^{a\mu} U_4(x)$, $U_4^\dagger(x) \to \mathrm{e}^{-a\mu} U_4^\dagger(x)$ [3, 4]. We found that this approach reproduced the correct expression for the pressure in the continuum case.

Lattice actions replace the QCD action with a discrete analog. This discretization leads to errors, known as cutoff effects, that vanish as the lattice spacing is sent to zero. We calculated these errors for the pressure as a Taylor series in the lattice spacing $a$. We found that the naive discretization produced errors of $\mathcal{O}(a^2)$. In numerical terms, this implied a 20% error at a lattice spacing $a = 1/8T$ ($N_\tau = 8$). Although naive fermions are never used in simulations, understanding their cutoff effects is still important because their dispersion relation is identical to that of domain-wall and overlap fermions. For $p \approx 0$, all three formulations show identical cutoff effects[1].

"Improvement" refers to the reduction of cutoff errors by adding extra terms to the action. Improvement increases the cost of simulating an action; on the other hand it is generally acknowledged to be necessary for reducing cutoff effects in practical simulations to negligible levels. Measurements using improved actions have been able to reproduce experimental quantities for the first time to within the accuracy of their errors [5].

For staggered fermions, the two most popular improvement schemes are the Naik and p4 schemes. If the quark mass is small, the primary source of discretization errors comes from the derivative term of the Dirac action. In both schemes, this error is reduced by replacing the usual one-link difference by a combination of one-link and three-link terms.

[1] Nevertheless, chiral actions are undoubled because their dispersion relation is subject to a constraint that is not satisfied at large momenta. This excludes the far corners of the Brillouin zone from contributing to the dispersion relation.

Thus without improvement one would expect a 20% deviation from the continuum limit for these fermions at $N_\tau = 8$. Studies with staggered fermions have shown that the deviation is somewhat smaller in actual simulations, say about 10%. In improved formulations on the other hand, the error on lattices with the same spacing is less than 5% even in the free case.

## Outline of the Thesis

In this thesis, we shall present preliminary results for an improved version of the domain-wall operator. The improvement scheme is similar to the Naik action in that it employs three-link terms. However, since we are improving the Wilson action, we add three-link terms to both the first and second derivatives. Such an action was studied first by G. Hamber and H. Wu [6] about three decades ago; accordingly it is known as the Hamber-Wu action. Both numerical and free-field calculations with this operator confirm that the corresponding domain-wall operator produces $\mathcal{O}(a^2)$-improved observables.

This thesis is organized as follows: In chapter 2, we present the the Lagrangian of Quantum Chromodynamics (QCD) and discuss its symmetries. At finite temperature, these symmetries influence the nature of the QCD phase diagram. We are especially interested in the phase diagram in the $(m_l, m_s)$-plane, where $m_l$ and $m_s$ are the masses of the up/down (assumed degenerate) and strange quarks respectively. Our current knowledge of this diagram comes from a combination of renormalization group arguments and lattice simulations, and we briefly present what is known.

In chapter 3, we introduce the formalism of lattice QCD. We stress that the lattice is a regulator whose advantage lies in the fact that it preserves gauge-invariance. At the same time, it renders the QCD action in a form suitable for numerical simulations.

Nevertheless the lattice is not a perfect regulator. It is well-known that no regulator can preserve gauge- and chiral-invariance simultaneously [7]. The lattice however seems to do just that for the simplest lattice Dirac action anti-commutes with the matrix $\gamma_5$. This ambiguity is resolved when we realize that the lattice Dirac action actually describes sixteen degenerate Dirac fermions in the continuum limit. This is the famous fermion doubling problem. Of these sixteen species (called "tastes"), eight have positive chirality and eight have negative chirality. The net chiral charge is zero and this cancels the anomaly. As we have already mentioned, the incompatibility of the lattice with chiral symmetry was resolved via the Ginsparg-Wilson relation. This brings us to domain-wall and overlap fermions, two formulations that satisfy this relation.

Chapters 4, 5 and 6 describe original work. In chapter 4, we determine the size of cutoff errors in thermodynamic observables for various actions. We

present a general formalism for calculating these errors. Next we turn to the two improved variants of the staggered action viz. the Naik and the p4 actions. We show how a $\mathcal{O}(a^n)$ rotation-invariant propagator leads to $\mathcal{O}(a^n)$-improved observables. After computing the size of these errors for staggered and Wilson fermions, we turn to the chiral fermions. Here we find that cutoff errors are of the same order as for naive fermions. We trace this back to the fact that domain-wall fermions have the same dispersion relation as naive fermions. Lastly, we also introduce a chemical potential in these formalisms and check that this leads to the expected value for the pressure in the continuum limit. We also show that fermions that are improved to a certain order stay that way in the presence of a chemical potential.

In chapter 5, we present results of actual simulations. Our focus will be on the results rather than the simulation details. We present our results for various observables, both at zero and finite temperature. Since this was an exploratory study, zero-temperature ensembles were generated only at one $\beta$-value close to the critical coupling. By measuring meson masses and the string tension, we were able to determine the value of the lattice spacing $a$ at that coupling.

The observable relevant to the chiral phase transition is the disconnected chiral susceptibility, which shows a peak at the transition. Indeed, our measurements showed just such a peak from which we obtained $\beta_c \simeq 2.04$ as the transition coupling. We also measured the Polyakov loop susceptibility, which shows a peak at the point where nuclear matter becomes deconfined. Unfortunately our measurements failed to resolve any peak-like structure for this quantity.

The Polyakov loop is actually a good order parameter only in the absence of quarks. When there are dynamical quarks in the system however, quark number susceptibilities can be used as order parameters. Second-order susceptibilities measure the fluctuation in conserved charges. They are therefore small in the confined phase, in which the charges are carried by hadrons, and large in the deconfined phase, when the charges are carried by quarks. Therefore as the temperature is varied, they can be expected to transit from a small value to a large one. Similarly, the fourth-order susceptibilities can be expected to show a peak at the deconfinement temperature.

We measured the lowest-order diagonal and off-diagonal light and strange susceptibilities viz. $\chi_2^{l,s}$ and $\chi_{11}^{l,s}$. Using these, we also determined the charge, baryon number and isospin susceptibilities. Many of these quantities could not be measured to sufficient precision within our limited statistics, but in two of the susceptibilities viz. isospin and charge, our measurements were sufficiently clean so as to allow us to extract a value for the deconfinement coupling $\beta_d$.

We obtained a value $\beta_d \simeq 2.03$ from fits to both susceptibilities.

The chiral symmetry of domain-wall fermions is broken if the fifth dimension is finite in extent. This breaking takes the form of an additive mass renormalization $m_{\rm res}$ to the quark mass. $m_{\rm res}$ is called the residual mass and our simulations revealed that it increased quite sharply as one moved toward stronger coupling. In fact, $m_{\rm res}$ was larger than the light quark mass $m_l = 0.003$ for some $\beta$-values. This variation distorted the chiral susceptibility and was the most important source of systematic error in our determination of $\beta_c$. This was because the disconnected chiral susceptibility diverges as $1/m^\alpha$ for some $\alpha$ near the transition point, and $m$ was not constant in this region. On the other hand, quark number susceptibilities are not very sensitive to the quark mass. By correcting for this effect, we found that the $\beta_c$ moved slightly to the left to 2.03, bringing it into agreement with the deconfinement coupling. Finally, we estimated the error from cutoff effects and the fact that the pion was heavy, as also the fact that our scale had been determined at a coupling which was different from the critical coupling. Based on all this, we were able to determine a value $T_c = 171(17)(10)$ MeV for the transition temperature, where the first error was due to the variation of $m_{\rm res}$, while the second combined continuum and chiral extrapolation errors.

In chapter 6, we present the improved domain-wall operator, based on the Hamber-Wu kernel. We present a derivation of the operator and present results for the free case which show that the pressure obtained with this operator shows negligible cutoff error. After that, we present results from simulations on high-temperature ensembles. We measure quark number susceptibilities using both the unimproved and improved domain-wall operator. The unimproved measurements exceed the Stefan-Boltzmann limit by about 10% while the improved measurements correctly attain the Stefan-Boltzmann limit. Finally in chapter 7, we summarize our work and present an outlook for the future.

# Chapter 2

# Chiral Symmetry and the QCD Phase Diagram

Quantum Chromodynamics (QCD) is acknowledged as providing us with a correct description of the strong force [8]. The strong force is experienced by particles that carry a quantum number called *color*, so named because it can take one of three values. It is the QCD analog of the familiar charge in electrodynamics.

At a fundamental level, colored matter is made of spin-1/2 fermions called *quarks*. Just as in Quantum Electrodynamics (QED), fermions interact through the exchange of massless, spin-1 particles called *gluons*. In sharp contrast to QED however, gluons also carry color and can interact among themselves by exchanging other gluons. This difference stems from the fact that the equations of motion of the gauge fields in QCD are nonlinear, as opposed to the Maxwell equations which are linear.

The QCD Lagrangian is given by

$$\begin{aligned}\mathcal{L}_{\text{QCD}} &= \sum_{f=1}^{N_f} \overline{\psi}_f(x)\left(\mathrm{i}\gamma^\mu\partial_\mu - m_f\right)\psi_f(x) - \frac{1}{4}\left(F^a_{\mu\nu}(x)\right)^2 \\ &+ \sum_{f=1}^{N_f}\left[\overline{\psi}_f(x)\gamma^\mu t^a\psi_f(x)\right]\cdot gA^a_\mu(x). \\ &= \mathcal{L}_{\text{dirac}} + \mathcal{L}_{\text{YM}} + \mathcal{L}_{\text{int}}.\end{aligned} \tag{2.1}$$

It is no accident that this Lagrangian is similar to the QED Lagrangian. In fact the Lagrangian (2.1) was obtained by generalizing the gauge symmetry

of the Maxwell equations: If we transform the fermion fields as

$$\psi(x) \to \exp\left(\mathrm{i}\alpha^a(x)t^a\right)\psi(x), \qquad \overline{\psi}(x) \to \overline{\psi}(x)\exp\left(-\mathrm{i}\alpha^a(x)t^a\right), \tag{2.2}$$

and simultaneously make a gauge transformation

$$A^a_\mu(x) \to A^a_\mu(x) + \frac{1}{g}\partial_\mu\alpha^a(x) + f^{abc}A^b_\mu(x)\alpha^c(x), \tag{2.3}$$

then the action is unchanged. The spinor $\psi$ is actually a triplet $(\psi_r, \psi_g, \psi_b)^T$ where $r$, $g$ and $b$ stand for red, green and blue respectively *i.e.* the three values that the color can take.

The transformations eqs. (2.2) and (2.3) are local *i.e.* they depend on the spacetime coordinate $x$. The fermion transformation is also a unitary transformation *i.e.* the matrices $t^a$ belong to the algebra of $SU(3)$ viz.[1]

$$\left[t^a, t^b\right] = t^a t^b - t^b t^a = \mathrm{i}f^{abc}t^c, \tag{2.4}$$

The requirement of gauge-invariance dictates (or constrains) what type of interactions are allowed. If we demand invariance under parity and charge conjugation, then the above Lagrangian is the only one that can be written down using operators of dimension less than or equal to four. Apart from this, gauge invariance is also necessary to ensure that the theory is renormalizable. This is necessary for the theory to make sensible predictions.

## 2.1 The Global Symmetries of QCD

Eq. (2.1) actually describes $N_f$ species (flavors) of quarks. The interactions of QCD do not distinguish among different flavors, nor have we introduced additional flavor-mixing terms. Thus, unlike the weak force, QCD does not transform quarks of one flavor to another.

Nevertheless, *if the quarks all have the same mass* $m$, the Dirac structure of the theory still gives rise to a symmetry among the flavors. To see what it is, let us collect the $N_f$ flavors into one big spinor $\Psi = (\psi_1, \ldots, \psi_{N_f})^T$. Then the QCD Lagrangian takes the form ($M \equiv m \cdot \mathbb{I}_{N_f \times N_f}$)

$$\begin{aligned}\mathcal{L}_{\mathrm{QCD}} &= \overline{\Psi}(x)\left(\mathrm{i}\gamma^\mu\partial_\mu - M\right)\Psi(x) \\ &\quad + gA^a_\mu(x)\cdot\Psi(x)\gamma^\mu t^a\Psi(x) - \frac{1}{4}\left(F^a_{\mu\nu}(x)\right)^2.\end{aligned} \tag{2.5}$$

[1]The $f^{abc}$ are known as the *structure constants* of the group and are antisymmetric in the indices $a$, $b$ and $c$.

We immediately see that eq. (2.5) is invariant under

$$\Psi(x) \to U\Psi(x), \qquad \overline{\Psi}(x) \to \overline{\Psi}(x)U^\dagger, \tag{2.6}$$

where $U \in U(N_f)$ is a unitary matrix. Unlike the gauge transformations, these rotations are global *i.e.* spacetime-independent.

If $m = 0$, the symmetry space is enlarged even further. This is because the Dirac spinor is composed of left- and right-handed spinors, defined by

$$P_L = \frac{1}{2}(1 - \gamma^5) \qquad P_R = \frac{1}{2}(1 + \gamma^5), \tag{2.7a}$$

$$\Psi_L = P_L\Psi, \qquad \Psi_R = P_R\Psi, \tag{2.7b}$$

$$\overline{\Psi}_L = \overline{\Psi}P_L, \qquad \overline{\Psi}_R = \overline{\Psi}P_R. \tag{2.7c}$$

Note that the hermitian conjugate of a left-handed particle is a right-handed antiparticle and conversely: $\overline{\Psi}_L = \Psi^\dagger\gamma^0 P_L = \Psi^\dagger P_R\gamma^0 = (P_R\Psi)^\dagger\gamma^0 = \overline{(\Psi_R)}$. Among the terms of eq. (2.5), only the mass term mixes left- and right-handed components viz. ($A_\mu = A^a_\mu t^a$, $\not{V} = \gamma^\mu V_\mu$ for any vector $V$)

$$\overline{\Psi}(x)\not{A}\Psi(x) = \overline{\Psi}_L(x)\not{A}\Psi_L(x) + \overline{\Psi}_R(x)\not{A}\Psi_R(x), \tag{2.8a}$$

$$\overline{\Psi}(x)\not{\partial}\Psi(x) = \overline{\Psi}_L(x)\not{\partial}\Psi_L(x) + \overline{\Psi}_R(x)\not{\partial}\Psi_R(x), \tag{2.8b}$$

$$m\overline{\Psi}\Psi = m\left(\overline{\Psi}_L\Psi_R + \overline{\Psi}_R\Psi_L\right). \tag{2.8c}$$

The two components thus decouple for $m = 0$, allowing us to perform separate $U(N_f)$ transformations

$$\Psi_L \to U_L\Psi_L, \qquad \overline{\Psi}_L \to \overline{\Psi}_L U_L^\dagger, \tag{2.9a}$$

$$\Psi_R \to U_R\Psi_R, \qquad \overline{\Psi}_R \to \overline{\Psi}_R U_R^\dagger. \tag{2.9b}$$

The symmetry group is thus enlarged to $U_L(N_f) \times U_R(N_f)$. Since $U(N_f)$ is isomorphic to $U(1) \times SU(N_f)$, the complete group of symmetries for $m = 0$ is given by $U(1)_L \times U(1)_R \times SU(N_f)_L \times SU(N_f)_R$.

By Nöther's theorem, these symmetries give rise to $2N_f^2$ conserved currents. These currents are

$$U(1)_L : \overline{\Psi}_L\gamma^\mu\Psi_L, \tag{2.10a}$$

$$U(1)_R : \overline{\Psi}_R\gamma^\mu\Psi_R, \tag{2.10b}$$

$$SU(N_f)_L : \overline{\Psi}_L\gamma^\mu T^i\Psi_L, \quad i = 1, \ldots, N_f^2 - 1, \tag{2.10c}$$

$$SU(N_f)_R : \overline{\Psi}_R\gamma^\mu T^i\Psi_R, \quad i = 1, \ldots, N_f^2 - 1. \tag{2.10d}$$

The matrices $T^i$ are the generators of $SU(N_f)$. However these are not the true conserved currents of QCD. Apart from these continuous symmetries, QCD is also invariant under parity $\mathcal{P}$ and charge conjugation $\mathcal{C}$. Under parity, the space components of a vector reverse sign while the time component remains unchanged. However, if the vector in question is an axial vector *i.e.* it has an intrinsic "handedness", then it does not change sign under the operation. Similarly, the operation of charge conjugation reverses the sign of all four components of a vector but leaves the components of an axial four-vector invariant.

Thus, under either $\mathcal{C}$ or $\mathcal{P}$, $\overline{\Psi}_L\gamma^\mu\Psi_L \leftrightarrow -\overline{\Psi}_R\gamma^\mu\Psi_R$, The true conserved currents therefore are actually given by

$$U(1)_V : \overline{\Psi}\gamma^\mu\Psi = \overline{\Psi}_L\gamma^\mu\Psi_L + \overline{\Psi}_R\gamma^\mu\Psi_R, \tag{2.11a}$$

$$U(1)_A : \overline{\Psi}\gamma^\mu\gamma^5\Psi = \overline{\Psi}_L\gamma^\mu\Psi_L - \overline{\Psi}_R\gamma^\mu\Psi_R, \tag{2.11b}$$

$$\begin{aligned} SU(N_f)_V : \overline{\Psi}\gamma^\mu T^i\Psi, \quad i = 1, \ldots, N_f^2 - 1 \\ = \overline{\Psi}_L\gamma^\mu T^i\Psi_L + \overline{\Psi}_R\gamma^\mu T^i\Psi_R, \end{aligned} \tag{2.11c}$$

$$\begin{aligned} SU(N_f)_A : \overline{\Psi}\gamma^\mu\gamma^5 T^i\Psi, \quad i = 1, \ldots, N_f^2 - 1 \\ = \overline{\Psi}_L\gamma^\mu T^i\Psi_L - \overline{\Psi}_R\gamma^\mu T^i\Psi_R. \end{aligned} \tag{2.11d}$$

The subscripts $V$ and $A$ stand for "vector" and "axial vector" respectively. The complete symmetry group of the strong interactions is thus given by $U(1)_V \times U(1)_A \times SU(N_f)_V \times SU(N_f)_A$.

Corresponding to each of these currents is a conserved charge. These charges have the same algebra as their symmetry group. The physical states transform according to irreducible representations of the algebra. Thus each state is labelled by a number, called the quantum number, which denotes the irreducible representation to which the state belongs.

The quantum number corresponding to $U(1)_V$ is the baryon number *i.e.* the number of quarks minus antiquarks irrespective of their flavor. All indications so far are that baryon number is exactly conserved by the Standard Model [9].

To understand what the $SU(N_f)_V$ symmetry is, let us specialize to $N_f = 2$. If we denote the two flavors by $u$ and $d$ (for up and down), then we find that the conserved charges are

$$Q^i = \int \mathrm{d}^3x \Psi^\dagger(x)\sigma^i\Psi(x), \quad i = 1, 2, 3. \tag{2.12}$$

The $\sigma^i$ are the Pauli spin matrices *i.e.* the generators of $SU(2)$. The charge

$Q^3$ in particular is given by

$$Q^3 = \int \mathrm{d}^3x \left[u^\dagger(x)u(x) - d^\dagger(x)d(x)\right]. \tag{2.13}$$

The up and down quarks have equal but opposite charges. This tells us that the symmetry in question is *isospin*. It is well-known that the strong interactions do not distinguish between the proton and the neutron. The conservation of the charge (2.13) is a restatement of that fact in the quark language.

### 2.1.1 Spontaneously Broken Chiral Symmetry

The situation with respect to the other two symmetries is a little more intricate. Let us first take the case of $U(1)_A$. This symmetry is broken when one tries to quantize the theory. As is well-known, quantum field theories contain divergences because of which a regulator must be introduced. It turns out that it is not possible to regulate the theory in such a way that both gauge- and chiral-invariance are preserved. We take gauge-invariance to be fundamental and require that the regulator preserve gauge symmetry. The price we pay for it is the anomalous non-conservation of the $U(1)_A$ current viz. [7]

$$\partial_\mu j^{\mu 5}(x) = N_f \frac{g^2}{32\pi^2} \epsilon^{\mu\nu\rho\sigma} F^a_{\mu\nu} F^a_{\rho\sigma}. \tag{2.14}$$

Lastly, let us discuss the case of $SU(N_f)_A$. The known hadrons do not group into multiplets that transform according to irreducible representations of $SU(N_f)_A$. Today we know that this is because the interactions of QCD dynamically break this symmetry. The scale at which this occurs is a characteristic length scale of QCD. It is denoted by $\Lambda_{\mathrm{QCD}}$ and its value is about 200 MeV. Note how quantum effects give rise to a scale that was *not* present in the classical theory. This breaking gives rise to $N_f^2 - 1$ Goldstone bosons. Since quarks are actually neither massless nor even degenerate, these bosons acquire masses. Nevertheless, they are still much lighter than the lightest baryon viz. the proton.

We classify quarks as light or heavy, depending on whether their masses are smaller or greater than $\Lambda_{\mathrm{QCD}}$. In the real world, the up and down quarks (masses $\approx$ 2 and 5 MeV respectively) are very light, while the strange quark ($\approx$ 100 MeV) may also be included with some reservations. The hypothesis of spontaneously broken $SU(2)_A$ and $SU(3)_A$ has proved to be very useful in modeling the interactions of QCD at low energy. The three pions viz. $\pi^\pm$ and $\pi^0$ are actually the Goldstone bosons of broken $SU(2)_A$. Note that they are degenerate upto a small mass splitting due to electromagnetic effects. This

shows the extent to which spontaneously broken $SU(2)_A$ is a good picture. If we include the kaons and the eta, we can form a set of eight mesons which we take to correspond to the generators of broken $SU(3)_A$. Note that the degeneracy is less pronounced; all eight however are much lighter than the lightest baryon viz. the proton.

Although we cannot yet prove from first principles that $SU(3)_A$ is dynamically broken, a wealth of evidence exists that this is indeed the case. On the one hand, there is numerical evidence from lattice simulations. On the other hand, the assumption of a spontaneously broken $SU(3)_A$ explains many properties of the low-energy dynamics of QCD. Indeed, calculations that start from this assumption have by now been formalized into a theory known as chiral perturbation theory ($\chi$PT) [10]. $\chi$PT has been very successful in accounting for the splitting of meson masses, pion scattering lengths, baryon form factors, etc. It is also used to extrapolate the results of lattice simulations down to very light or zero quark masses. $\chi$PT succeeds in the very regime that perturbative QCD breaks down. Thus our low-energy picture of QCD is not one of quarks interacting via gluon exchange but rather one of Goldstone bosons interacting among themselves and with baryons.

The other three quarks have masses of $\mathcal{O}(1 - 100 \text{ GeV})$. It does not make sense to talk of an $SU(6)_{A,V}$ symmetry. The global symmetries that we have discussed in this section are very badly broken by these three flavors. On the other hand, low-energy nuclear physics is mostly governed by the dynamics of the three light quarks alone. We shall specialize to the case $N_f = 3$ from now on.

## 2.2 Chiral Symmetry Restoration

The picture we have sketched out above is valid at zero temperature. Now the coupling constant of QCD $\alpha_s$ evolves with energy; however in contrast to QED it gets smaller at higher energies. This means that unlike QED or $\phi^4$ theory, QCD evolves toward, rather than away from, the Gaussian fixed point (free field theory) as the energy is increased. This property of QCD is known as *asymptotic freedom*.

The average energy of a system may also be raised by increasing the temperature of a system. Due to asymptotic freedom, we may expect that at high temperatures the interactions will be sufficiently weak so that the ground state is actually better described by the perturbative picture rather than the non-perturbative one. The prospect that nuclear matter could look very different at high temperatures gave rise to the field of finite-temperature QCD. It is now known that the above expectations were correct. At a temperature

$T \sim \Lambda_{\rm QCD}$, nuclear matter undergoes a transition to a new state, known as the *quark-gluon plasma*, that is chirally symmetric and in which quarks and gluons are not confined within hadrons[2].

Although the basic picture has been confirmed, several questions remain: Is the transition a genuine thermodynamic transition (first- or second-order), or is it merely a crossover? On a more theoretical level, how does the nature of this transition depend on the number of light flavors $N_f$ and their masses? Of course, we cannot tune the masses of quarks in experiments; however by studying the problem in some special limits (for e.g. three massless flavors), we may gain more insight into the nature of the transition.

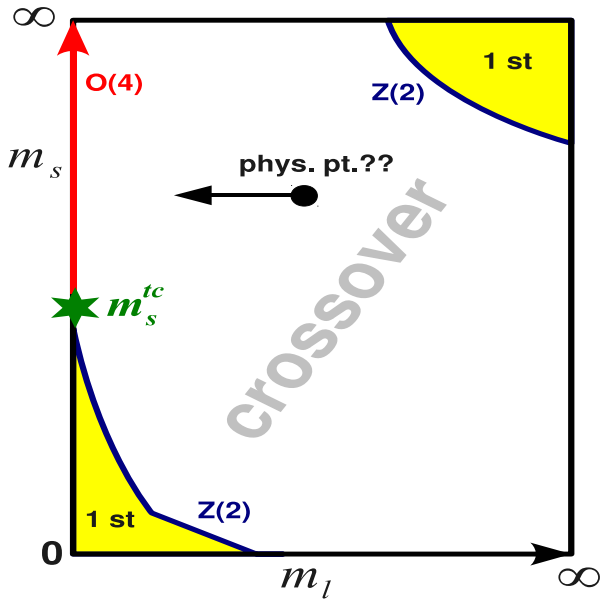


Figure 2.1: The QCD phase diagram in the $(m_l, m_s)$-plane (Fig. borrowed from S. Mukherjee, SEWM 2010).

Fig. 2.1 summarizes our current knowledge about the chiral phase transition. It is conventional to treat the up and down quarks as having the same mass $m_l$. Depending upon the values of $m_l$ and $m_s$, the transition may be either first-order, second-order or a crossover, and this is what fig. 2.1 shows. Let us quickly summarize this figure: The quark masses $m_l$ and $m_s$ run from 0 to $\infty$ as one moves away from the origin (bottom left) to any of the far corners of the diagram. In the limit of infinite quark mass, the corresponding flavor(s) simply drops out *i.e.* the top right corner corresponds to pure gauge

[2]The transition from a hadronic phase to one consisting of quarks and gluons is called *deconfinement*.

("quenched") QCD, for example.

Renormalization Group-based arguments [1] tell us that for two light flavors, the transition is expected to be second-order, belonging to the $O(4)$ universality class. This is the red line along the $y$-axis. For three massless flavors, the transition is first-order. As the masses are increased, the first-order region comes to an end along a critical line. This second-order transition belongs to the $Z(2)$ universality class. The critical line extends all the way to the $y$-axis, where it meets the $O(2)$ line at a point called the tricritical point $(0, m_s^{tc})$. The exact location of this point is still unknown.

For the case of quenched or pure gauge QCD on the other hand, the transition is again first-order. As the theory is "unquenched" *i.e.* the quark masses are introduced, this transition too ends on a critical line belonging to the $Z(2)$ universality class.

No analytical method exists for the general case of arbitrary quark masses. This question must be studied numerically. Numerical studies have shown that when the light and strange quark mass values are close to the real-world ones ($m^{\rm phy} = (m_l^{\rm phy}, m_s^{\rm phy})$), the transition is just a crossover *i.e.* it lies beyond each of the second-order lines. The question mark next to the physical point is because its exact location relative to the phase transition regions is still unknown. For example, imagine keeping the strange mass fixed at its physical value and decreasing $m_l$. If $m_s^{\rm phy}$ is sufficiently small then the $Z(2)$ transition will be encountered first. On the other hand, if $m_s^{\rm phy}$ is large, then we will see a crossover transition all the way upto $m_l = 0$, at which point we encounter the $O(4)$ second-order transition. As yet, we cannot rule out either scenario though the evidence seems to point toward the latter one [11, 12].

We mentioned that the general case must be studied numerically. That numerical method is Lattice QCD. Lattice QCD is the only method we have for extracting the values of observables related to the non-perturbative properties of QCD by starting from the fundamental Lagrangian (2.1). The lattice has provided us with evidence that the picture we sketched out in this chapter viz. spontaneously broken chiral symmetry and confined matter, is correct. It has also confirmed that a transition occurs at higher temperatures. Lattice QCD is necessary because perturbation theory converges poorly at low energies, but also because phenomena such as chiral symmetry breaking are inherently non-perturbative *i.e.* they do not show up at any order in perturbation theory. The lattice is defined in Euclidean time. Therefore it can only compute time-independent phenomena. On the other hand, that is just how the partition function is defined in the path-integral approach. This makes the lattice an ideal tool for the study of QCD thermodynamics. In the next chapter, we shall introduce the formalism of Lattice QCD.

# Chapter 3

# Quantum Chromodynamics on a Lattice

In a quantum field theory, the value of an observable $\mathcal{O}$ is given by the following viz.

$$\langle \mathcal{O} \rangle = \frac{\int \mathcal{D}[\psi, \overline{\psi}, A] \mathcal{O}(\psi, \overline{\psi}, A) \exp\left(\mathrm{i}S[\psi, \overline{\psi}, A]\right)}{\int \mathcal{D}[\psi, \overline{\psi}, A] \exp\left(\mathrm{i}S[\psi, \overline{\psi}, A]\right)} \tag{3.1}$$

The integral is a functional integral over the space of all field configurations $(\psi, \overline{\psi}, A)$. The contribution to the integral from a particular configuration is weighted by a phase factor $\mathrm{e}^{\mathrm{i}S}$ where $S$ is the action functional *i.e.* the spacetime integral of the Lagrangian for the configuration in question. Note that all paths are equally probable; the only difference is in their relative phases. The denominator, which is simply the sum of the phase factors for all the configurations, is called the generating functional.

Often, the action can be written as $S = S_0 + gS_I$, where the coupling constant $g$ is small and eq. (3.1) can be evaluated exactly for $g = 0$. In that case, $\langle \mathcal{O} \rangle$ can be calculated approximately by expanding the weight factor viz.

$$\mathrm{e}^{S} = \mathrm{e}^{S_0} \left(1 + gS_I + \frac{g^2}{2!} S_I^2 + \dots\right), \tag{3.2}$$

and evaluating eq. (3.1) upto some order $g^n$ by evaluating $\langle \mathcal{O} \rangle_0$, $\langle \mathcal{O} S_I \rangle_0$, $\langle \mathcal{O} S_I^2 \rangle_0$, etc. The subscript '0' is because each term is evaluated at $g = 0$. This forms the starting point for perturbation theory.

For several time-independent quantities (such as the spectrum of the theory), a useful trick is to Wick-rotate the action to Euclidean space $x_4 = \mathrm{i}x^0$. This converts the oscillatory factor $\mathrm{e}^{\mathrm{i}S}$ into a decaying exponential $\mathrm{e}^{-S_E}$ ($S_E$ is the Euclidean action). The rate of decay is controlled by the smallest eigenvalue of $S_E$. This approach is often used to isolate the ground state of a

theory.

The Wick-rotated quantity looks a lot like the thermal expectation value of $\mathcal{O}$ in the grand canonical ensemble viz.

$$\langle \mathcal{O} \rangle = \frac{\int \mathcal{D}[\psi, \overline{\psi}, A] \mathcal{O}(\psi, \overline{\psi}, A) \exp\left(-S_E[\psi, \overline{\psi}, A]\right)}{\int \mathcal{D}[\psi, \overline{\psi}, A] \exp\left(-S_E[\psi, \overline{\psi}, A]\right)} \tag{3.3}$$

Note that in the Wick-rotated counterpart, eq. (3.3), all configurations do *not* contribute with the same probability. Rather, the greatest contribution comes from the configuration with the least action *i.e.* the classical (in Euclidean space) configuration, etc.[1] From the viewpoint of the thermal analogy, the Wick-rotated path-integral is just the expectation value of the observable in the grand canonical ensemble. It is well-known that in this ensemble, the probability that $\mathcal{O}$ shall take the value $\mathcal{O}_i$ is proportional to $\exp(-S_{E_i})$. If we choose a set of $N$ configurations from this ensemble, then $\langle \mathcal{O} \rangle$ is given by

$$\langle \mathcal{O} \rangle = \lim_{N \to \infty} \frac{1}{N} \sum_{i=1}^{N} \mathcal{O}_i, \tag{3.4}$$

where the $\mathcal{O}_i$ are the values that $\mathcal{O}$ takes on each of the configurations. As $N \to \infty$, most of the configurations in eq. (3.3) have values $\mathcal{O}_i \approx \langle \mathcal{O} \rangle$.

Eq. (3.4) is the fundamental equation governing the Monte Carlo approach to Quantum Field Theory [13]. In this approach, one generates a set of configurations that approximates the grand canonical ensemble *i.e.* the probability of occurrence of a particular configuration is proportional to $\mathrm{e}^{-S_E}$, where $S_E$ is the action of the configuration. Once we have a sufficiently large number of configurations, any observable can be measured directly by using eq. (3.4).

Thus the main task in the Monte Carlo approach is to generate such an ensemble. This is something that needs to be done numerically *i.e.* using a computer. We shall not go into the details of how this is done, but Monte Carlo methods have a long history in relation to statistical mechanics and several algorithms have been developed for this purpose. Many of these algorithms have been borrowed and adapted to suit the peculiar needs of QCD. A detailed discussion can be found in [14–16] for e.g.

[1] The Wick-rotated action is often the same as the Hamiltonian of the original theory. Thus, the minimum value of the action is actually the energy of the ground state.

## 3.1 The Lattice as a Regulator

Before that, there is one problem that needs to be dealt with. Numerical methods can only handle a finite number of degrees of freedom. On the other hand, the path-integral in eqs. (3.1) and (3.3) refer to an infinite set of paths, each path itself being continuous. To adapt these equations to a numerical setting, it is necessary to discretize them somehow.

The simplest possible discretization is to replace spacetime by a lattice. A lattice (generally hypercubic) is a grid of evenly-spaced points on which the fields are defined. The lattice spacing (usually denoted by $a$) acts as an ultraviolet cutoff on the degrees of freedom. This renders the degrees of freedom countable. In numerical work, the lattice is also not infinite in extent but finite with periodic or antiperiodic boundary conditions. Thus one also has an infrared cutoff and together the two ensure that the number of degrees of freedom is finite.

In fact, it is well-known that quantum field theory has infinities that arise from the infinite degrees of freedom. Even in perturbation theory as one goes beyond lowest order, one encounters divergences due to the fact that the loop integrals run all the way from zero to infinity. These divergences are dealt with by introducing a cutoff that renders all quantities finite. From this point of view, the lattice is a regulator that cuts off the infinite degrees of freedom.

It is very important that the regulator respects the symmetries of the theory. Thus for example, a naive cutoff viz. $\int_0^\Lambda \mathrm{d}p$, is never used because this violates gauge-invariance which leads to problems with renormalizability. Similarly, in lattice QCD one cannot simply discretize $\psi(x) \to \psi_n$, $A^a_\mu(x) \to A^a_{\mu n}$, etc. The great advantage of lattice QCD is that it was shown by Kenneth Wilson how to discretize eq. (3.3) in a gauge-invariant manner [17].

In the following section, we shall retrace Wilson's construction. We shall see that unlike in the continuum, the gauge degrees of freedom are not the gauge potentials $A_\mu$ drawn from the algebra of the group $SU(3)$, but rather the group matrices themselves. Since the group $SU(3)$ is compact unlike its algebra, its volume is finite and no gauge-fixing is required. We shall also see that the discretizing the fermion action is non-trivial; this is the famous fermion doubling problem. This problem is closely related to the question of putting chiral symmetry on the lattice: It turns out that one cannot have chiral symmetry and avoid the doubling problem at the same time.

## 3.2 The Wilson Line

Let us recall how QCD is made gauge-invariant: Since the quark fields at different spacetime points transform independently ($V(x), V(y) \in SU(3)$)

$$\psi(x) \to V(x)\psi(x), \qquad \psi(y) \to V(y)\psi(y), \tag{3.5}$$

to define a meaningful derivative we must introduce an object $U(x, y)$ (called the comparator) which transforms as [19]

$$U(x, y) \to V(x)U(x, y)V^\dagger(y) \tag{3.6}$$

and use it to define the *covariant derivative* viz.

$$n^\mu D_\mu \psi(x) = \lim_{\epsilon \to 0} \frac{\psi(x + \epsilon n) - U(x + \epsilon n, x)\psi(x)}{\epsilon}. \tag{3.7}$$

Here, $n$ is an arbitrary unit vector. For infinitesimally separated points we have

$$U(x + \epsilon n, x) = 1 + \mathrm{i}g\epsilon n^\mu A^a_\mu(x)t^a + \mathcal{O}(\epsilon^2), \tag{3.8}$$

where the $t^a$ are the generators of $SU(3)$ and the coefficients $A^{a\mu}(x)$ multiplying them are the gauge potentials. Thus, $D_\mu = \partial_\mu - \mathrm{i}gA^a_\mu t^a$.

Conversely, if we know the gauge potentials $A^a_\mu(x)$, we can construct the comparator from them viz.

$$U(x, y; \mathcal{C}) = \mathcal{P}_\mathcal{C} \exp\left(\mathrm{i}g \int_x^y dz^\mu A^a_\mu(z)t^a\right). \tag{3.9}$$

The symbol $\mathcal{P}_\mathcal{C}$ stands for "path-ordering" along the curve $\mathcal{C}$ joining $y$ to $x$[2].

$U(x, y; \mathcal{C})$ is called the *Wilson line* [17][3]. Eq. (3.9) tells us that the Wilson line measures the net phase picked up by the fermion field as it is transported parallel to itself along the curve $\mathcal{C}$ from $y$ to $x$. This phase depends on the path $\mathcal{C}$, as can be seen by noting that it does not vanish if $\mathcal{C}$ is a closed curve. Rather

$$U(x, x; \mathcal{C}) = \mathcal{P}_\mathcal{C} \exp\left(\mathrm{i}g \oint \mathrm{d}z^\mu A^a_\mu(z)t^a\right). \tag{3.10}$$

[2]Since the $A^a_\mu t^a$ are matrices, they do not commute in general and an ordering prescription is needed to define matrix products. The above prescription puts matrices further along the curve as one moves from $y$ to $x$ to the right.

[3]The Wilson line construction also occurs in the early works of Schwinger, and most notably in the Aharanov-Bohm effect. F. Wegner was also led to such a construction as a result of generalizing the Z(2) symmetry of the Ising model to a local symmetry [18].

Now consider the following product of links viz.

$$\begin{aligned} U_{\mu\nu}(x) &= U(x, x+\epsilon\hat{\mu})U(x+\epsilon\hat{\mu}, x+\epsilon\hat{\mu}+\epsilon\hat{\nu}) \\ &\quad \times U(x+\epsilon\hat{\mu}+\epsilon\hat{\nu}, x+\epsilon\hat{\nu})U(x+\epsilon\hat{\nu}, x), \\ &= 1 + \mathrm{i}g\epsilon^2 F^a_{\mu\nu}(x)t^a + \mathcal{O}(\epsilon^4). \end{aligned} \tag{3.11}$$

In the last line, we have introduced the *field strength tensor* $F^a_{\mu\nu}$, defined by $F^a_{\mu\nu} = \partial_\mu A^a_\nu - \partial_\nu A^a_\mu + g f^{abc} A^b_\mu A^c_\nu$. This product is an approximation to a Wilson loop around a small square of side $a$ in the $\mu\nu$-plane. We may write

$$\begin{aligned} U_{\mu\nu}(x) &\approx \exp\Big(\mathrm{i}ga^2 F^a_{\mu\nu}(x)t^a\Big), \\ &= 1 + \mathrm{i}ga^2 F^a_{\mu\nu}(x)t^a - \frac{g^2a^4}{2}\left(F^a_{\mu\nu}(x)t^a\right)\left(F^b_{\mu\nu}(x)t^b\right) + \ldots \end{aligned} \tag{3.12}$$

Since the $t^a$ are traceless

$$\begin{aligned} \mathrm{Tr}\Big(1 - U_{\mu\nu}(x)\Big) &\approx \frac{g^2a^4}{2} F^a_{\mu\nu}(x)F^b_{\mu\nu}(x)\mathrm{Tr}(t^a t^b) \\ &= \frac{g^2a^4}{4}\Big(F^a_{\mu\nu}(x)\Big)^2 + \mathcal{O}(a^6) \end{aligned} \tag{3.13}$$

The special case of the Wilson line, when the curve $\mathcal{C}$ is closed, is known as the *Wilson loop*. It transforms under gauge transformations as $U(x,x;\mathcal{C}) \to V(x)U(x,x;\mathcal{C})V^\dagger(x)$. Thus the trace of the Wilson loop is gauge-invariant.

We are ready to motivate the action of Lattice QCD. Before doing so, let us switch to Euclidean spacetime via $x^4 = \mathrm{i}x^0$, $A_4(x) = \mathrm{i}A_0(x)$. This has the advantage that the action becomes positive-definite, something that will be very important to the sequel.

Lattice QCD approximates Euclidean spacetime by a four-dimensional lattice of spacing $a$. The fermion fields live on the sites $n \equiv (n_1, n_2, n_3, n_4)$ of this lattice viz. $\psi(x) \to \psi_n$, $\overline{\psi}(x) \to \overline{\psi}_n$, with $x_\mu = an_\mu$. The gauge fields are not discretized; rather one puts the comparator $U(an, an+\hat{\mu}) \equiv U_\mu(n)$ on the *link* between $n$ and $n+\hat{\mu}$.

The covariant derivative is replaced by the following difference viz.

$$\begin{aligned} D_\mu\psi(x) &\to \frac{U(n, n+\hat{\mu})\psi_{n+\hat{\mu}} - \psi_n}{a}, \\ &= \frac{U_\mu(n)\psi_{n+\hat{\mu}} - \psi_n}{a}. \end{aligned} \tag{3.14}$$

The RHS equals the LHS upto terms of $\mathcal{O}(a)$; importantly however, the RHS is gauge-covariant even for $a \neq 0$. Similarly, rather than simply discretize the

Euclidean gauge action we replace it by

$$
\begin{aligned}
S_G &= \sum_n a^4 \Big[ \frac{1}{g^2} \sum_{\mu,\nu} \mathrm{ReTr}\Big(1 - U_{\mu\nu}(x)\Big)\Big] \qquad (3.15)\\
&= \sum_n a^4 \Big[ \frac{2N_c}{g^2} \sum_{\nu<\mu} \Big(1 - \frac{1}{N_c}\mathrm{ReTr}U_{\mu\nu}(n)\Big)\Big],\\
&\to \int \mathrm{d}^4x \sum_{\mu,\nu} \frac{1}{4} \left(F^a_{\mu\nu}(x)\right)^2 \text{ as } a \to 0. \qquad \text{(eq.(3.13))}
\end{aligned}
$$

where $U_{\mu\nu}(n)$ is given by eq. (3.11) *i.e.* it is the product of links around the elementary square (plaquette) of the lattice situated at $x$. A pictorial representation of links and plaquettes is shown in fig. 3.1.

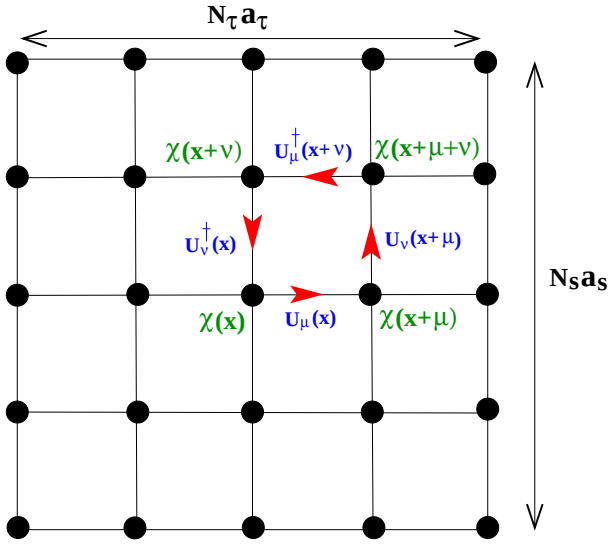


Figure 3.1: Graphical representation of the fundamental fields of lattice QCD. Quark fields (denoted by $\chi(x)$) sit at the sites of the lattice while gauge fields are replaced by unitary $SU(3)$ matrices (denoted by $U_\mu(x)$ and represented by arrows) that sit on the links. The gauge action is given by the product of links around the smallest possible closed curve *i.e.* the plaquette (Figure borrowed from S. Mukherjee).

The lattice approximation to the generating functional is given by

$$\mathcal{Z} = \int \prod_{n,\mu} \mathrm{d}\psi_n \mathrm{d}\overline{\psi}_n \mathrm{d}U_\mu(n) \mathrm{e}^{-(S_F+S_G)}, \tag{3.16a}$$

$$S_F = \sum_n a^4 \left[ \frac{1}{2a} \sum_{\mu=1}^{4} \gamma_\mu \left( U_\mu(n)\psi_{n+\hat{\mu}} - U_\mu^\dagger(n)\psi_{n-\hat{\mu}} \right) \right] + \sum_n a^4 m \overline{\psi}_n \psi_n, \tag{3.16b}$$

$$S_G = \sum_n a^4 \Big[ \frac{2N_c}{g^2} \sum_{\nu<\mu} \Big( 1 - \frac{1}{N_c} \mathrm{ReTr} U_{\mu\nu}(n) \Big) \Big] \tag{3.16c}$$

Often, the fermion fields are integrated out before simulating. This gives rise to a determinant viz.

$$\mathcal{Z} = \int \prod_n \mathrm{d}U_\mu(n) \det D[U] \mathrm{e}^{-S_G[U]}. \tag{3.17}$$

The way to include fermions is to generate an ensemble with a probability distribution $\det D \mathrm{e}^{-S_G}$ rather than just $\mathrm{e}^{-S_G}$. Evaluating a determinant is expensive; moreover this must be done for each gauge field. This makes dynamical fermion simulations much more expensive than pure gauge simulations.

To retain the probabilistic interpretation, we must have $\det D \geqslant 0$. We shall see how this is achieved for various fermion actions later.

## 3.3 The Fermion Doubling Problem

Fermions present a problem for lattice QCD. To see what that is, let us write down the action of a free Dirac particle on the lattice. A straightforward discretization yields (for $m = 0$)

$$S = \sum_x a^4 \sum_{\mu=1}^{4} \overline{\psi}(x) \gamma_\mu \left( \frac{\psi_{x+\hat{\mu}} - \psi_{x-\hat{\mu}}}{2a} \right). \tag{3.18}$$

We've approximated the derivative by a *symmetric* difference, so that the Dirac operator is hermitian. To find the propagator, we go over to momentum space and invert

$$D^{-1}(pa) = -\mathrm{i} \frac{\sum_\mu \gamma_\mu \sin(p_\mu a)}{\sum_\mu \sin^2(p_\mu a)}. \tag{3.19}$$

For $a \to 0$ and near the origin of the Brillouin zone, this reduces to

$$D^{-1}(p) \approx -\mathrm{i}\frac{\sum_\mu \gamma_\mu p_\mu}{\sum_\mu p_\mu^2}, \tag{3.20}$$

which is just the continuum propagator.

Unfortunately, the periodicity of $\sin(p_\mu a)$ means that similar results are obtained at the other corners of the Brillouin zone. Thus for instance, for $\widetilde{p}_\mu = (2\pi - p_1, p_2, p_3, p_4)$ we have

$$\sin(\widetilde{p}_1 a) = -\sin(p_1 a), \qquad \sin(\widetilde{p}_k a) = \sin(p_k a) \qquad (k = 2, 3, 4).$$

Define a new set of $\gamma$-matrices viz. $\widetilde{\gamma}_1 = \gamma_1$ and $\widetilde{\gamma}_k = -\gamma_k$ for $k = 2, 3, 4$. These are related to the original ones by a similarity transformation[4]. The new propagator is given by

$$D^{-1}(\widetilde{p}a) = -(-\mathrm{i})\frac{\sum_\mu \widetilde{\gamma}_\mu \sin(\widetilde{p}_\mu a)}{\sum_\mu \sin^2(\widetilde{p}_\mu a)}, \tag{3.21}$$

which is the same as the old propagator except for an overall sign. Similar results are obtained at all corners of the Brillouin zone. Thus the latticized version of the Dirac equation actually describes 16 degenerate species (called tastes) in the continuum. This is the famous *fermion doubling problem.*

Doubling arises because the Dirac propagator vanishes at all the corners of the Brillouin zone. This is related to the fact that the Dirac equation is a first-order equation. Such a situation does not arise for a bosonic field such as the Klein-Gordon field because the relevant equation is a second-order one viz.

$$\partial^2\phi(x) \approx \sum_\mu \phi_{x+\hat{\mu}} + \phi_{x-\hat{\mu}} - 2\phi_x; \tag{3.22a}$$

$$\to \tilde{\phi}_p \left[ 2\sum_{\mu=1}^{4} \big(\cos(p_\mu a) - 1\big) \right], \qquad \text{(momentum space)}$$

$$D^{-1}(ap) = \frac{1}{4}\frac{1}{\sum_\mu \sin^2\left(\frac{p_\mu a}{2}\right)}. \tag{3.22b}$$

This also reduces to the continuum Klein-Gordon propagator as $a \to 0$. However the presence of $p_\mu/2$ instead of $p_\mu$ means that the propagator has a period equal to twice the Brillouin zone. Since it does not vanish at the far corners,

[4]Let $S = \gamma_1$. Then $S^{-1}\gamma_1 S = \gamma_1$ while $S^{-1}\gamma_k S = -\gamma_k$ for $k = 2, 3, 4$.

there are no doublers.

Thus the latticized Dirac equation is actually a theory of $2^d$ species (called tastes) of fermions in the continuum. In the next two sections, we shall look at the two most popular approaches to circumvent this doubling problem. The first viz. staggered fermions employs an ingenious trick due to Susskind [21] to reduce the number of tastes from sixteen to four. An alternative approach, due to Kenneth Wilson [20], adds an irrelevant term (*i.e.* a term that vanishes in the continuum limit) that lifts the degeneracy of the tastes, making fifteen of them heavy while leaving the relevant taste light. Unfortunately, the additional term breaks chiral symmetry.

### 3.3.1 Staggered Fermions

It is possible to diagonalize the naive action, eq. (3.18) in spin space as follows viz.

$$\psi_n \to T_n \psi_n, \qquad \overline{\psi}_n \to \overline{\psi}_n T_n^\dagger, \qquad T_n^\dagger = T_n^{-1}. \tag{3.23}$$

The matrix $T_n$ is given by $T_n = \gamma_1^{n_1}\gamma_2^{n_2}\gamma_3^{n_3}\gamma_4^{n_4}$. Denoting the transformed fields by $\chi_n$, $\overline{\chi}_n$, we find that the action becomes

$$S_{stag} = \frac{1}{2}\sum_n \sum_{\mu=1}^{4} \eta_\mu(n)\, \overline{\chi}_n \left(\chi_{n+\hat{\mu}} - \chi_{n-\hat{\mu}}\right) + m \sum_n \overline{\chi}_n \chi_n. \tag{3.24}$$

The factor $\eta_\mu(n) = (-1)^{\sum_{\nu<\mu} n_\nu}$ is the only remnant of the original $\gamma$-matrix structure. More importantly, since the action is now identical for each spin component, we may discard all but one them and work with the resulting one-component theory. This is the great advantage of staggered fermions over other formulations – they are a factor four less expensive in simulations than the next cheapest viz. Wilson fermions.

Another advantage of staggered fermions is that they preserve a $U(1)$ symmetry that is the remnant of the original chiral symmetry viz.

$$\chi_n \to \mathrm{e}^{\mathrm{i}\theta\Gamma_5}\chi_n, \qquad \overline{\chi}_n \to \overline{\chi}_n \mathrm{e}^{\mathrm{i}\theta\Gamma_5}, \qquad \Gamma_5 = (-1)^{\sum_\mu n_\mu}. \tag{3.25}$$

Of course, we need to show that this reduced theory goes over to the Dirac theory in the continuum limit. This is somewhat involved and we shall not go into the details [14, 15]. What is done is to combine the fields at the corners of the elementary hypercube into (one or more) Dirac spinors. In $2d$ dimensions, this hypercube has $2^{2d}$ corners; accordingly the reconstruction gives rise to $2^{2d-2}$ spinors. Susskind's trick thus gets rid of doublers in $1+1$ dimensions

but only reduces them from 16 to 4 in 3+1 dimensions. The fermions are called "staggered" fermions because they are reconstructed from different, adjacent vertices.

The staggered operator $D_s$ is antihermitian and also $\Gamma_5$-hermitian viz. $\Gamma_5 D_s \Gamma_5 = D_s^\dagger$. The antihermiticity implies that its eigenvalues are imaginary, while $\Gamma_5$-hermiticity implies that they come in complex conjugate pairs. Together, they imply that $\det D_s$ is real and non-negative.

### 3.3.2 Wilson Fermions

A very different approach to the doubling problem was taken by Kenneth Wilson in 1983 [20]. It consisted of adding a second derivative term to the usual Dirac action. Just as for the bosonic action, this operator does not vanish at the far corners of the Brillouin zone, and it lifts the degeneracy in the propagator that was responsible for the doubling by giving the fermions at the far corners masses of $\mathcal{O}(1/a)$.

The Wilson action is given by

$$S_W = \frac{1}{2}\sum_x \bar{\psi}_x \left( \sum_{\mu=1}^{4} \gamma_\mu (\psi_{x+\hat{\mu}} - \psi_{x-\hat{\mu}}) - r \sum_{\mu=1}^{4} (\psi_{x+\hat{\mu}} + \psi_{x-\hat{\mu}} - 2\psi_x) \right) + \sum_x m \bar{\psi}_x \psi_x. \tag{3.26}$$

The new term is the one proportional to $r$. It approximates a second derivative and when expanded in powers of the lattice spacing, turns out to be proportional to $a \sum_\mu \partial_\mu^2 \psi_x$ *i.e.* it vanishes in the continuum limit. The propagator is given by $(m = 0)$

$$D_W^{-1}(ap) = \frac{2r \sum_\mu \sin^2(p_\mu a/2) - \mathrm{i} \sum_\mu \gamma_\mu \sin(p_\mu a)}{\sum_\mu \sin^2(p_\mu a) + r^2 \left( 2 \sum_\mu \sin^2(p_\mu a/2) \right)^2}. \tag{3.27}$$

The $r$-term acts like a mass term, albeit a momentum-dependent one. The degeneracy is lifted because the fermions at the far corners of the Brillouin zone get masses of $\mathcal{O}(1/a)$. Thus there are no doublers.

The elimination of doublers is unfortunately achieved at the cost of chiral symmetry. The Wilson term acts like a mass term and therefore $\{D_W, \gamma_5\} \neq 0$ where $D_W$ is the Wilson operator. On the other hand, the naive and staggered actions are chiral-invariant but they contain doublers.

Before moving on, let us mention two things in connection with the Wilson

action. First, the Wilson action is often written as

$$\begin{aligned} S = &\frac{1}{2}\sum_x \overline{\psi}_x \sum_{\mu=1}^{4} \Big[(r-\gamma_\mu)U_\mu(x)\psi_{x+\hat{\mu}} + (r+\gamma_\mu)U_\mu^\dagger(x)\psi_{x-\hat{\mu}}\Big] \\ &+ (4+m)\sum_x \overline{\psi}_x\psi_x. \end{aligned} \tag{3.28}$$

One almost always chooses $r = 1$, and rescales the fields $\psi \to (2m+8r)^{-1/2}\psi$, $\overline{\psi} \to (2m+8r)^{-1/2}\overline{\psi}$ so that the Wilson operator takes the form $D_W = 1 - \kappa \not{D}$ where

$$\not{D} = \sum_{\mu=1}^{4}(r-\gamma_\mu)U_\mu(x)\delta_{x',x+\hat{\mu}} + (r+\gamma_\mu)U_\mu^\dagger(x)\delta_{x',x-\hat{\mu}}, \tag{3.29a}$$

$$\kappa = \frac{1}{2m+8r}. \tag{3.29b}$$

Second, the Wilson operator is neither hermitian nor antihermitian but instead satisfies a property called $\Gamma_5$-hermiticity viz. $\Gamma_5 D_W \Gamma_5 = D_W^\dagger$. $\Gamma_5$-hermiticity implies that $H_W = \Gamma_5 D_W$ has real eigenvalues. Just as for the staggered operator, the eigenvalues of the $H_W$ can be either positive or negative. However unlike the staggered case, these eigenvalues need not come in opposite-sign pairs. This means that $\det H_W$ is not necessarily non-negative. As we have seen, this is necessary for $\det H_W$ to have a probabilistic interpretation.

The way out is to simulate *two* flavors of Wilson quarks, $\det H_W^2 = \det D_W^\dagger D_W$, and take the *square root* of the determinant to obtain a single flavor. Unlike in the staggered formulation, taking the square root in this case is uncontroversial because the Wilson operator is a local operator. Furthermore, there is a gap in the spectrum of $H_W$, for non-zero quark mass and at sufficiently small lattice spacing, that prevents eigenvalues from crossing the origin. Thus, at least on sufficiently fine lattices, the rooting procedure is uncontroversial for Wilson fermions.

Continuum QCD with quarks has three important symmetries viz. Lorentz-invariance, gauge-invariance and, in the limit of massless quarks, chiral-invariance[5]. We have already seen that the lattice breaks Lorentz-invariance at finite $a$ but strictly preserves gauge-invariance. The situation with chiral symmetry is much more intricate, as we shall see.

[5]Massless QCD is also scale-invariant, but this is spoilt by the conformal anomaly. We shall not discuss scale-invariance in this thesis.

## 3.4 Chiral Symmetry and the Lattice

From the above discussion, it would seem that it is not possible to maintain strict chiral-invariance, $\{\gamma_5, D\} = 0$ of the Dirac action whilst simultaneously getting rid of the doublers. This is indeed true. The relation between chiral symmetry, doubling and the anomaly was clarified by Karsten and Smit [24][6]. An anomaly is a symmetry of a classical field theory that is broken by quantum corrections. Quantum Field Theories contain divergences because of which a regulator (such as the lattice) must be introduced. In continuum QCD, the $U(1)_A$ symmetry is broken because it is impossible to find a regulator that preserves gauge- and $U(1)_A$-invariance simultaneously. We take gauge-invariance to be fundamental and give up conservation of the $U(1)_A$ current. This anomalous non-conservation is responsible, for instance, for $\pi^0 \to \gamma\gamma$ decay.

If a symmetry is to be anomalous in the continuum limit, then any regulator must break it explicitly. If we however insist that the regulator (*i.e.* the lattice) preserve the symmetry exactly, then it cannot be anomalous in the continuum. This is where the doublers come in. One always has an even number of doublers with equal and opposite chiral charges and the theory is anomaly-free in the continuum because the net chiral charge is zero. Shortly afterward, Nielsen and Ninomiya proved a theorem that stated the impossibility of having a doubler-free, analytic and chiral fermion operator on the lattice [25].

### 3.4.1 Chiral Fermions

Today we know that there is a loophole in the argument: It is possible to have a fermion operator that is invariant under an exact symmetry which in turn reduces to chiral symmetry in the continuum. That symmetry stems from a relation that Paul Ginsparg and Kenneth Wilson proposed should be obeyed by the fixed point of a chiral action under "blocking" [29] viz.

$$\{\gamma_5, D\} = aD\gamma_5 D \qquad \text{(Ginsparg-Wilson)} \tag{3.30}$$

Here, $D$ is the Dirac operator $S_E = -\sum_{x,x'} \overline{\psi}_x D_{x,x'} \psi_{x'}$ and $a$ is the lattice spacing. We see that $D$ is chiral-invariant in the continuum. However, the Ginsparg-Wilson relation implies that $D$ has an exact symmetry even at $a \neq 0$, as first pointed out by M. Lüscher viz. [30]

$$\psi \to \gamma_5 \left(1 + \frac{a}{2} D\right) \psi, \qquad \overline{\psi} \to \overline{\psi} \left(1 - \frac{a}{2} D\right) \gamma_5. \tag{3.31}$$

[6]The material in this section and the next is from the lectures by D. Kaplan [22].

Again, in the continuum limit this reduces to the usual chiral transformation.

In the continuum, the anomaly arises because the path-integral measure is not invariant under chiral transformations. Similarly, the path-integral measure on the lattice is not invariant under eq. (3.31). As a result, one has an anomaly and an index theorem viz.

$$\mathrm{Tr}\,(\gamma_5 D) = (n_- - n_+) = 2N_f\nu, \tag{3.32}$$

where $n_\pm$ is the number of positive(negative)-chirality zero modes, $N_f$ is the number of flavors and the topological index $\nu$ of a lattice configuration is *defined* by eq.(3.32) above.

The existence of an exact symmetry implies that operators computed on the lattice are protected from additive renormalization just as in the continuum. We may also expect a realistic spectrum of hadrons. In thermodynamic simulations too, phase transitions may be expected to belong to the same universality class as continuum QCD. Thus it would be advantageous to find such an operator.

## 3.5 Domain-Wall Fermions

Historically, Domain-Wall Fermions (DWF) were discovered first and their relation to the Ginsparg-Wilson equation later. The DWF formalism is of Dirac fermions in five dimensions $(x, y, z, t, s)$ with a mass term $M_5(s)$ that is $s$-dependent. This mass term is arbitrary except that it should satisfy $M_5(-\infty) < 0$, $M_5(\infty) > 0$ (In simulations, one generally takes $M_5(s) = \pm M_5\ \epsilon(s)$).

When the spectrum of this theory is computed, one finds massive eigenmodes with masses of $\mathcal{O}(M_5)$. Intriguingly however, one also finds a massless mode $\Psi(x, s)$ (we use the shorthand $x = (x, y, z, t)$) attached to the four-dimensional hyperplane $s = 0$, the plane where $M_5$ switches sign. The corresponding eigenfunction is localized to that hyperplane, its support decaying exponentially with $|s|$.

The massless mode is chiral, $\gamma_5\Psi(x, s) = \pm\Psi(x, s)$, and its chirality depends only on our choice of sign in $\pm M_5\ \epsilon(s)$. Furthermore, if we turn on a *four-dimensional* background gauge field at $s = 0$, one has a current that flows in or out of $s = 0$ from or into the bulk. From the four-dimensional point of view, this appears as an anomalous non-conservation of chiral charge.

Thus in the domain-wall formalism, (i) one obtains a four-dimensional chiral fermion whose mass is zero due to topology ($M_5(\pm\infty) = \pm M_5$) and not due to fine-tuning, (ii) the low-energy theory consequently has chiral symmetry

even though the five-dimensional theory does not, and (iii) the only effect of the lack of chiral-invariance on the low-energy theory is the anomaly! This shows that domain-wall fermions are indeed chiral lattice fermions.

### 3.5.1 Domain-Wall Fermions on the Lattice

The lattice formulation of domain-wall fermions is the discrete analog of a model considered by Lüscher [31]. This model has $M_5(s<0)=\infty$, $M_5(s>0)=-M_5$ where $M_5$ is a constant. The spectrum of the theory contains a massless, left-handed fermion localized at $s=0$. Lüscher showed that its propagation in the four-dimensional hyperplane had an amplitude $D^{-1}(x-y)$ where

$$D=\Big[1+\gamma_5\epsilon(H)\Big],\quad H=\gamma_5\left(\not{\partial}_4-M_5\right),\quad \epsilon(H)=\frac{H}{\sqrt{H^\dagger H}}=\frac{H}{\sqrt{H^2}}. \tag{3.33}$$

In fact, the operator $D$ is the overlap operator [26–28]. It is the only known solution to the Ginsparg-Wilson equation, eq.(3.30). Thus we see that domain-wall fermions have an exact chiral symmetry.

Unfortunately, this is true only if the fifth dimension is infinite in extent, something that can never be achieved in a lattice simulation. On the lattice, one must have $M_5(s<0)=M_5(s>L_s)=\infty$, $M_5(0\leqslant s\leqslant L_s)=-M_5$ for some $L_s$. One then finds that there are two massless modes in the theory, of opposite chiralities and localized at $s=0$ and $L_s$. The overlap between these modes (which are after all only a finite distance away from each other) alters the low-energy spectrum so that one instead has a single, massive fermion whose mass (called the *residual mass* $m_{\rm res}$) depends upon the overlap. However, at least for smooth gauge fields and at weak coupling, $m_{\rm res}$ vanishes exponentially with increasing $L_s$. $m_{\rm res}$ must be determined in every domain-wall simulation as it quantifies the residual chiral symmetry breaking. We shall return to this question when we look at the results of such simulations later.

The lattice version of the above model is given by [32]

$$\begin{aligned}
S_5&=\sum_{(x,s),(x',s')}\overline{\psi}_{x,s}\left(D^{\parallel}_{x,x'}\delta_{s,s'}+D^{\perp}_{s,s'}\delta_{x,x'}\right)\psi_{x',s'},\\
D^{\parallel}_{x,x'}&=\frac{1}{2}\sum_{\mu=1}^{4}\Big[(1-\gamma_\mu)\delta_{x',x+\hat{\mu}}+(1+\gamma_\mu)\delta_{x',x-\hat{\mu}}\Big]-(4-M_5)\delta_{x,x'},\\
D^{\perp}_{s,s'}&=\frac{1}{2}\Big[(1-\gamma_\mu)\delta_{x',x+\hat{\mu}}+(1+\gamma_\mu)\delta_{x',x-\hat{\mu}}-2\delta_{s,s'}\Big].
\end{aligned} \tag{3.34}$$

We recognize $D^{\parallel}_{x,x'}$ as the Wilson operator, albeit with a large, negative mass $-M_5$. In fact, the full operator is just the Wilson operator in five dimensions. The presence of the Wilson term insures that the spectrum is free of doublers.

We can also give the fermion a mass $m$ by introducing a coupling between the $s = 0$ and $s = L_s$ hyperplanes viz.

$$D^{\perp}_{s,s'} \to D^{\perp}_{s,s'} - \frac{m}{2}\Big[(1+\gamma_5)\delta_{s,1}\delta_{s',L_s} + (1-\gamma_5)\delta_{s,L_s}\delta_{s',0}\Big]. \tag{3.35}$$

While we impose (anti)periodic boundary conditions along the spatial(temporal) direction(s), the only boundary conditions along the fifth direction are the ones provided by the mass term itself. For $m = 0$, there is no coupling between the two end walls. For $m = 1$, the mass terms look like antiperiodic boundary conditions. In this case, there are no light modes at the walls. This latter observation was picked up by Furman and Shamir [32], and later by Vranas [33] to introduce the concept of *Pauli-Villars fermions*: Add to the fermionic action a set of scalar fields $\phi$, $\phi^\dagger$ with the same action but with $m = 1$. When the fermion and scalar fields are integrated out in the path integral, the resulting determinant is

$$\mathcal{Z}(\beta, m) = \int \mathcal{D}U \frac{\det D(m)}{\det D(1)} \mathrm{e}^{-\beta S_G[U]}. \tag{3.36}$$

The heavy fields cancel the contributions of the bulk modes while leaving the low-energy physics unaffected. The addition is reminiscent of the Pauli-Villars regulator in QED and for this reason, domain-wall fermions are often referred to as "doubly-regularized fermions."

## 3.6 Overlap Fermions

It might seem that perfect chiral symmetry is not possible since one can never set $L_s = \infty$ in a simulation. However, Neuberger and Narayanan were able to find a closed-form analytic expression for the operator. This operator is the *overlap* operator, and it is given by [26, 27]

$$D_{ov}(-M_5) = \Big[1 + \gamma_5 \epsilon(H)\Big], \quad \epsilon(H) = \frac{H}{\sqrt{H^\dagger H}} = \frac{H}{\sqrt{H^2}} \quad H = \gamma_5 D_W(-M_5). \tag{3.37}$$

Note the similarity between eqs. (3.37) and (3.33); the latter is just the lattice analog of the former. Whereas in the definition of $H$ in eq. (3.33), what appeared was the continuum Dirac operator, in eq. (3.37), one has the Wilson operator $D_W(-M_5)$, again for a large, negative mass $-M_5$, instead.

Remember that $D_W$ is $\gamma_5$-hermitian, $\gamma_5 D_W \gamma_5 = D_W^\dagger$. This implies that the matrix $H$ defined above is hermitian. Now $\epsilon(H)$ is the sign function of a hermitian matrix and is defined as follows: If $UHU^{-1} = \Lambda$ where $\Lambda$ is diagonal, then

$$\epsilon(H) = U^{-1}\epsilon(\Lambda)U, \qquad \epsilon(\Lambda) = \mathrm{diag}\left(\epsilon(\Lambda_{11}), \ldots, \epsilon(\Lambda_{nn})\right). \tag{3.38}$$

For a real number, $\epsilon(x) = x/|x|$ and is defined for all $x \neq 0$. Since the eigenvalues of a hermitian matrix are real, $\epsilon(\Lambda_{ii})$ is unambiguous unless $\Lambda_{ii}$ is zero.

It is easily seen that the overlap operator satisfies the Ginsparg-Wilson equation, eq. (3.30) viz.

$$\begin{aligned} \left\{\gamma_5, (1+\gamma_5\epsilon)\right\} &= \epsilon + 2\gamma_5 + \gamma_5\epsilon\gamma_5, \\ (1+\gamma_5\epsilon)\,\gamma_5\,(1+\gamma_5\epsilon) &= \epsilon + \gamma_5(1+\epsilon^2) + \gamma_5\epsilon\gamma_5, \end{aligned} \tag{3.39}$$

and equality follows because $\epsilon^2 = 1$.

This concludes our introductory survey of lattice QCD. In the next few chapters, we shall describe our work. We shall present the results of our simulations in chapter 5 but before we do that, we take up one important aspect of lattice simulations: Remember that the lattice is a theory with a cutoff whereas before extracting values for observables one must actually remove the cutoff *i.e.* send $a \to 0$. In a numerical simulation, this formal procedure is not possible. At best, one can repeat the simulations for more than one value of the cutoff and extrapolate. However, lattice simulations are expensive and it is often not possible to repeat them in this fashion. What we need is a method to estimate deviations due to non-zero $a$ *i.e.* cutoff errors, and this is what we shall turn to next.

In the next chapter, we will calculate cutoff errors in thermodynamic observables for different lattice actions. We shall do this by calculating the pressure on the lattice and expanding it in a Taylor series in the lattice spacing. We will be especially interested in the leading-order correction. For the canonical staggered, Wilson and chiral actions, this begins at $\mathcal{O}(a^2)$ — a rather large error at current lattice spacings. This motivates us to reduce these errors by including extra terms in the action. In the staggered case this procedure leads to the Naik and p4 actions. In a later chapter, we shall use a similar procedure to improve the domain-wall action. Lastly, we shall also introduce a chemical potential in the domain-wall and overlap formalisms and verify that this leads to the correct expression for the pressure in the continuum limit.

# Chapter 4

# Cutoff Effects in Fermionic Observables

## 4.1 The Need for Improvement

Lattice simulations begin by placing matter(gauge) fields on the sites(links) of a discrete lattice. The lattice spacing[1] acts as a cutoff and thus regulates divergences which must then be subtracted before sending the spacing to zero. The cutoff also affects finite quantities (observables) and therefore the limit $a \to 0$ must be taken to obtain their correct (*i.e.* continuum) values.

This is not a straightforward task because the lattice is a dimensionless formulation and the value of $a$ is never explicitly specified. What taking the continuum limit really means is that one increases the number of sites in each direction while keeping the *physical length* along that direction *i.e.* the volume $V$ or temperature $T$ fixed.

This procedure has some practical limitations. The number of degrees of freedom grows with the number of sites and this increases the cost of simulations. In addition, the strength of the signal (observable) relative to the statistical noise decreases with increasing spacing.[2] As a result, one needs much more statistics at smaller lattice spacings. This problem is especially severe in thermodynamic simulations where typical observables such as the pressure ($P$), energy density ($\varepsilon$), etc. have a mass dimension of four. As a result, one is constrained to work with rather coarse lattices.

[1] Henceforth denoted by $a$.

[2] This may be understood as follows: Lattice simulations do not return the physical value $\mathcal{O}$ of an observable but rather its dimensionless analog $\mathcal{O}a^d$ where $d$ is the dimension of $\mathcal{O}$. This vanishes as $a^d$ as $a \to 0$. On the other hand, a divergence $\mathcal{D} \propto a^{-d'}$ falls off more slowly, as $a^{d-d'}$.

The dependence of an observable $\mathcal{O}$ on the lattice spacing $a$ has the generic form[3]

$$\mathcal{O}(a) = \mathcal{O}a^d\big(1 + c_1 a + c_2 a^2 + \dots\big). \tag{4.1}$$

The leading $a^d$ behavior is physical, while the rest of the terms quantify the *cutoff* error. The values of the coefficients $c_n$ depend upon our choice of discretization. In most cases, a straightforward discretization (nearest-neighbor differences and plaquette terms) leads to $\mathcal{O}(a)$ or $\mathcal{O}(a^2)$ errors. By systematically adding terms to the action (such as next-nearest neighbor differences or rectangle terms) one can eliminate these errors so that the cutoff error begins at $\mathcal{O}(a^4)$ or higher [34]. While these additional terms do increase the cost of simulation, they also obviate the need for going to larger lattices. Reducing cutoff errors in this fashion is referred to as *improvement*.

### 4.1.1 QCD at High Temperatures

At high temperatures, strongly-interacting matter undergoes a crossover transition from hadronic matter to a *Quark-Gluon Plasma* in which quarks and gluons are no longer confined within hadrons. This is a consequence of the asymptotic freedom of QCD due to which the coupling constant grows weaker at higher energies.

The existence of such a transition was predicted by early lattice studies. It has also been confirmed experimentally in the heavy-ion collision experiments currently underway at the Relativistic Heavy Ion Collider (RHIC) at Brookhaven. However it is clear, both from lattice studies as well as from experiment, that quarks continue to interact strongly even in the liberated state. Consequently, one needs a non-perturbative method such as the lattice to compute quantities such as the equation of state ($P$ versus $\varepsilon$) or the speed of sound $c_s$ ($= \mathrm{d}P/\mathrm{d}\varepsilon$), which are useful in the phenomenology of these collisions.

However cutoff errors can strongly distort the measured values of these quantities. We see an example of this in fig. 4.1, which also demonstrates the importance of improvement. A calculation using the standard Wilson action and on a coarse lattice seems to indicate that $P/T^4$ exceeds its ideal gas value of $8\pi^2/45 \approx 1.755$. This however is only a lattice artifact. Measurements at several values of the spacing converge to a value that is about 10% less at the highest temperatures. On the other hand, $P/T^4$ as measured using improved gauge actions on the same coarse lattice never exceeds the Stefan-Boltzmann limit[4] and in fact is quite close to the continuum value.

[3] Sometimes, a non-analytic $a^n \ln a$ behavior is also seen.

[4] The limit of ideal, massless particles (fermions or bosons); henceforth denoted SB.

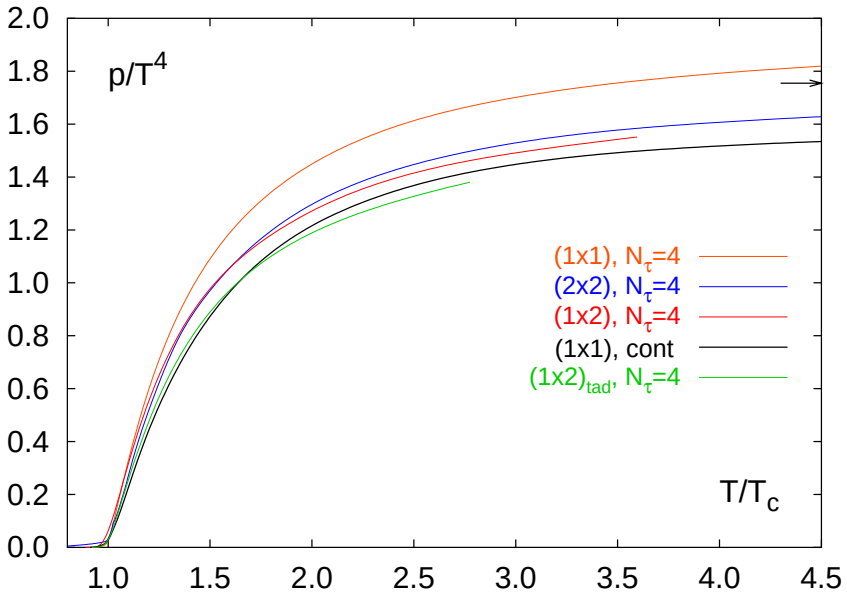


Figure 4.1: (i) The pressure in the pure gauge theory calculated with an unimproved $(1 \times 1)$ versus different improved actions. Note that the unimproved pressure exceeds the ideal gas value shown by the arrow. (ii) A continuum extrapolation of measurements with the unimproved action shows that the pressure actually misses the ideal gas value by $\sim$10% even at the largest temperatures. (iii) This behavior is reproduced fairly well by improved actions even at $N_\tau = 4$ (Figure taken from [35]).

### 4.1.2 Cutoff Effects in the Fermion Sector

Cutoff effects in the gauge sector of QCD have been reduced to a large extent through the use of improved gauge actions. The introduction of fermions however introduces new kinds of cutoff errors. These may be best understood by studying an ideal gas of fermions on the lattice. This is because simulations have shown that fermionic observables actually attain the SB limit quite quickly above the transition temperature.

In the ideal gas limit, one has exact expressions (upto integrals that can be done numerically) for thermodynamic quantities. We may also expand the integrands in a Taylor series in $a$ and evaluate each Taylor coefficient by integration. This approach leads to a series of the type eq. (4.1). While the zeroth-order term shall always give the continuum result, we are especially interested in the leading correction. We shall see that it is of $\mathcal{O}(a^2)$ for naive and Wilson fermions. Since this implies quite a large error ($\sim$20% at $N_\tau = 8$) in observables, we are motivated to improve these actions by adding extra

terms to them. Two different ways of doing this shall lead us to the Naik and p4 actions. By explicit calculation, we shall verify that the error for these actions begins at $\mathcal{O}(a^4)$.

The Naik and p4 actions have actually been implemented in QCD simulations where they have shown good scaling behavior. Our interest in them however was from the viewpoint of understanding improvement. What we are really interested in is fermions with chiral symmetry. In particular, we are interested in how these actions fare with respect to thermodynamics. We shall see that bulk observables computed with them show $\mathcal{O}(a^2)$ errors similar to unimproved fermions. This behavior can be traced to the fact that near the origin of the Brillouin zone, both overlap and domain-wall fermions have the same dispersion relation as naive fermions. We conjecture how this behavior can be improved though we do not prove this explicitly. This will be done in a later chapter. Of the two chiral actions viz. domain-wall and overlap, we shall place greater emphasis on the former as our simulations have been performed using them. However overlap fermions are simpler from the viewpoint of analytical calculations. Moreover they can be thought of as a (important) limiting case of domain-wall fermions. Thus we shall work with the overlap formalism as well whenever convenient.

The introduction of fermions also broadens the scope of the QCD phase diagram. While quenched QCD has no free parameters save for the gauge coupling, $2+1$-flavor QCD has two more viz. the light and strange quark masses $m_l$ and $m_s$. However QCD also conserves flavor *i.e.* the number of quarks minus antiquarks of each flavor. Accordingly, we may introduce *chemical potentials* ($\mu_l$, $\mu_s$) corresponding to each quark flavor and study the phase diagram in say, the $T-\mu_{l,s}$ plane[5]. We shall have more to say about lattice QCD at finite chemical potential in section 4.7.

We would also like to introduce a chemical potential $\mu$ in the lattice action. For staggered and Wilson fermions, the usual way to do so is as an imaginary part to the gauge field component $A_4(x)$ viz. $U_4(x) \to e^{\mu} U_4(x)$, $U_4^\dagger(x) \to e^{-\mu} U_4^\dagger(x)$, where the $U_4$'s are the gauge links in the time direction. This prescription has been shown to eliminate $\mu^2/a^2$-divergences in staggered- and Wilson-type fermions [3]. We shall also use this prescription to introduce $\mu$ in the overlap and domain-wall formalisms. We shall justify this by showing that the continuum pressure is correctly reproduced and that $\mu^2/a^2$-divergences do not arise [36, 37]. We will also give explicit results for the $\mu$-dependence of cut-off effects in leading and next-to-leading order in a large-$N_\tau$ expansion of bulk thermodynamics. Just as for staggered- and Wilson-type fermions, a

[5]QCD also conserves the net charge, baryon number and isospin; thus we may also introduce $\mu_Q$, $\mu_B$ and $\mu_I$. However, these are just simple linear combinations of $\mu_l$ and $\mu_s$.

non-vanishing chemical potential only modifies the expansion coefficients but does not change the structure of the expansion, *i.e.* actions that are improved to $\mathcal{O}(a^n)$ at $\mu = 0$ remain improved to that order also for $\mu > 0$.

## 4.2 Quantifying Cutoff Effects in Thermodynamic Observables

We shall illustrate the procedure outlined above in the case of the simplest possible discretization viz. the naive action. For simplicity we shall work with a single flavor and color of fermion. Now the partition function at temperature $T$ and non-vanishing chemical potential $\mu$ for free fermions defined on a lattice of size $N_\sigma^3 \times N_\tau$ is given by[6]

$$\mathcal{Z}(V,T,\mu,m) = \int \prod_x \mathrm{d}\bar{\psi}_x \mathrm{d}\psi_x \mathrm{e}^{-S_F}, \tag{4.2a}$$

$$S_F = \frac{1}{2}\sum_x \Bigg( \sum_{k=1}^{3} (\bar{\psi}_x \gamma_k \psi_{x+\hat{k}} - \bar{\psi}_x \gamma_k \psi_{x-\hat{k}}) + \mathrm{e}^{\mu}\bar{\psi}_x\gamma_4\psi_{x+\hat{4}} - \mathrm{e}^{-\mu}\bar{\psi}_x\gamma_4\psi_{x-\hat{4}} \Bigg) + \sum_x m\bar{\psi}_x\psi_x. \tag{4.2b}$$

We note that the transformation

$$\psi(\mathbf{x},x_4) \to \mathrm{e}^{-\mu x_4}\psi(\mathbf{x},x_4), \qquad \overline{\psi}(\mathbf{x},x_4) \to \mathrm{e}^{\mu x_4}\overline{\psi}(\mathbf{x},x_4), \tag{4.3}$$

leaves the path integral invariant while shifting the entire $\mu$-dependence to the last time slice. The Euclidean action thus depends on $\mu$ only through the combination $\mu/T$.

In momentum space the action becomes

$$S_F = \sum_p \Big( \sum_{k=1}^{3} \mathrm{i}\gamma_k \sin p_k + \mathrm{i}\gamma_4 \sin(p_4 - \mathrm{i}\mu) + m \Big), \tag{4.4}$$

and hence the path-integral evaluates to

$$\mathcal{Z}(V,T,\mu,m) = \prod_p \Big( \sum_{k=1}^{3} \sin^2 p_k + \sin^2(p_4 - \mathrm{i}\mu) + m^2 \Big)^2. \tag{4.5}$$

[6] $a = 1$ from now on unless explicitly stated otherwise.

Since $\ln \mathcal{Z} = PV/T$ in the infinite-volume limit,

$$\frac{P}{T^4} = 2\left(\frac{N_\tau}{N_\sigma}\right)^3 \sum_{(\mathbf{p},p_4)} \ln\Big(\sum_{k=1}^{3} \sin^2 p_k + \sin^2(p_4 - \mathrm{i}\mu) + m^2\Big). \tag{4.6}$$

The sums over the space components become integrals in the infinite-volume limit. The sum over $p_4$ however remains a sum even in the limit $N_\tau \to \infty$ because the temporal extent $N_\tau a$ defines the inverse temperature $T^{-1}$ of the system, which is finite for $T \neq 0$.

We shall evaluate this sum by replacing it by a contour integral. Since this is something that we will do all the time, we shall describe the procedure in detail below. Let us denote $\sum_{k=1}^{3} \sin^2 p_k + m^2 \equiv \omega^2$. We want a closed-form expression for $\mathcal{S} = \sum_{p_4} \ln(\omega^2 + \sin^2(p_4 - \mathrm{i}\mu))$. Now,

$$\begin{aligned} \frac{\mathrm{d}\mathcal{S}}{\mathrm{d}\omega^2} &= \sum_{k=1}^{N_\tau} \frac{1}{\omega^2 + \sin^2(p_4 - \mathrm{i}\mu)}, \\ &= \sum_{k=1}^{N_\tau} \frac{1}{\omega^2 + \sin^2\left(\frac{2\pi}{N_\tau}(k+\frac{1}{2}) - \mathrm{i}\mu\right)}. \end{aligned} \tag{4.7}$$

In the second line, we have replaced $p_4$ by its value on a discrete lattice. The factor of $1/2$ arises because we have imposed antiperiodic boundary conditions in the time direction (as we should for a fermionic system). Now consider the function

$$H(z) = \frac{1}{z\left(z^{N_\tau} + \mathrm{e}^{\mu N_\tau}\right)} \frac{1}{\omega^2 - \frac{1}{4}\left(z - \frac{1}{z}\right)^2}. \tag{4.8}$$

The first fraction has simple poles at $z_k \equiv \exp\left[(2k+1)\pi/N_\tau - \mathrm{i}\mu\right]$, $k = 1, \ldots, N_\tau$.[7] Its residues at these poles are

$$\lim_{z \to z_k} (z - z_k) H(z) = -\frac{\mathrm{e}^{-\mu N_\tau}}{N_\tau} \frac{1}{\omega^2 + \sin^2\left(\frac{2\pi}{N_\tau}(k+\frac{1}{2}) - \mathrm{i}\mu\right)}, \tag{4.9}$$

*i.e.* its residues are the terms of the sum in eq.(4.7). It also has poles at

$$\begin{aligned} \omega^2 &= \frac{1}{4}\left(z - \frac{1}{z}\right)^2, \\ z &= \pm\omega \pm \sqrt{1+\omega^2} \equiv \omega_{1\ldots4}, \end{aligned} \tag{4.10}$$

[7] The function is regular at $z = 0$.

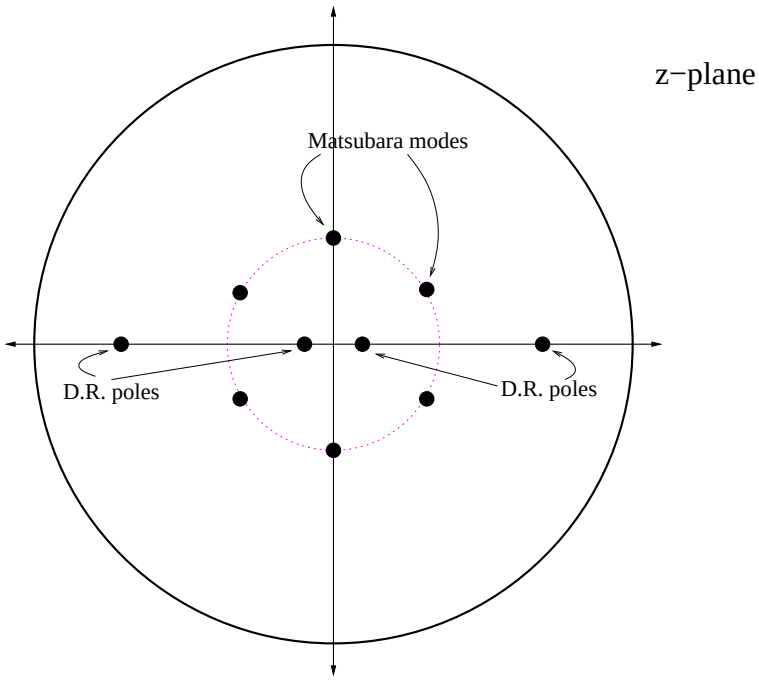


Figure 4.2: The contour of integration for $N_\tau = 6$. The dotted line is a circle of radius $\mathrm{e}^{\mu/T}$. "D.R." stands for dispersion relation. These are the poles of the propagator.

with residues

$$\lim_{z\to\omega_i}(z-\omega_i)H(z) = \frac{-4\omega_i}{\omega_i^{N_\tau}+\mathrm{e}^{\mu N_\tau}}\prod_{j\neq i}(\omega_i-\omega_j)^{-1}. \tag{4.11}$$

To simplify the above expression, let us denote $\omega^2 \equiv \sinh^2 E$. Then we immediately see that the four poles are related to each other as $\pm\mathrm{e}^{E}$, $\pm\mathrm{e}^{-E}$. The corresponding residues are given by

$$z = \mathrm{e}^{E}: \qquad -\frac{1}{\mathrm{e}^{EN_\tau}+\mathrm{e}^{\mu N_\tau}}\frac{1}{2\cosh E\sinh E}, \tag{4.12a}$$

$$z = -\mathrm{e}^{E}: \qquad -\frac{1}{(-)^{N_\tau}\mathrm{e}^{EN_\tau}+\mathrm{e}^{\mu N_\tau}}\frac{1}{2\cosh E\sinh E}, \tag{4.12b}$$

$$z = \mathrm{e}^{-E}: \qquad \frac{1}{\mathrm{e}^{-EN_\tau}+\mathrm{e}^{\mu N_\tau}}\frac{1}{2\cosh E\sinh E}, \tag{4.12c}$$

$$z = -\mathrm{e}^{-E}: \qquad \frac{1}{(-)^{N_\tau}\mathrm{e}^{-EN_\tau}+\mathrm{e}^{\mu N_\tau}}\frac{1}{2\cosh E\sinh E}. \tag{4.12d}$$

From now on, we shall assume that $N_\tau$ is even. Consider the contour shown

in fig. 4.2. For $N_\tau > 1$, $H(z) \to 0$ faster than $1/z^2$ and the integral vanishes as the contour goes to infinity. By the residue theorem, the sum over its residues is also equal to zero. This gives

$$\begin{aligned}\frac{\mathrm{e}^{-\mu N_\tau}}{N_\tau}\frac{\mathrm{d}\mathcal{S}}{\mathrm{d}\omega^2} &= \frac{\mathrm{e}^{-\mu N_\tau}}{N_\tau}\sum_{k=1}^{N_\tau}\frac{1}{\omega^2+\sin^2\left(\frac{2\pi}{N_\tau}(k+\frac{1}{2})-\mathrm{i}\mu\right)},\\ &= \frac{-\mathrm{e}^{-\mu N_\tau}}{\sinh E\cosh E}\left(\frac{1}{\mathrm{e}^{(E-\mu)N_\tau}+1}-\frac{1}{\mathrm{e}^{(-E-\mu)N_\tau}+1}\right). \qquad (4.13)\end{aligned}$$

Now let us use

$$\frac{\mathrm{d}\mathcal{S}}{\mathrm{d}\omega^2} = \frac{\mathrm{d}\mathcal{S}}{\mathrm{d}E}\frac{\mathrm{d}E}{\mathrm{d}\omega^2} = \frac{\mathrm{d}\mathcal{S}}{\mathrm{d}E}\cdot 2\sinh E\cosh E,$$

to obtain

$$\frac{\mathrm{d}\mathcal{S}}{\mathrm{d}E} = -2N_\tau\left(\frac{1}{\mathrm{e}^{(E-\mu)N_\tau}+1}-\frac{1}{\mathrm{e}^{(-E-\mu)N_\tau}+1}\right), \qquad (4.14)$$

which upon integrating yields

$$\mathcal{S} = 2\Big(\ln\left(1+\mathrm{e}^{-(E-\mu)N_\tau}\right)+\ln\left(1+\mathrm{e}^{(E+\mu)N_\tau}\right)\Big).$$

The factor of 2 is the spin degeneracy. The first term too is familiar as the partition function for spin-1/2 fermions. The second term is divergent because it contains the zero-point contribution, which we subtract as follows viz.[8]

$$\ln\left(1+\mathrm{e}^{(E+\mu)N_\tau}\right) = \ln\left(1+\mathrm{e}^{-(E+\mu)N_\tau}\right)+N_\tau(E+\mu) \to \ln\left(1+\mathrm{e}^{-(E+\mu)N_\tau}\right).$$

After this zero-point redefinition, our theory describes fermions and antifermions. The expression for the pressure eq.(4.6) becomes

$$\begin{aligned}\frac{P}{T^4} &= 2\left(\frac{N_\tau}{N_\sigma}\right)^3\sum_{\mathbf{p}}\left\{\ln\left(1+\mathrm{e}^{-(E-\mu)N_\tau}\right)+\ln\left(1+\mathrm{e}^{-(E+\mu)N_\tau}\right)\right\},\\ &= 2\left(\frac{N_\tau}{N_\sigma}\right)^3\sum_{\mathbf{p}}\left\{\ln\left(1+\mathrm{e}^{-(E-\mu)/aT}\right)+\ln\left(1+\mathrm{e}^{-(E+\mu)/aT}\right)\right\}. \qquad (4.15)\end{aligned}$$

This is starting to look like the continuum expression, but we must remember

[8]Such a subtraction must be performed in numerical work as well as in actual simulations. In both cases, this is done by evaluating the pressure on a $T = 0$ lattice and subtracting it from the finite-temperature value.

that $E$ is not equal to $\sqrt{|\mathbf{p}|^2 + m^2}$. In fact,

$$\begin{aligned}\frac{E(a\mathbf{p}, am)}{a} &= \sqrt{|\mathbf{p}|^2 + m^2} \\ &\quad - \frac{a^2}{6}\left(\sqrt{(|\mathbf{p}|^2 + m^2)^3} + \frac{1}{2}\frac{\sum_{k=1}^{3} p_k^4}{\sqrt{|\mathbf{p}|^2 + m^2}}\right) + \mathcal{O}(a^4).\end{aligned} \tag{4.16}$$

The variable $E/a$ (we divide by the lattice spacing to obtain the dimensionful analog), viewed as a function of $|\mathbf{p}|$ and $m$, defines the *dispersion relation* of the lattice action. Given a Taylor expansion such as above, one may proceed in two ways: If the bare mass of the quark which we wish to simulate is small, then the cutoff error is dominated by $\mathbf{p}$ and setting $m = 0$ provides a reasonable estimate for it. On the other hand, if the bare mass is large, then it dominates the error and we set $\mathbf{p} = 0$ instead. Since we are interested in $2 + 1$-flavor QCD rather than charm quark simulations, we shall adopt the former approach. Substituting eq.(4.16) into eq.(4.15), we get

$$\begin{aligned}\frac{P}{T^4} &= 2\left(\frac{N_\tau}{N_\sigma}\right)^3 \sum_{\mathbf{p}} \Bigg\{ \ln\left(1 + \mathrm{e}^{-(|\mathbf{p}|-\mu)/T}\right) \\ &\quad + \frac{(aT)^2}{3}\frac{1}{1 + \mathrm{e}^{(|\mathbf{p}|-\mu)/T}}\frac{|\mathbf{p}|^4 - \sum_{k=1}^{3} p_k^4}{|\mathbf{p}|T^3} + \mathcal{O}(a^4)\Bigg\} + (\mu \to -\mu).\end{aligned} \tag{4.17}$$

We were careful to substitute $N_\tau = 1/aT$ in eq.(4.15) so that we could keep track of quantities that stayed constant as the spacing was sent to zero. Now we see that we have a Taylor series in $aT = 1/N_\tau$. The last step is to convert the sum over $\mathbf{p}$ into an integral by using $\mathrm{d}p_k = 2\pi/N_\sigma$. Since the Taylor coefficients are homogeneous functions of $p_k/T$, we shall actually use $\mathrm{d}q_k = \mathrm{d}p_k/T = 2\pi N_\tau/N_\sigma$ as our integration measure. Thus we arrive at our final expression viz. ($z \equiv \exp \mu/T$)

$$\begin{aligned}\frac{P}{T^4} &= 2\int \frac{\mathrm{d}^3 q}{(2\pi)^3} \ln\left(1 + z\mathrm{e}^{-q}\right) \\ &\quad + \frac{2}{3N_\tau^2}\int \frac{\mathrm{d}^3 q}{(2\pi)^3}\frac{1}{1 + z^{-1}\mathrm{e}^{q}}\frac{2q^4 - \sum_k q_k^4}{q} + \mathcal{O}\left(\frac{1}{N_\tau^4}\right) \\ &\quad + \left(\mu \to -\mu\right).\end{aligned} \tag{4.18}$$

Each integral in this series can be evaluated exactly, even for finite $\mu$. The $\mu$-dependence of the series is non-trivial; we will discuss it in section 4.7. Setting

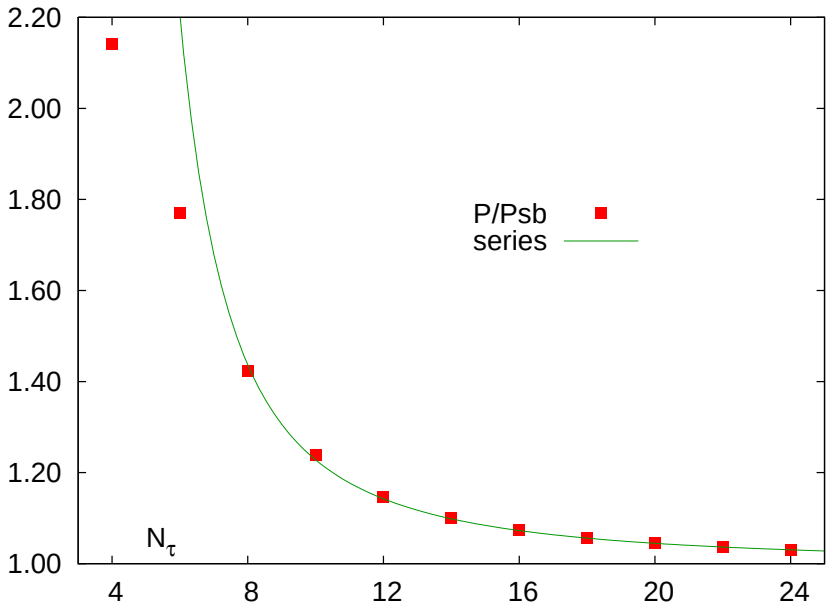


Figure 4.3: $P/P_{SB}$ for naive fermions. The green line is the series from eq. (4.19).

$\mu = 0$ for now, we obtain the following series for the pressure viz.

$$\frac{P}{T^4} = \frac{7\pi^2}{180}\left\{1 + \frac{248}{147}\left(\frac{\pi}{N_\tau}\right)^2 + \frac{635}{147}\left(\frac{\pi}{N_\tau}\right)^4 + \frac{3796}{189}\left(\frac{\pi}{N_\tau}\right)^6\right\} + \mathcal{O}\left(\frac{1}{N_\tau^8}\right). \tag{4.19}$$

## 4.3 Improved Staggered Fermions

Eq.(4.19) tells us that cutoff errors with the naive action begin at $\mathcal{O}(a^2)$. In fig. 4.3, we calculate $P/T^4$ numerically for different values of $N_\tau$ and compare these to the continuum result. We see that the deviation is $\sim 40\%$ even at $N_\tau = 8$. This is an unacceptably large value and we are motivated to improve the action so that the error may be brought down to reasonable levels.

For $m = 0$, the Dirac operator only consists of the derivative term. This term is generally approximated by the symmetric difference viz.

$$\partial_\mu \psi(x) \approx \frac{\psi(x + a\hat{\mu}) - \psi(x - a\hat{\mu})}{2a}. \tag{4.20}$$

A Taylor expansion reveals that the RHS is equal to the LHS upto terms that

start at $\mathcal{O}(a^2)$. However we may also approximate

$$\partial_\mu \psi(x) \approx c_{10} \frac{\psi(x + a\hat{\mu}) - \psi(x - a\hat{\mu})}{2a} + c_{30} \frac{\psi(x + 3a\hat{\mu}) - \psi(x - 3a\hat{\mu})}{6a}. \quad (4.21)$$

Choosing $c_{10} = 9/8$, $c_{30} = -1/8$ sets the $\mathcal{O}(a^2)$ error to zero. Deviations from the continuum are now of $\mathcal{O}(a^4)$ and hence much smaller[9]. In fact, we have just described the construction of the Naik action.

In more than one dimension, we can form other differences viz.

$$\begin{aligned}
\partial_\mu \psi(x) \approx\ & c_{10} \frac{\psi(x + a\hat{\mu}) - \psi(x - a\hat{\mu})}{2a} \\
& + c_{12} \sum_{\nu \neq \mu} \left\{ \frac{\psi(x + a\hat{\mu} + 2a\hat{\nu}) - \psi(x - a\hat{\mu} + 2a\hat{\nu})}{2a} \right\} \\
& + c_{12} \sum_{\nu \neq \mu} \left\{ \frac{\psi(x + a\hat{\mu} - 2a\hat{\nu}) - \psi(x - a\hat{\mu} - 2a\hat{\nu})}{2a} \right\}. \qquad (4.22)
\end{aligned}$$

In momentum space, this becomes

$$\begin{aligned}
\mathrm{i} p_\mu \psi(p) &= \left[ c_{10} + 2c_{12} \sum_{\nu \neq \mu} \cos(2p_\nu a) \right] \frac{\mathrm{i}}{a} \sin(p_\mu a) \psi(p), \\
&= \left[ c_{10} + 2c_{12} \sum_{\nu \neq \mu} \left( 1 - \frac{(2p_\nu a)^2}{2} \right) \right] \frac{\mathrm{i}}{a} \left( p_\mu a - \frac{a^3}{6} p_\mu^3 \right) \psi(p) + \mathcal{O}(a^4), \\
&= \left[ (c_{10} + 6c_{12}) \left( p_\mu - \frac{a^2}{6} p_\mu^3 \right) - 4 p_\mu c_{12} \sum_{\nu \neq \mu} a^2 p_\nu^2 \right] \mathrm{i} \psi(p) + \mathcal{O}(a^4), \\
&= \left[ (c_{10} + 6c_{12}) - a^2 \left( \frac{c_{10} + 6c_{12}}{6} p_\mu^2 + 4c_{12} \sum_{\nu \neq \mu} p_\nu^2 \right) \right] \mathrm{i} p_\mu \psi(p) + \mathcal{O}(a^4).
\end{aligned} \quad (4.23)$$

The first condition on these coefficients is obviously $c_{10} + 6c_{12} = 1$. There are two different sources of $\mathcal{O}(a^2)$ errors with different coefficients, so it is not possible to eliminate these. Let us instead make the action *rotation-invariant* at $\mathcal{O}(a^2)$ by choosing $c_{10} + 6c_{12} = 24c_{12}$. Then we have $c_{10} = 3/4$, $c_{12} = 1/24$ and the derivative term becomes $\mathrm{i} p_\mu (1 - a^2 p^2/6) + \mathcal{O}(a^4)$ where $p^2 = \sum_\mu p_\mu^2$.

[9]Since we have approximated the derivative by *symmetric* differences, there are no odd powers of $a$ in the Taylor expansion.

### 4.3.1 Rotation-Invariance of the Action

It is possible to proceed further and carry out the program to the one-loop level. This has been done for both the Naik as well as p4 actions [38, 39]. However let us stop here and ask instead, "What is the advantage of making the Dirac operator rotation-invariant upto a certain order?" The lattice propagator is given by $\sum_\mu \gamma_\mu D_\mu / \sum_\mu D_\mu^2$, where $D_\mu$ is our approximation to $\partial_\mu$. Now the poles of the propagator define the dispersion relation of the system. These are the solutions to $D^2 \equiv \sum_\mu D_\mu^2 = 0$. In the continuum, the dispersion relation is simply $p^2 = 0$. Rotation-invariance implies that $D^2$ is a function of $p^2$ upto some order $n$, namely

$$D^2(ap_\mu) = (ap)^2 + b_4(ap)^4 + \ldots b_{2n}(ap)^{2n} + F\left((ap_\mu)^{2n+2}\right). \tag{4.24}$$

Next we ask,"How well does the lattice dispersion relation approximate the continuum one?" If we put $p^2 = 0$ above, we see that $D^2 = 0$ upto terms of $\mathcal{O}(a^{2n+2})$. *This means that the dispersion relation is* $\mathcal{O}(a^n)$*-improved*: $E = |\mathbf{p}| + \mathcal{O}(a^{2n+2})$.

The significance of this becomes evident if we look back at eqs.(4.15) and (4.16). In the course of summing over the Matsubara modes, we were led to define a variable $E$ viz. $\sinh^2 E = \sum_{i=1}^3 \sin^2 p_i$ (for $m = 0$). Remembering that $p_4 = iE$, we see that the equation was actually $\sum_{\mu=1}^4 \sin^2 p_\mu = 0$ *i.e.* $E$ was the solution to the dispersion relation.

In fact, the net effect of summing over the Matsubara modes is always to cast the expression for the pressure into the form given by eq.(4.15) viz.

$$\frac{P}{T^4} = 2\left(\frac{N_\tau}{N_\sigma}\right)^3 \sum_{\mathbf{p}} \left\{ \ln\left(1 + \mathrm{e}^{-(E-\mu)/aT}\right) + \ln\left(1 + \mathrm{e}^{-(E+\mu)/aT}\right) \right\}.$$

What changes from one action to another is simply the definition of $E$. Thus, *improving* $E$ *upto a certain order improves the pressure upto the same order.* This is the importance of rotation-invariance.

One may ask why one cannot simply eliminate corrections to the propagator (as in the Naik action) instead of just making them rotation-invariant. For the simple cases described above, both choices work equally well. However, it is an empirical fact that rotation-invariant actions perform better than improved actions with respect to thermodynamics. For example, if we compute

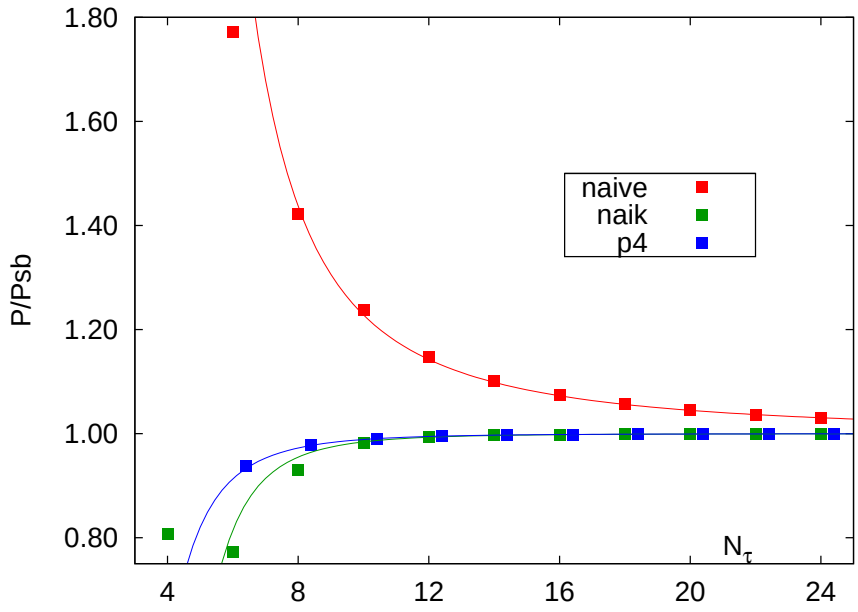


Figure 4.4: The performance of the Naik and p4 actions as compared with the naive action. The solid lines are the series, eqs. (4.19) and (4.25). The p4 points are displaced slightly relative to the Naik ones for clarity.

the series expansion for both the Naik and p4 actions, we get

$$\begin{aligned}
\text{Naik}: & \frac{7\pi^2}{180}\left\{1-\frac{1143}{980}\left(\frac{\pi}{N_\tau}\right)^4-\frac{365}{77}\left(\frac{\pi}{N_\tau}\right)^6\right\}+\mathcal{O}\left(\frac{1}{N_\tau^8}\right), \\
\text{p4}: & \frac{7\pi^2}{180}\left\{1-\frac{1143}{980}\left(\frac{\pi}{N_\tau}\right)^4+\frac{73}{2079}\left(\frac{\pi}{N_\tau}\right)^6\right\}+\mathcal{O}\left(\frac{1}{N_\tau^8}\right).
\end{aligned} \tag{4.25}$$

Both actions are $\mathcal{O}(a^2)$-improved and their $\mathcal{O}(a^4)$-corrections are the same. However, p4 fermions have smaller sub-leading errors.

Similarly, by numerically integrating the following expression viz.

$$\frac{P}{T^4}=2N_\tau^3\sum_{k=1}^{N_\tau}\int\frac{\mathrm{d}^3p}{(2\pi)^3}\ln\left[D^2\left(\mathbf{p},\frac{2\pi}{N_\tau}\left(k+\frac{1}{2}\right)\right)\right], \tag{4.26}$$

we obtain figure 4.4. Here again we see that the p4 action has smaller errors on coarser lattices than the Naik action.

Another reason for preferring rotation-invariance over improvement is that it might not be possible to eliminate the error term in some cases. We shall see

an example of this when we improve the domain-wall operator later. In that case, the need to maintain a property called the *projection property* forces us to leave the action unimproved but rotation-invariant at $\mathcal{O}(a^2)$. The resulting pressure is nevertheless $\mathcal{O}(a^2)$-improved.

It must be mentioned that the above improvement is only achieved for $m = 0$. For nonzero $m$, one has $\mathcal{O}((am)^2)$-errors. This is because the dispersion relation is now $p^2 + m^2 = 0$. Thus, analogous to eq.(4.24), we would like to have

$$\begin{aligned} D'^2(ap, am) &= a^2(p^2 + m^2) \\ &\quad + b_4 a^4 (p^2 + m^2)^2 + \ldots b_{2n}(p^2 + m^2)^n a^{2n} \\ &\quad + F\left((ap_\mu)^{2n+2}, (am)^{2n+2}\right). \end{aligned} \tag{4.27}$$

whereas what we actually have is

$$\begin{aligned} D^2(ap, am) &= (ap)^2 + (am)^2 \\ &\quad + b_4 (ap)^4 + \ldots b_{2n}(ap)^{2n} \\ &\quad + F\left((ap_\mu)^{2n+2}\right). \end{aligned} \tag{4.28}$$

Setting $p^2 = -m^2$ yields $D^2 = b_4(am)^4 + \ldots$ *i.e.* $(E^2 - |\mathbf{p}|^2)/m^2 = 1 + \mathcal{O}((am)^2)$. For the light quarks, this error isn't very large. For the charm quark on the other hand, additional tuning is required.

Lastly, we mention that rotation-invariance is also the reason why thermodynamics with Wilson fermions shows $\mathcal{O}(a^2)$ errors (as we shall see) despite the Wilson term being an $\mathcal{O}(a)$-term.

## 4.4 Thermodynamics with Wilson Fermions

We have already come across the Wilson action in sec. 3.3.2. In the following, we shall set $r = 1$ as it is the natural choice for many simulations and it also simplifies our calculations.

The Wilson pressure is given by

$$\frac{P}{T^4} = 2\left(\frac{N_\tau}{N_\sigma}\right)^3 \sum_p \left( \sum_{\mu=1}^{4} \sin^2 p_\mu + \left(2\sum_{\mu=1}^{4} \sin^2 \frac{p_\mu}{2}\right)^2 \right).$$

The dispersion relation is now a quadratic in $\sin^2(p_4/2)$ ($\sin^2 p_4 = 2\sin^2(p_4/2) - 2\sin^4(p_4/2)$). It will have four solutions of which only one, say $\omega^2$, reduces to the correct dispersion relation as $a \to 0$. The sum over Matsubara modes is

carried out as before by contour integration. However the presence of half-angles means that the function $H(z)$ (eq. (4.8)) must now be

$$H(z) = \frac{1}{z\left(z^{2N_\tau}+1\right)} \frac{1}{\omega^2 - \frac{1}{4}\left(z - \frac{1}{z}\right)^2}. \tag{4.29}$$

with poles at $z_k = \exp \mathrm{i}\pi(k+1/2)$. The net result is simply the following expression for the pressure viz.

$$\frac{P}{T^4} = 2\left(\frac{N_\tau}{N_\sigma}\right)^3 \sum_{\mathbf{p}} \left\{ \ln\left(1+\mathrm{e}^{-(E-\mu)/aT}\right) + \ln\left(1+\mathrm{e}^{-(E+\mu)/aT}\right) \right\}. \tag{4.30}$$

A Taylor series expansion of this equation shows yields

$$\frac{P}{T^4} = \frac{7\pi^2}{180}\left\{1 + \frac{248}{147}\left(\frac{\pi}{N_\tau}\right)^2 + \frac{635}{147}\left(\frac{\pi}{N_\tau}\right)^4 + \frac{133,517}{8316}\left(\frac{\pi}{N_\tau}\right)^6\right\} + \mathcal{O}\left(\frac{1}{N_\tau^8}\right). \tag{4.31}$$

We see that cutoff errors begin at $\mathcal{O}(a^2)$. This, as we have already mentioned, is due to the fact that the Wilson dispersion is rotation-invariant up to $\mathcal{O}(a^2)$. Fig. 4.5 plots the Wilson pressure for three different values of $r$.

Understanding the cutoff effects of the Wilson operator is important to us because it forms the core (or "kernel") of chiral-invariant fermion formlations such as hypercube, domain-wall or overlap fermions. We are especially interested in domain-wall fermions because we carried out simulations with them. Accordingly, we turn to these fermions next.

## 4.5 Thermodynamics with Domain-Wall Fermions

For a discussion of cutoff effects, rather than start from eq. (3.34), it is more convenient to work with an equivalent four-dimensional operator, first obtained by R. Edwards and U. Heller [40] by integrating out the fields in the fifth dimension. We shall not derive this operator but start by stating it directly viz.

$$\frac{D(m)}{D(1)} = \frac{1+m}{2} + \frac{1-m}{2}\gamma_5 \frac{T^{-L_s}-1}{T^{-L_s}+1}. \tag{4.32}$$

We will mostly consider the case $m = 0$ as well as $L_s = \infty$ (Relaxing these conditions is easy but the formulae become a little more cumbersome). In appendix B, we explain the symbols that appear above and also invert the

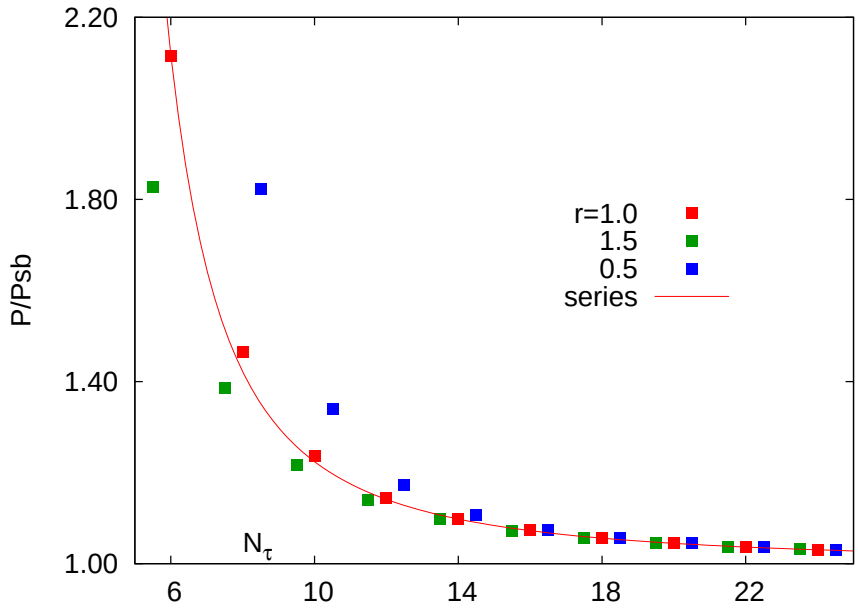


Figure 4.5: $P/P_{SB}$ for Wilson fermions as a function the inverse lattice spacing and for three different values of $r$. The green and blue points are displaced by $N_\tau = \pm 0.5$ for clarity. The curve "series" refers to eq. (4.31).

operator to obtain the propagator. We obtain

$$D^{-1}(p) = 1 + \frac{\mathrm{i}\sum_\mu \gamma_\mu \sin p_\mu}{S^2 + W^2 - 1 + \sqrt{(1+S^2+W^2)^2 - 4W^2}}, \tag{4.33}$$

where $W = 1 - M_5 + \sum_\mu (1 - \cos p_\mu)$ and $S^2 = \sum_\mu \sin^2 p_\mu$. This propagator has a pole at

$$\begin{aligned}
(1 - S^2 - W^2)^2 &= (1 + S^2 + W^2)^2 - 4W^2, \\
\Rightarrow \quad S^2 &= 0, \qquad 1 - S^2 - W^2 > 0, \\
\Rightarrow \quad S^2 &= 0, \qquad -1 < W < 1, \\
i.e. \ \sum_{\mu=1}^{4} \sin^2 p_\mu &= 0, \qquad -1 < 1 - M_5 + \sum_\mu (1 - \cos p_\mu) < 1.
\end{aligned} \tag{4.34}$$

We see that domain-wall fermions have the same dispersion relation as naive fermions viz. $\sum_\mu \sin^2 p_\mu = 0$. This has solutions near all the corners of the Brillouin zone. It is the constraint $|W| < 1$ that makes all the difference [41]. Note that $M_5$ is as yet a free parameter. It can be chosen so that the constraint

is satisfied at any one of the corners. Of course, we would like the massless mode to "live" at the origin of the Brillouin zone. Setting $p_\mu = 0$ above, we get

$$-1 < 1 - M_5 < 1, \quad i.e. \quad 0 < M_5 < 2. \tag{4.35}$$

A convenient choice in free-field calculations is $M_5 = 1$. In simulations, $M_5$ is often different from its free-field value and other considerations apply to its choice. Note that for $2 < M_5 < 4$, $4 < M_5 < 6$, ..., $8 < M_5 < 10$, we have fermions at the other corners $(\pi, 0, 0, 0)$, $(\pi, \pi, 0, 0)$, ..., $(\pi, \pi, \pi, \pi)$ of the Brillouin zone. Thus, depending on the choice of $M_5$, one may have {1,4,6,4,1} flavors of light fermions (the Pascal numbers).

Next, we turn to the pressure. It is given by

$$\begin{aligned} \frac{P}{T^4} &= 2\left(\frac{N_\tau}{N_\sigma}\right)^3 \ln\det D, \\ &= 2\left(\frac{N_\tau}{N_\sigma}\right)^3 \sum_{(\mathbf{p},p_4)} \ln\left[1 + \frac{S^2 + W^2 - 1}{\sqrt{(1 + S^2 + W^2)^2 - 4W^2}}\right]. \end{aligned} \tag{4.36}$$

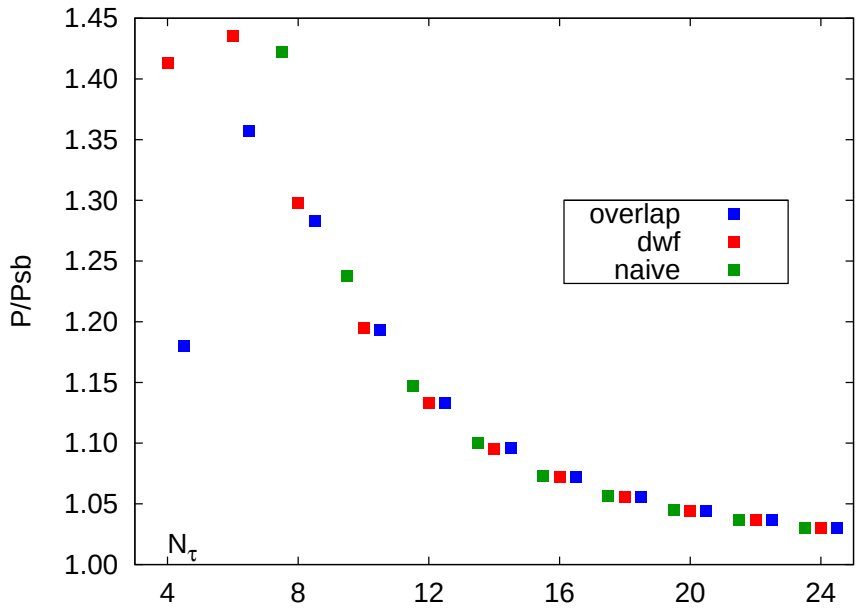


Figure 4.6: The DWF pressure as a function of $N_\tau$. The overlap and naive fermion pressures have also been included for comparison purposes. These are displaced by $N_\tau = \pm 0.5$ relative to the DWF pressure for clarity. Note the agreement of the naive values with the DWF/overlap ones in the scaling regime.

As a first step, we may numerically integrate this expression and obtain the ideal gas pressure as a function of $N_\tau$, the inverse cutoff. Our results are shown in fig. 4.6. We see, not surprisingly, that the overlap and DWF values agree for larger $N_\tau$ (but not for smaller ones). We have also plotted the pressure of naive fermions for the same values of $N_\tau$ and these too agree with the DWF/overlap values in the scaling regime. This is understandable because after all the dispersion relations are the same in all three cases.

## 4.6 The Relation between the DWF and Overlap Formalisms

Let us rewrite the argument of the logarithm in eq.(4.36) as follows viz.

$$\frac{S^2+W^2-1}{\sqrt{(1+S^2+W^2)^2-4W^2}} = \frac{W-1}{2W}\sqrt{\frac{S^2+(W+1)^2}{S^2+(W-1)^2}}+\frac{W+1}{2W}\sqrt{\frac{S^2+(W-1)^2}{S^2+(W+1)^2}}. \tag{4.37}$$

Near the continuum limit, $S^2 \to 0$, $W \to 1$ and the second term vanishes while the first term reduces to

$$\begin{aligned} \frac{W-1}{2W}\sqrt{\frac{S^2+(W+1)^2}{S^2+(W-1)^2}} &\to \frac{W-1}{\sqrt{S^2+(W-1)^2}}, \\ \ln\left(1+\frac{S^2+W^2-1}{\sqrt{(1+S^2+W^2)^2-4W^2}}\right) &\to \ln\left(1+\frac{W-1}{\sqrt{S^2+(W-1)^2}}\right). \end{aligned} \tag{4.38}$$

The RHS of the second line leads to the overlap pressure (eq. (C.5b) with $W-1 \equiv A$). Eq. (4.38) tells us that overlap fermions are not just the $L_s \to \infty$ limit of domain-wall fermions. Rather, one must take the double limit $L_s \to \infty$, $a \to 0$ in that order. This is the reason why the overlap and DWF pressures disagree in fig. 4.6 for small values of $N_\tau$.

Since the two expressions agree in the scaling regime, we may compute the series expansion from the (simpler) overlap expression. The procedure is the same as before, but now the function $H(z)$ (ch. 4) has branch cuts in the $z$-plane and we must show that their contribution vanishes in the large-$N_\tau$ limit [37]. However, the final result may be anticipated: Overlap fermions

have the same series expansion as naive fermions viz.

$$\frac{P}{T^4} = \frac{7\pi^2}{180}\left\{1 + \frac{248}{147}\left(\frac{\pi}{N_\tau}\right)^2 + \frac{635}{147}\left(\frac{\pi}{N_\tau}\right)^4 + \frac{3796}{189}\left(\frac{\pi}{N_\tau}\right)^6\right\} + \mathcal{O}\left(\frac{1}{N_\tau^8}\right). \tag{4.39}$$

## 4.7 Lattice QCD at Finite Chemical Potential

Lastly, we would like to discuss the important question of QCD simulations at finite chemical potential $\mu$ ($\mu = \mu_l$ or $\mu_s$). On the lattice, it can be introduced as follows viz.

$$U_4(x) \to \mathrm{e}^{\mu} U_4(x), \qquad U_4^\dagger(x) \to \mathrm{e}^{-\mu} U_4^\dagger(x), \tag{4.40}$$

where $U_4(x)$, $U_4^\dagger(x)$ are the gauge links along the temperature direction. When done this way, $\mu$ appears as an imaginary, constant background gauge field $A_4' = A_4 - \mathrm{i}\mu$. This generalized gauge invariance is responsible for the cancellation of quadratic divergences in the continuum. On the lattice too, this prescription removes divergences that would otherwise go as $\mu^2/a^2$ [3].

However this prescription renders the Dirac operator non-hermitian and the action $S$ complex. This is a problem for lattice QCD which relies on the probabilistic interpretation of $\mathrm{e}^{-S}$. Since $\mathrm{e}^{-S}$ becomes complex, importance-sampling methods break down. This is the famous sign problem of Lattice QCD.

To date, there is no *ab initio* method for simulating QCD at arbitrary $\mu$. However it is at least possible to obtain information at small $\mu$ by means of measurements at $\mu = 0$. One way is by expanding the partition function in a Taylor series in $\mu/T$ about $\mu = 0$ viz. [42]

$$\begin{aligned}\frac{P(\mu_l,\mu_s)}{T^4} = \frac{P(0,0)}{T^4} &\\ + \chi_2^l\left(\frac{\mu_l}{T}\right)^2 + \chi_2^s\left(\frac{\mu_s}{T}\right)^2 + \chi_{11}^{ls}\left(\frac{\mu_l}{T}\right)\left(\frac{\mu_s}{T}\right) &\\ + \chi_4^l\left(\frac{\mu_l}{T}\right)^4 + \chi_4^s\left(\frac{\mu_s}{T}\right)^4 + \chi_{22}^{ls}\left(\frac{\mu_l}{T}\right)^2\left(\frac{\mu_s}{T}\right)^2 + \ldots,&\end{aligned} \tag{4.41}$$

and measuring the Taylor coefficients via simulations at $\mu = 0$. These Taylor coefficients are called *Quark Number Susceptibilities* (QNS).

Just like the pressure, these quantities can suffer from cutoff effects if the lattice is too coarse. We compute these errors for the generic case of an $\mathcal{O}(a^n)$-improved action in appendix A. Fortunately we find that actions that

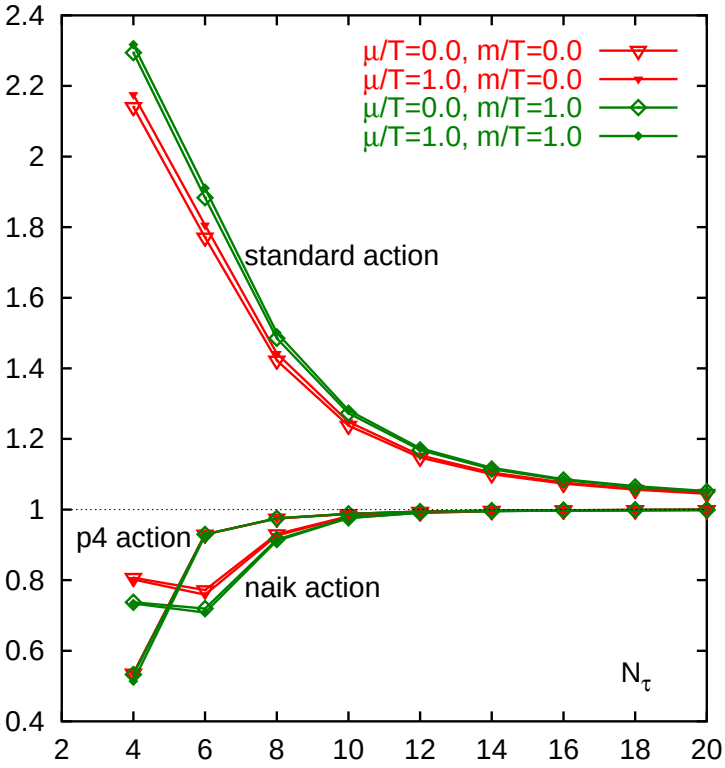


Figure 4.7: $P/T^4$ for free fermions, both improved and unimproved, at zero and nonzero $\mu$ and $m$. A slight $\mu$-dependence is seen; however improvement still holds at finite $\mu$.

| | $\chi_2$ | | $\chi_4$ | |
|---|---|---|---|---|
| | $N_\tau = 4$ | $N_\tau = 8$ | $N_\tau = 4$ | $N_\tau = 8$ |
| Unimproved | 79.2% | 19.8% | 113% | 28.3% |
| Improved | 5.1% | 0.3% | 8.0% | 0.5% |

Table 4.1: Cutoff error in the first two QNS induced by the chemical potential for unimproved and improved fermions. The first column gives the value for $N_\tau = 4$ while the latter gives the value for $N_\tau = 8$.

are improved upto a certain order at $\mu = 0$ stay that way at $\mu \neq 0$ and no further improvement is necessary. This is best seen from fig. 4.7 where the free pressure is plotted, both for zero and nonzero $\mu$, as a function of $N_\tau$ for the naive as well as improved actions.

Of course, a slight $\mu$-dependence is introduced and this is also seen when the Taylor series expansion, eq. (4.18), is computed. The Taylor coefficients become $\mu$-dependent and this leads to corrections in the susceptibilities. Cutoff errors for the first two non-trivial susceptibilities for both naive and improved staggered fermions for two values of the cutoff are presented in table 4.1.

### 4.7.1 Overlap and DWF at Finite-$\mu$

We would like to introduce the chemical potential in the same way as for staggered and Wilson fermions. In the overlap formalism however, we encounter a problem: The Wilson operator $D_W$ is not $\gamma_5$-hermitian at $\mu \neq 0$. Rather one has $\gamma_5 D_W(\mu)\gamma_5 = D^\dagger(-\mu)$. This implies that $H \equiv \gamma_5 D_W$ is not hermitian. To deal with this situation, Bloch and Wettig [4] proposed the following analytic continuation the sign function viz. $\epsilon(x + \mathrm{i}y) = \epsilon(x)$. With this definition, $\epsilon^2 = 1$ just like at $\mu = 0$.

This is important because the overlap satisfies the Ginsparg-Wilson relation, eq.(3.30) viz.

$$\begin{aligned} \left\{\gamma_5, (1+\gamma_5\epsilon)\right\} &= \epsilon + 2\gamma_5 + \gamma_5\epsilon\gamma_5, \\ (1+\gamma_5\epsilon)\,\gamma_5\,(1+\gamma_5\epsilon) &= \epsilon + \gamma_5(1+\epsilon^2) + \gamma_5\epsilon\gamma_5, \end{aligned} \tag{4.42}$$

and equality follows because of $\epsilon^2 = 1$. Thus we see that *if* the sign function is defined as above, the overlap operator satisfies the Ginsparg-Wilson relation even at $\mu \neq 0$. The other "natural" definition viz. $\epsilon(H) = H/\sqrt{H^\dagger H}$ fails in this respect.

Bloch and Wettig also showed [4] that the above extension of the overlap is equivalent to what would be obtained by introducing a chemical potential in the DWF formalism in the usual way *i.e.* $U_4(x) \to e^{\mu} U_4(x)$, $U_4^\dagger(x) \to e^{-\mu} U_4^\dagger(x)$ and taking the double limit $\lim_{a\to 0}\lim_{L_s\to\infty}$. Everything thus falls into place and we have a solid theoretical foundation for proceeding to simulate QCD thermodynamics with domain-wall fermions. Accordingly, we stop our theoretical discussion here and in the next chapter take a look at the results of such a simulation.

# Chapter 5

# DWF Thermodynamics at $N_\tau = 8$

Chiral symmetry plays a very important role in the Standard Model. The $SU(3)$ part of chiral symmetry, while spontaneously broken, still protects operators from additive renormalization. Chiral symmetry breaking is responsible for determining the low-energy spectrum of QCD viz. light mesons that do not form parity multiplets. The $U(1)$ part is anomalously broken and this mechanism is responsible for the $\pi^0 \to \gamma\gamma$ decay.

Similarly, a central question in QCD thermodynamics is the nature of the phase transition in which chiral symmetry is restored. Here again, the spectrum plays an important role in determining the characteristics of the transition, as can be seen from models of the Hadron Resonance Gas (HRG) type [43, 44]. For QCD with two massless flavors, this transition is a second-order phase transition belonging to the $O(4)$ universality class (since $O(4)$ is isomorphic to $SU(2) \times SU(2)$) while for three massless flavors, it is a first-order transition.

The location and nature of the chiral phase transition have been extensively studied using lattice techniques with several different fermion actions [45–47, 51–53]. Recently, the most detailed studies of the transition temperature have been performed with different variants of the staggered fermion action [45–47, 51]. Although staggered fermions are computationally inexpensive, they have the disadvantage that they do not preserve the full $SU(2) \times SU(2)$ chiral symmetry of continuum QCD, but only a $U(1)$ subgroup. This lack of chiral symmetry is immediately apparent in the pion spectrum for staggered quarks in which there is only a single pseudo-Goldstone pion, the other pions acquiring additional mass from $O(a^2)$ flavor-mixing terms in the action. As we have already discussed, it is important to realize the spectrum accurately for an accurate determination of the transition.

It is therefore important to study the QCD phase transition using a different fermion discretization scheme. The obvious alternative is the Wilson fermion formulation. As is well-known however, Wilson fermions break chiral symmetry completely at finite lattice spacing and it is restored only in the continuum limit, the same limit in which the breaking of $SU(2) \times SU(2)$ chiral symmetry in the staggered fermion formulation disappears.

Domain-Wall Fermions (DWF) have an exact chiral symmetry, the Ginsparg-Wilson condition, even at finite lattice spacing $a$. The DWF formulation is of Wilson fermions in five-dimensions with a large, negative mass $-M_5$ (the domain-wall height) and non-trivial boundary conditions in the fifth ($s$-) direction. The spectrum of this theory consists of massless modes that are localized at the four-dimensional hyperplanes at the two ends of the fifth dimension viz. $s = 0$ and $s = L_s$. These modes have opposite chiralities. In any simulation, the fifth dimension is of finite extent and consequently the two chiral modes "mix." This mixing results in an effective mass, called the residual mass $m_{\rm res}$, of the massless mode. For weak gauge fields this mixing vanishes exponentially as $L_s$ is increased; that is why domain-wall fermions are regarded as chiral fermions just like overlap or hypercube fermions.

Since DW fermions preserve all the symmetries of the continuum, their phase transitions should belong to the same universality class as QCD. It is thus natural to explore the QCD phase diagram with domain-wall fermions. Around ten years ago, the Riken-Brookhaven-Columbia (RBC) collaboration conducted exploratory studies with domain-wall fermions at $N_\tau = 4$ and 6 [52]. These early results were quite encouraging, showing a clear signal for a physical, finite temperature transition. However, these were two-flavor calculations on quite coarse lattices with quarks whose masses were of the order of the strange quark. Besides, $m_{\rm res}$ too was found to be quite large on these coarse lattices.

Given the substantial increase in computer capability and the deeper understanding of domain wall fermions that has been achieved over the past decade, it is natural to return to this approach. Now significantly smaller quark masses and much finer lattices with $N_\tau = 8$ can be studied and important aspects of residual chiral symmetry breaking can be recognized and explored.

In this chapter, we shall describe such a study of the QCD finite-temperature transition region using DW fermions at $N_\tau = 8$. We start by presenting our results in sections 5.1 and 5.2. In the former we discuss our determination of the lattice spacing $a$, while in the latter we discuss various finite-temperature observables such as the chiral condensate and the disconnected chiral susceptibility, the Polyakov loop and its susceptibility as well as various quark number

susceptibilities are discussed. The chiral symmetry restoration coupling is defined to be the peak of the disconnected chiral susceptibility $\chi_{\text{disc}}$. Similarly, we define the deconfinement crossover to occur at the inflection point $\beta_d$ of the isospin ($\chi_I$) or charge ($\chi_Q$) susceptibilities. We extract these values from our data.

Of concern in any DWF simulation is the magnitude of the residual mass $m_{\text{res}}$. In section 5.3, we present our results for this important quantity. Unfortunately, $m_{\text{res}}$ changes drastically as the coupling is varied, becoming larger than the light quark mass around the transition coupling. This results in a distortion of the curve for $\chi_{\text{disc}}$, introducing a systematic error in the determination of $\beta_c$. We determine this systematic error.

Finally, in section 5.4 we convert our value for $\beta_c$ to a temperature $T_c$. This was not straightforward because we had not generated zero-temperature ensembles in this exploratory study. Thus, we had to make a careful extrapolation and also estimate the error introduced by doing so. Lastly, we present our conclusions and outlook for the future.

## 5.1 Zero-Temperature Observables

Measurements at zero temperature are essential for two reasons:

- They are necessary to determine the lattice spacing. This is generally done by measuring either (i) the string tension $T$ between a quark-antiquark pair, or (ii) some hadron mass for eg. the pion, rho or nucleon mass ($m_\pi$, $m_\rho$ or $m_N$), or (iii) both. Of course, one really determines their dimensionless counterparts $a^2T$, $am_\pi$, etc. but since the physical values of these quantities are very well-known, the lattice spacing $a$ can be determined as well. Note that finite-temperature ensembles cannot be used for this purpose as hadrons dissociate at these temperatures.

- Observables in Quantum Field Theory contain divergences which must be subtracted. It is well-known that the introduction of the temperature leads to no new divergences. Since in finite-temperature studies we are often interested only in the temperature-dependent part of quantities, we may remove divergences by calculating something both at $T \neq 0$ and $T = 0$ and subtracting the latter from the former.

Unfortunately, zero-temperature ensembles are expensive to generate. Indeed, in more detailed simulations the bulk of computer time is taken up in their generation. This is partly because of the larger size of these lattices — one approximates $T = 0$ by taking $N_\tau$ to be much larger than its finite-temperature value — but also partly because the presence of light hadrons and

chiral symmetry breaking means that the Dirac operator has small eigenvalues due to the Goldstone modes. This leads to a larger *condition number i.e.* the ratio of the largest to the smallest eigenvalue. Matrices with large condition numbers take longer to invert.

Since this was an exploratory study, and since even finite-temperature DWF ensembles are expensive to generate, we did not generate zero-temperature ensembles *except* at one $\beta$-value, to get a rough estimate of the lattice spacing. The value chosen was $\beta = 2.025$ because it is, as we shall see later, quite close to the transition temperature.

### 5.1.1 The Static Quark Potential

To determine the lattice scale, we measured the static quark-anti-quark correlation function, $W(r,t)$, on 148 configurations (every 5 MD trajectories from 300-1035) on these zero temperature configurations. The quantity $W(r,t)$ is the product of two spatially separated sequences of temporal gauge links connecting spatial hyperplanes, each containing links that have been fixed to Coulomb gauge [48, 49]:

$$w(\mathbf{r},t) = U_4(\mathbf{r},0)U_4(\mathbf{r},1)\ldots U_4(\mathbf{r},t-1), \tag{5.1a}$$

$$W(r,t) = \frac{1}{N_{\text{pairs}}(r)} \sum_{|\mathbf{r_1}-\mathbf{r_2}|=r} \text{Tr}\big[w(\mathbf{r_1},t)\cdot w(\mathbf{r_2},t)\big]. \tag{5.1b}$$

where $N_{\text{pairs}}(r)$ is the number of pairs of lattice points with a given spatial separation $r$. In our calculation the results obtained from orienting the "time" axis along each of the four possible directions are also averaged together. The time dependence of $W(r,t)$ was then fit to an exponential form viz.

$$W(r,t) = c(r)\exp\left[-V(r)\ t\right], \tag{5.2}$$

in order to extract the static quark potential $V(r)$. $V(r)$ in turn was fit to the Cornell form

$$V(r) = -\frac{\alpha}{r} + \sigma r + V_0, \qquad \left(r^2\frac{dV(r)}{dr}\right)_{r=r_0} = 1.65, \tag{5.3}$$

from which the Sommer parameter $r_0$ was determined. Table 5.1 gives the details of the fit which determines the parameters $\alpha$ and $\sigma$ of Eq. 5.3 and results in a value of $r_0/a = 3.08(9)$. For the physical value of $r_0$, we use the current standard result $r_0 = 0.469(7)$ fm [50]. This gives a lattice spacing $a \approx 0.15$ fm, or $a^{-1} \approx 1.3$ GeV. It should be emphasized that this value for

| $\beta$ | $r_0/a$ | $a^{-1}$ (GeV) | t fit range | r fit range | $\chi^2$/dof. |
|---|---|---|---|---|---|
| 2.025 | 3.08(9) | 1.30(4) | $(4, 9)$ | $(\sqrt{3}, 6)$ | 1.03 |

Table 5.1: Results for $r_0$. The errors are calculated by the jackknife method, with data binned into blocks, each containing 10 molecular dynamics time units.

$r_0$ has been determined for a single light quark mass and no extrapolation to the physical value of the light quark mass has been performed. This failure to extrapolate to a physical value for the light quark mass is likely to result in an overestimate of the lattice spacing $a$ by about 3%.

### 5.1.2 Meson mass spectrum

In addition to the static quark potential, we also calculated the meson spectrum on the same zero temperature ensemble at $\beta = 2.025$. The meson spectrum was determined using 55 configurations, separated by 10 MD time units, from 500 and 1040. Table 5.2 gives the results for $m_\rho$ and $m_\pi$ for three different valence mass combinations, as well as their values in the chiral limit from linear extrapolation. Equating the physical value of $m_\rho = 776$ MeV with the chirally extrapolated lattice value gives a lattice scale of $a^{-1} = 1.26(11)$ GeV, which is consistent with the scale determined from $r_0$. Examining the data for the light pseudoscalar meson, we find $m_\pi \approx 308$ MeV, somewhat larger than twice the mass of the physical pion. For the kaon, we have $m_K \approx 496$ MeV, very close to the physical kaon mass.

| $m_x^{val}$ | $m_y^{val}$ | $m_{\text{avg}}$ | fit range | $m_\rho a$ | $\chi^2$/dof | $m_\pi a$ | $\chi^2$/dof |
|---|---|---|---|---|---|---|---|
| 0.003 | 0.003 | 0.0030 | 8-16 | 0.646(63) | 0.3(4) | 0.2373(20) | 2.4(11) |
| 0.003 | 0.037 | 0.0200 | 8-16 | 0.716(23) | 0.8(7) | 0.3815(15) | 2.0(10) |
| 0.037 | 0.037 | 0.0370 | 8-16 | 0.776(10) | 2.2(11) | 0.4846(11) | 1.2(8) |
| | $-m_{\text{res}}$ | | | 0.617(56) | | 0.073(6) | |

Table 5.2: The calculated masses $m_\rho$ and $m_\pi$ for various combinations of valence quark mass. The last line represents extrapolation of the light quark mass to $m_{\text{avg}} = (m_x + m_y)/2 = -m_{\text{res}}$.

## 5.2 Finite-Temperature Observables

### 5.2.1 Chiral condensate

For QCD with massless quarks, there is a true phase transition from a low-temperature phase with spontaneous chiral symmetry breaking to a high-temperature phase where chiral symmetry is restored. If the quarks have a finite, common mass $m_f$ that explicitly breaks chiral symmetry, the existence of a chiral phase transition persists for masses up to a critical quark mass, $m_f < m_f^{\text{crit}}$, above which the theory undergoes a smooth crossover rather than a singular phase transition as the temperature is varied. The value of $m_f^{\text{crit}}$ is poorly known and depends sensitively on the number of light quark flavors. For a transition region dominated by two light quark flavors $m_f^{\text{crit}}$ is expected to vanish and the transition to be second order only for massless quarks. For three or more light flavors, a first order region $0 \leqslant m_f < m_f^{\text{crit}}$ should be present.

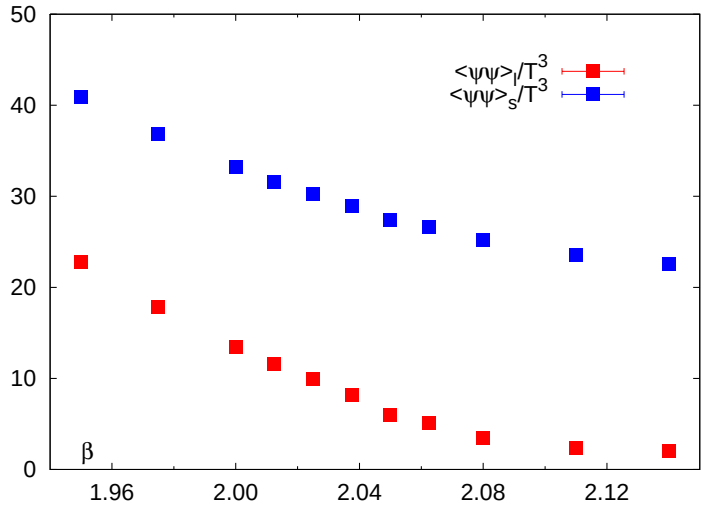


Figure 5.1: The light and strange quark condensates.

The order parameter that best describes the chiral phase transition is the chiral condensate, $\langle\overline{\psi}\psi\rangle$, which vanishes in the symmetric phase but attains a non-zero expectation value in the chirally broken phase. For quark masses above $m_f^{\text{crit}}$, the chiral condensate will show only analytic behavior, but both the light and strange quark chiral condensates, $\langle\overline{\psi}_l\psi_l\rangle, \langle\overline{\psi}_s\psi_s\rangle$, and the disconnected part of their chiral susceptibilities, $\chi_l, \chi_s$, still contain information about the chiral properties of the theory in the vicinity of the crossover transition. The chiral condensate and the disconnected chiral susceptibility for a

single quark flavor are defined as:

$$\langle\overline{\psi}\psi\rangle = \frac{T}{V}\frac{\partial \ln Z}{\partial m} = \frac{1}{N_\sigma^3 N_\tau}\langle \mathrm{Tr} D^{-1}\rangle, \tag{5.4}$$

$$\chi_{\mathrm{disc}} = \frac{T}{V}\langle\left(\mathrm{Tr}D^{-1}\right)^2\rangle - \langle \mathrm{Tr}D^{-1}\rangle^2 = \frac{1}{VT^2}\left[\langle\left(\overline{\psi}\psi\right)^2\rangle - \langle\overline{\psi}\psi\rangle^2\right]. \tag{5.5}$$

where $m$ is the mass of the quark being examined, $T$ is the temperature, $V$ the spatial volume and $N_\tau$ and $N_\sigma$ are the number of lattice sites in the temporal and spatial directions respectively.

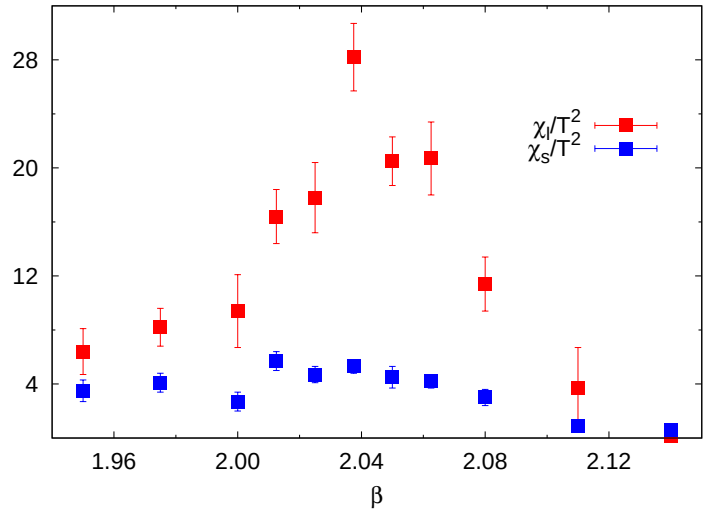


Figure 5.2: The light and strange quark susceptibilities.

On our finite-temperature ensembles, we calculated both the light ($m_l = 0.003$) and strange ($m_s = 0.037$) chiral condensates using 5 stochastic sources to estimate $\langle\overline{\psi}_q\psi_q\rangle$ on every fifth trajectory. Using multiple stochastic sources on a given configuration allows us to extract an unbiased estimate of the fluctuations in $\overline{\psi}_q\psi_q$ and to calculate the disconnected chiral susceptibility. The Polyakov loop is calculated after every trajectory.

Figures 5.1 and 5.2 show the chiral condensate and the disconnected part of the chiral susceptibility. Examining the light and strange quark chiral condensates, it is difficult to precisely determine an inflection point. Such an inflection point could be used to locate the mid-point of a thermal crossover. We can also study the disconnected chiral susceptibility. This is computed from the fluctuations in the chiral condensate and will show a peak near the location of the inflection point of the chiral condensate. We shall identify this peak with the location of the chiral crossover. The light chiral susceptibility

shown in fig. (5.2), has a clear peak near $\beta = 2.0375$.

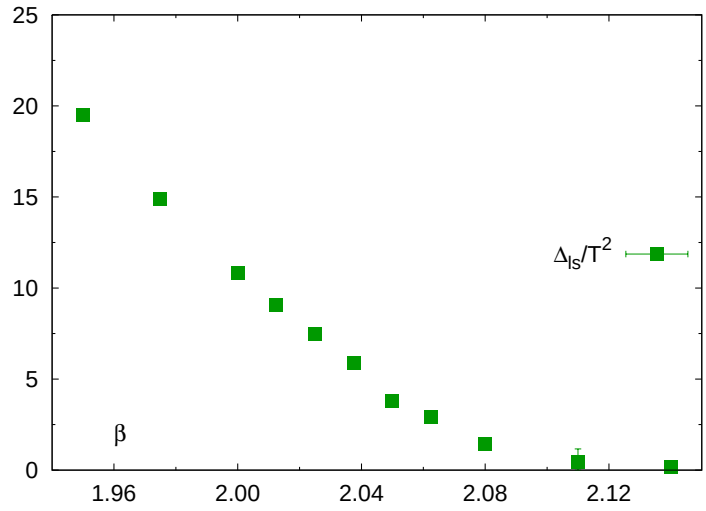


Figure 5.3: Removing the leading divergence by defining $\Delta_{ls} = \langle\overline{\psi}_l\psi_l\rangle - (m_l/m_s)\langle\overline{\psi}_s\psi_s\rangle$.

From fig.(5.1), we see that neither the strange nor the light condensate goes to zero as $\beta$ is increased. This is partly because chiral symmetry is explicitly broken by the quark mass, but also because of the presence of divergences. Like most QFT observables, the quark condensate contains divergences that need to be subtracted. One way of doing this is by computing the chiral condensate at the same coupling and at zero-temperature and subtracting it from the finite-temperature condensate. For this however, we need to generate zero-temperature ensembles at each $\beta$-value. Since these ensembles are much more expensive to generate, and since this was an exploratory study, we did not do so.

If the fermion action has a chiral symmetry, it is known (from continuum calculations as well as from staggered simulations) that the leading divergence is of the form $m_f/a^2$, where $m_f$ is the mass of the fermion. This is a divergence which vanishes in the chiral limit, $m_f \to 0$. On the other hand, in the case of fermions without chiral symmetry (Wilson, or domain-wall at finite $L_s$), a $1/a^3$ divergence also exists. In the domain-wall case however, this divergence vanishes exponentially with $L_s$. As we shall see, it can be neglected at $L_s = 32$. This implies that the leading divergence in the chiral condensate is of the form $m_f/a^2$.

This leads us to define the *subtracted chiral condensate*, which is free of the

above divergence viz.

$$\Delta_{ls} = \langle\overline{\psi}_l\psi_l\rangle - \frac{m_l}{m_s}\langle\overline{\psi}_s\psi_s\rangle.$$

This effectively removes the $m_l/a^2$ term from $\langle\overline{\psi}_l\psi_l\rangle$ while having no effect on the finite-temperature part or the contribution from vacuum chiral symmetry breaking. The result for such a subtracted light chiral condensate is shown in fig. 5.3[54].

### 5.2.2 Polyakov loop

Quarks and gluons do not appear as free particles in nature. The strongly-interacting particles that we observe are hadrons which are bound states of quarks or quarks and antiquarks. This feature of the strong force is called *confinement*.

Since QCD is believed to describe the strong force, QCD must exhibit confinement. However, confinement is a non-perturbative phenomenon and it does not show up in perturbation theory. As of today, no rigorous proof exists that QCD is confining.

However, lattice simulations have demonstrated that at least in the quenched case (*i.e.* when the quarks are infinitely heavy), QCD is confining. What one actually demonstrates is that the energy of a quark-antiquark pair grows linearly with the separation. It would thus cost an infinite amount of energy to dissociate the pair. Now the energy of a $q\bar{q}$-pair can be shown to be related to the logarithm of the Wilson loop viz.

$$V_{q\bar{q}}(R) = \sigma R = \lim_{T\to\infty}\left[-\frac{1}{T}\ln W(R,T)\right]. \tag{5.6}$$

The Wilson loop is a rectangle whose sides are of lengths $R$ and $T$. $R$ is the separation between the $q\bar{q}$ pair while $T$ is the time (which must be very large). The quantity $\sigma$ is called the string tension; its value is estimated to be around $(250\text{ GeV})^2$.

Similar to the chiral phase transition, one also has a phase transition in which matter goes from a confined, hadronic state to a deconfined state in which the basic degrees of freedom are quarks and gluons. The order parameter in this case is derived from an observable known as the Polyakov loop. The Polyakov loop is a Wilson loop that wraps around the temperature direction. It is related to the free energy $F_Q$ of an isolated, static quark: $L \sim \exp(-F_Q/T)$. In the confined phase, producing an isolated quark requires infinite energy and the Polyakov loop vanishes. However at sufficiently high temperatures, the system becomes deconfined and the Polyakov loop acquires a non-vanishing

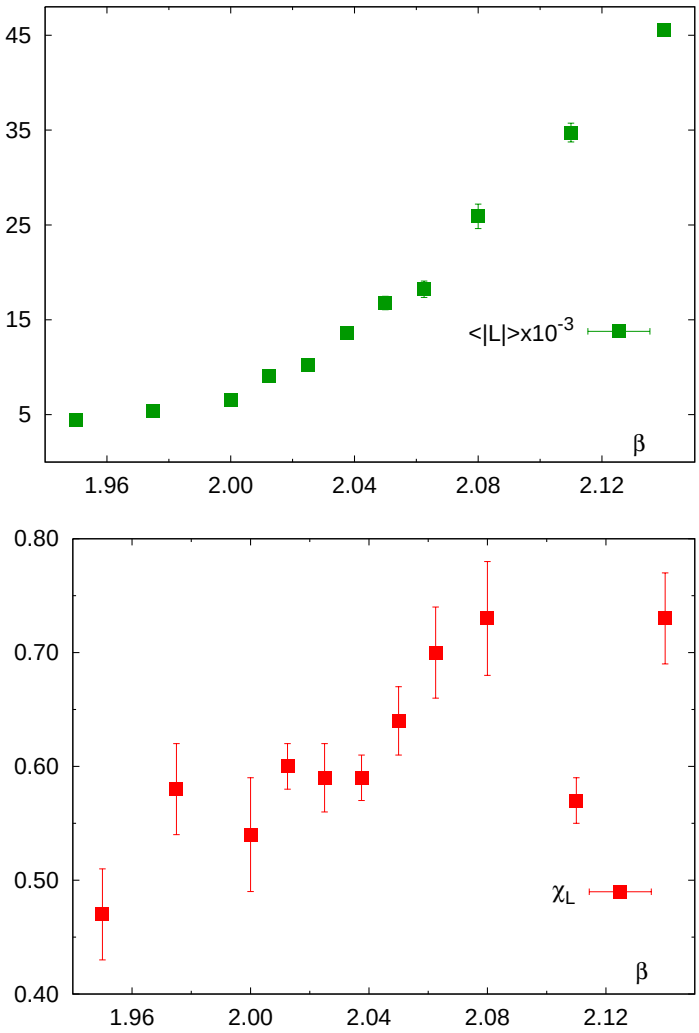


Figure 5.4: The Polyakov loop expectation value (top) and its susceptibility (bottom). Unlike the disconnected chiral susceptibility, no clear peak is seen in this susceptibility.

expectation value in a sufficiently large volume.

The Polyakov loop can be used to define an order parameter only in the absence of quarks. If one has dynamical quarks, new quark-antiquark pairs can be created out of the vacuum. No quark is truly isolated and a different order parameter is needed. We shall see in the next section that quark number susceptibilities can serve as order parameters for deconfinement when there are dynamical quarks in the system.

We have not yet defined the order parameter. It is the spacetime average

| $\beta$ | $\langle\overline{\psi}_l\psi_l\rangle/T^3$ | $\chi_l/T^2$ | $\langle\overline{\psi}_s\psi_s\rangle/T^3$ | $\chi_s/T^2$ | $\langle L\rangle$ $(10^{-3})$ | $\chi_L$ |
|---|---|---|---|---|---|---|
| 1.95 | 22.8(2) | 6.4(17) | 40.9(1) | 3.5(8) | 4.40(62) | 0.47(4) |
| 1.975 | 17.9(2) | 8.2(14) | 36.8(1) | 4.1(7) | 5.44(42) | 0.58(4) |
| 2.00 | 13.5(2) | 9.4(27) | 33.2(1) | 2.7(7) | 6.52(47) | 0.54(5) |
| 2.0125 | 11.6(2) | 16.4(20) | 31.6 | 5.7(7) | 9.02(53) | 0.60(2) |
| 2.025 | 9.9(2) | 17.8(26) | 30.2(1) | 4.7(6) | 10.18(61) | 0.59(3) |
| 2.0375 | 8.2(2) | 28.2(25) | 28.9(1) | 5.3(5) | 13.61(55) | 0.59(2) |
| 2.05 | 6.0(2) | 20.5(18) | 27.4(1) | 4.5(8) | 16.77(71) | 0.64(3) |
| 2.0625 | 5.1(2) | 20.7(27) | 26.6(1) | 4.2(5) | 18.22(86) | 0.70(4) |
| 2.08 | 3.5(2) | 11.4(20) | 25.2(1) | 3.0(6) | 25.91(129) | 0.73(5) |
| 2.11 | 2.37(7) | 3.7(30) | 23.51(5) | 0.9(2) | 34.74(99) | 0.57(2) |
| 2.14 | 2.03(2) | 0.15(2) | 22.59(7) | 0.6(3) | 45.6(20) | 0.73(4) |

Table 5.3: Results obtained for the light and strange quark chiral condensates and disconnected chiral susceptibilities as well as the Polyakov loop and its susceptibility.

of all possible Polyakov loops $L$ viz.

$$L = \frac{1}{3N_\sigma^3}\sum_{\mathbf{r}}\mathrm{Tr}\left(\prod_{\tau=0}^{N_\tau-1}U_4(\mathbf{r},t)\right) \tag{5.7}$$

$$\chi_L = N_\sigma^3\left\{\langle L^2\rangle - \langle L\rangle^2\right\}. \tag{5.8}$$

The quantity $\chi_L$ is the related susceptibility. As an order parameter, $L$ is expected to be zero in the confined phase and nonzero in the deconfined one. Depending on the nature of the transition, it should either change sharply or smoothly. In either case, the loop susceptibility should show a peak (which may or may not be infinite in the thermodynamic limit); the position of this peak can be used to assign a value for the deconfinement temperature $T_d$.

Figure 5.4 shows the Polyakov loop and its susceptibility. As in the case of the chiral condensate, it is difficult to precisely locate an inflection point in the $\beta$ dependence of the Polyakov loop although the region where the Polyakov loop begins to increase more rapidly is roughly coincident with the peak in chiral susceptibility. There is no well-resolved peak in the data for the Polyakov loop susceptibility, so we are unable to use this observable to locate the deconfinement transition coupling. We list our results for these finite temperature quantities in Table 5.3.

### 5.2.3 Quark Number Susceptibilities

Quark number susceptibilities have already been defined in eq. (4.41), which we reproduce here viz.

$$\begin{aligned}\frac{P(\mu_l,\mu_s)}{T^4} = \frac{P(0,0)}{T^4} \\ + \chi_2^l \left(\frac{\mu_l}{T}\right)^2 + \chi_2^s \left(\frac{\mu_s}{T}\right)^2 + \chi_{11}^{ls} \left(\frac{\mu_l}{T}\right)\left(\frac{\mu_s}{T}\right) \\ + \chi_4^l \left(\frac{\mu_l}{T}\right)^4 + \chi_4^s \left(\frac{\mu_s}{T}\right)^4 + \chi_{22}^{ls} \left(\frac{\mu_l}{T}\right)^2 \left(\frac{\mu_s}{T}\right)^2 + \ldots,\end{aligned}$$

It can be shown that the effect of taking two derivatives w.r.t. the chemical potential is equivalent to taking a single derivative w.r.t. the temperature [55]. Thus, we may expect$\chi_2^{l,s}$ to behave like the energy density *i.e.* smoothly transit from a low value to a high one as the temperature is increased. Similarly, $\chi_4^{l,s}$ can be expected to show a peak-like structure.

Apart from these basic quark number susceptibilities, one also has the derived susceptibilities $\chi_2^I$, $\chi_2^Q$, etc. These are susceptibilities related to the charges conserved by QCD, such as isospin ($I$), strangeness ($S$), electric charge ($Q$) and baryon number ($B$). These are simple linear combinations of the above susceptibilities viz.

$$\chi_2^S = \chi_2^s, \tag{5.9a}$$

$$\chi_2^I = \frac{1}{2}\left(\chi_2^u - \chi_{11}^{ud}\right), \tag{5.9b}$$

$$\chi_2^B = \frac{1}{9}\left(2\chi_2^u + \chi_2^s + 2\chi_{11}^{ud} + \chi_{11}^{us}\right), \tag{5.9c}$$

$$\chi_2^Q = \frac{1}{9}\left(5\chi_2^u + \chi_2^s - 4\chi_{11}^{ud} - 2\chi_{11}^{us}\right). \tag{5.9d}$$

As second derivatives of the partition function, these susceptibilities measure fluctuations in the quark number, charge, isospin, etc. This provides us with a qualitative understanding of their behavior: Charge fluctuations are small at low temperatures as charges are carried by rather heavy hadrons and they are large at high temperature because they are carried by almost massless quarks. Fluctuations of conserved charges thus reflect the deconfining aspects of the QCD transition.

The measurement of these susceptibilities on the lattice takes the form of determining operator traces. This is because the $\mu$-derivatives act on the

fermion determinant viz.

$$\frac{\partial}{\partial \mu_f} \ln \mathcal{Z} = \int \mathcal{D}U \frac{\mathrm{d}}{\mathrm{d}\mu_f} \det D(m_f, \mu_f) \mathrm{e}^{-S_G}, \tag{5.10a}$$

$$= \left\langle \mathrm{Tr}\left( D_f^{-1} \frac{\mathrm{d}D_f}{\mathrm{d}\mu_f} \right) \right\rangle,$$

$$\frac{\partial^2}{\partial \mu_f \partial \mu_g} \ln \mathcal{Z} = \left\langle \mathrm{Tr}\left( D_f^{-1} \frac{\mathrm{d}D_f}{\mathrm{d}\mu_f} \right) \cdot \mathrm{Tr}\left( D_g^{-1} \frac{\mathrm{d}D_g}{\mathrm{d}\mu_g} \right) \right\rangle \tag{5.10b}$$

$$- \left\langle \mathrm{Tr}\left( D_f^{-1} \frac{\mathrm{d}D_f}{\mathrm{d}\mu_f} \right) \right\rangle \left\langle \mathrm{Tr}\left( D_g^{-1} \frac{\mathrm{d}D_g}{\mathrm{d}\mu_g} \right) \right\rangle$$

$$\frac{\partial^2}{\partial \mu_f^2} \ln \mathcal{Z} = \left\langle \mathrm{Tr}\left( D_f^{-1} \frac{\mathrm{d}^2 D_f}{\mathrm{d}\mu_f^2} \right) \right\rangle - \left\langle \mathrm{Tr}\left( D_f^{-1} \frac{\mathrm{d}D_f}{\mathrm{d}\mu_f} \right)^2 \right\rangle \tag{5.10c}$$

$$+ \left\langle \mathrm{Tr}^2\left( D_f^{-1} \frac{\mathrm{d}D_f}{\mathrm{d}\mu_f} \right) \right\rangle - \left\langle \mathrm{Tr}\left( D_f^{-1} \frac{\mathrm{d}D_f}{\mathrm{d}\mu_f} \right) \right\rangle^2.$$

The angular brackets are a shorthand for $\frac{1}{\mathcal{Z}} \int \mathcal{D}U \det D_f \det D_g \ \mathrm{e}^{-S_G}$.

### 5.2.4 The Chemical Potential in the DWF formalism

We have already seen (Ch. 4) that introducing a chemical potential in the Domain-Wall formalism as $U_4(x) \to \mathrm{e}^{\mu} U_4(x)$, $U_4^\dagger(x) \to \mathrm{e}^{-\mu} U_4^\dagger(x)$ leads to the correct value for the pressure in the continuum in the sense that spurious divergences that go as $\mathcal{O}(\mu^2/a^2)$ are eliminated. It must be stressed that when introduced this way, $\mu$ couples to the links on all $s$-slices and not just the ones on the boundary where the light fermion lives. Now each $s$-slice may also be thought of as an additional fermion flavor. The other ($s \neq 0$) flavors are heavy with masses of $\mathcal{O}(1/a)$. The contribution of these flavors is removed by introducing fictitious, pseudofermionic fields called Pauli-Villars fields. These fermions are heavy, with $m_{\mathrm{PV}} = 1$. Thus the DW determinant is actually a ratio of two determinants, one for each flavor viz. ($f = u, d, s$)

$$\prod_{f=u,d,s} \frac{\det M_f(m = m_f, \mu_f)}{\det M_{\mathrm{PV}}(m = 1, \mu_f)},$$

To cancel out the effects of the heavy flavors, it is necessary to also couple the Pauli-Villars fields to the same chemical potential. In fact, this is the procedure that was shown to reproduce the correct continuum pressure in the DWF case [4]. In practice, the effect of dividing by $\det M_{\mathrm{PV}}$ is that each trace in eq.(5.10) receives an appropriate subtraction, $\mathrm{Tr}(D_f^{-1} D_f') \to \mathrm{Tr}(D_f^{-1} D_f' -$

| $\beta$ | meas | sep | #r.v. | $\chi_2^u$ | $\chi_2^s$ | $\chi_2^I$ | $\chi_2^Q$ |
|---|---|---|---|---|---|---|---|
| 1.95 | 73 | 10 | 200 | 0.16(22) | 0.02(10) | 0.092(16) | 0.120(20) |
| 1.975 | 61 | 10 | 200 | 0.06(20) | 0.06(14) | 0.140(16) | 0.170(20) |
| 2.0125 | 125 | 10 | 150 | 0.44(12) | 0.32(4) | 0.238(14) | 0.296(20) |
| 2.025 | 71 | 20 | 150 | 0.60(10) | 0.38(6) | 0.282(12) | 0.352(16) |
| 2.0375 | 96 | 20 | 150 | 0.60(12) | 0.32(4) | 0.320(12) | 0.410(16) |
| 2.05 | 81 | 25 | 150 | 0.76(10) | 0.50(8) | 0.382(18) | 0.486(22) |
| 2.0625 | 111 | 10 | 150 | 0.64(12) | 0.48(8) | 0.400(18) | 0.504(20) |
| 2.11 | 35 | 10 | 100 | 1.02(12) | 0.88(10) | 0.466(22) | 0.606(28) |
| 2.14 | 40 | 10 | 100 | 1.02(6) | 0.86(4) | 0.512(8) | 0.666(10) |

Table 5.4: Details of the calculation of quark number susceptibilities. The column labeled "meas" gives the number of measurements that were performed, that labeled "sep" gives the number of time units between those measurements while the "#r.v." column gives the number of random vectors used in each measurement.

$D_{f\mathrm{PV}}^{-1} D'_{f\mathrm{PV}}$), etc.

The computation of the inverse of a matrix is an extremely expensive process. However, we really only need its trace. This is computed stochastically as follows: If $\eta^{(m)}$, $n = 1, 2, \ldots$ are independent random vectors satisfying

$$\overline{\eta_i^\dagger \eta_j} = \lim_{n\to\infty} \frac{1}{n} \sum_{m=1}^{n} \eta_i^{(m)\dagger} \eta_j^{(m)} = \delta_{ij}, \tag{5.11}$$

then

$$\mathrm{Tr}\mathcal{O} = \overline{\eta_i^\dagger \mathcal{O}_{ij} \eta_j} = \lim_{n\to\infty} \frac{1}{n} \sum_{m=1}^{n} \eta_i^{(m)\dagger} \mathcal{O}_{ij} \eta_j^{(m)}. \tag{5.12}$$

Here, the overline denotes an average over the random vectors. This is faster than computing the full inverse of the matrix. In our simulations, we used 100-200 random vectors to determine the traces. Our measurements are summarized in Table 5.4.

In fig. (5.5), we show our results for the diagonal light and strange quark number susceptibilities $\chi_2^u$ and $\chi_2^s$, respectively. We see that these susceptibilities do transit from a low value to a high one as $\beta$ increases. However, it is difficult to assign any definite value of $\beta$ around which the transition takes place within the current statistical accuracy of our calculation. To a large extent this is because of the traces on the second line of eq.(5.10). These terms are the same as the ones in the off-diagonal susceptibility provided we set $f = g$. In fact, with our current limited statistics these susceptibilities

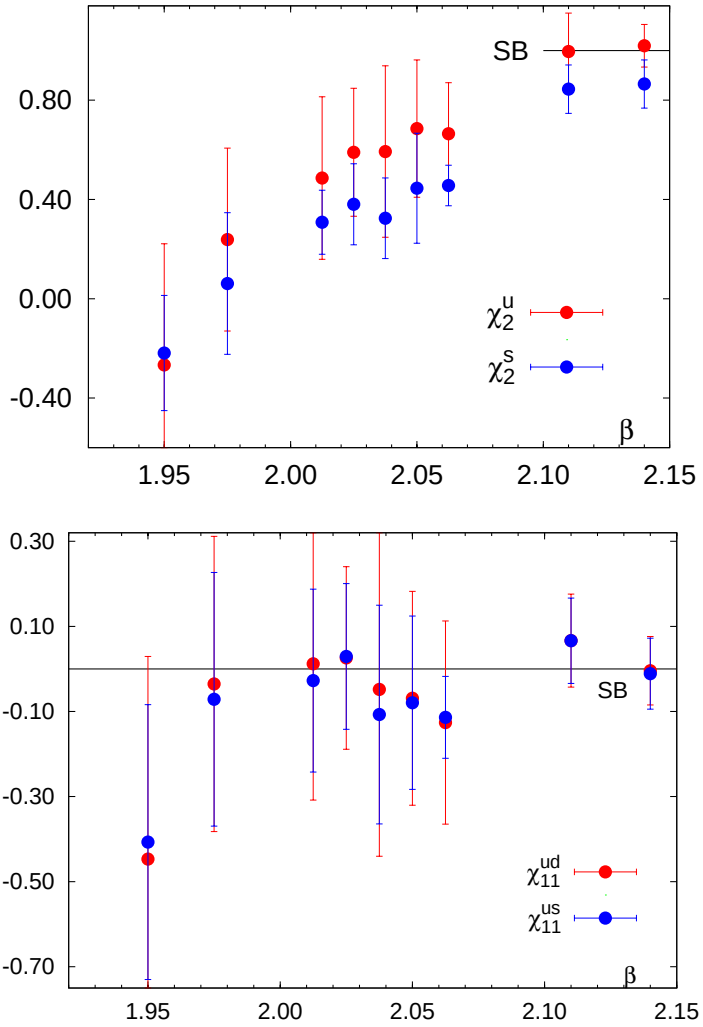


Figure 5.5: The diagonal (top) and off-diagonal susceptibilities (bottom).

vanish within errors and therefore only contribute noise.

However when we consider some of the conserved charge susceptibilities, specifically $\chi_2^I$ and $\chi_2^Q$, the diagonal and off-diagonal susceptibilities combine in such a way as to completely or partially cancel the noisy terms. Indeed, as fig.(5.6) shows, the signals are cleaner in this case and even show a smooth transition from a low to a high value.

We can even use this behavior to determine a transition temperature. We

tried to fit the data to two *Ansätze* viz.

$$f(\beta) = A\tanh(B(\beta - \beta_d)) + C, \tag{5.13a}$$
$$g(\beta) = a\beta^3 + b\beta^2 + c\beta + d, \tag{5.13b}$$
$$\beta_d = -b/3a. \tag{5.13c}$$

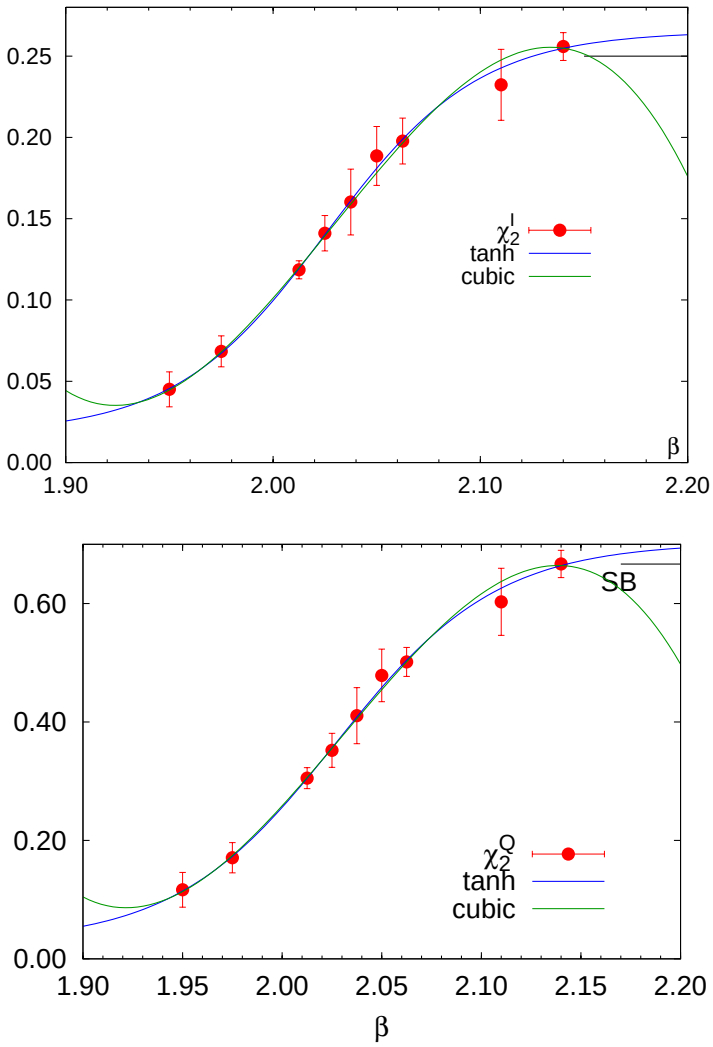


Figure 5.6: The signals are cleaner for $\chi_2^I$(top) and $\chi_2^Q$(bottom), allowing us to specify the transition coupling $\beta_c$ as the inflection point of a fit.

In the absence of further information, the cubic equation is the most natural fitting choice. On the other hand, we know that the curve must reach a plateau around the Stefan-Boltzmann limit. This makes the choice of the hyperbolic

tangent function a particularly tempting one. As can be seen from fig.(5.6), the best fit depends strongly on the choice of function. However, the inflection point determined in both cases is the same, although the errors are much larger for the cubic fit. This inflection point can serve as an estimate of the transition, although the slope of these observables also receives contributions from the regular part of the free energy.

| | $\chi_2^I$ | | | $\chi_2^Q$ | | |
|---|---|---|---|---|---|---|
| | best fit | error | % error | best fit | error | % error |
| $A$ | 0.123683 | 0.006582 | 5.321 | 0.338025 | 0.01983 | 5.867 |
| $B$ | 13.6692 | 1.338 | 9.79 | 12.3695 | 1.177 | 9.512 |
| $x_0$ | 2.02584 | 0.002439 | 0.1204 | 2.02711 | 0.002976 | 0.1468 |
| $C$ | 0.141598 | 0.00357 | 2.521 | 0.365072 | 0.01036 | 2.836 |
| | $\chi^2/\text{ndf} = 0.094$, $\beta_d = 2.026$. | | | $\chi^2/\text{ndf} = 0.089$, $\beta_d = 2.027$. | | |

Table 5.5: Best fit values to the tanh function for $\chi_2^I$ (left) and $\chi_2^Q$ (right).

| | $\chi_2^I$ | | | $\chi_2^Q$ | | |
|---|---|---|---|---|---|---|
| | best fit | error | % error | best fit | error | % error |
| $a$ | -47.5507 | 11.57 | 24.33 | -113.438 | 24.57 | 21.66 |
| $b$ | 289.412 | 70.83 | 24.48 | 690.827 | 150.6 | 21.81 |
| $c$ | -585.583 | 144.5 | 24.67 | -1398.37 | 307.7 | 22.01 |
| $d$ | 394.026 | 98.19 | 24.92 | 941.18 | 209.4 | 22.25 |
| | $\chi^2/\text{ndf} = 0.186$, $\beta_d = 2.089$. | | | $\chi^2/\text{ndf} = 0.089$, $\beta_d = 2.027$. | | |

Table 5.6: Best fit values to the cubic function for $\chi_2^I$ (left) and $\chi_2^Q$ (right).

To estimate systematic errors in the fits we performed fits for the entire data set as well as in limited ranges by leaving out one or two data points at the lower as well as upper edge of the $\beta$-range covered by our data sample. From this we find inflection points in the range $2.024 \leqslant \beta_0 \leqslant 2.037$ for $\chi_2^I$ and $2.024 \leqslant \beta_0 \leqslant 2.034$ for $\chi_2^Q$. Summarizing this analysis we therefore conclude that the inflection points in the electric charge and isospin susceptibilities coincide within statistical errors and are given by $\beta_0 = 2.030(7)$. This is in good agreement with the determination of a pseudo-critical coupling obtained from the location of peak in the chiral susceptibility, $\beta = 2.0375$, found in Section 5.2.1.

## 5.3 The Residual Mass

The residual mass is a measure of the degree to which exact chiral symmetry is broken by the finite extent of the fifth dimension. On the lattice, starting from a conserved, five-dimensional vector current

$$\begin{aligned}\mathcal{J}^a_\mu(x,s) = \frac{1}{2}\big[&\overline{\psi}(x+\hat{\mu},s)(1+\gamma_\mu)U^\dagger_\mu(x)t^a\psi(x,s) \\ &\overline{\psi}(x,s)(1-\gamma_\mu)U_\mu(x)t^a\psi(x+\hat{\mu},s)\big]\,.\end{aligned} \tag{5.14}$$

one can construct a four-dimensional axial current that is partially conserved viz. [58]

$$\mathcal{A}^{5a}_\mu(x) = \sum_{s=0}^{L_s-1}\epsilon\left(s-\frac{L_s-1}{2}\right)\mathcal{J}^a_\mu(x,s), \tag{5.15a}$$

$$\Delta_\mu\mathcal{A}^a_{5\mu}(x) = 2mJ^a_5(x) + 2J^a_{5q}(x). \tag{5.15b}$$

The function $\epsilon(x)$ is just the sign function, $\epsilon(x) = x/|x|$, $x \neq 0$ and $\Delta_\mu$ is just the forward difference. The current $\mathcal{A}^{5a}_\mu(x)$ is the four-dimensional axial current. In eq. (5.15b), the first term is just the pseudoscalar density viz.

$$\begin{aligned}J^a_5(x) = -\frac{1}{2}\Big[&\overline{\psi}(x,L_s-1)(1-\gamma_5)t^a\psi(x,0) \\ &-\overline{\psi}(x,0)(1+\gamma_5)t^a\psi(x,L_s-1)\Big].\end{aligned} \tag{5.16}$$

The second term is new, and only seen at finite $L_s$ viz.

$$\begin{aligned}J^a_{5q}(x) = -\frac{1}{2}\Big[&\overline{\psi}(x,L_s/2-1)(1-\gamma_5)t^a\psi(x,L_s/2) \\ &-\overline{\psi}(x,L_s/2)(1+\gamma_5)t^a\psi(x,L_s/2-1)\Big].\end{aligned} \tag{5.17}$$

This term is often called the "midpoint term."

The residual mass is defined as the ratio of the correlators of the midpoint term and the pseudoscalar density viz.

$$m_{\text{res}} = \lim_{t\to\infty} R(t) = \lim_{t\to\infty}\frac{\sum_{\mathbf{x},\mathbf{y}}\langle J^a_5(\mathbf{x},t)J^a_5(\mathbf{y},0)\rangle}{\sum_{\mathbf{x},\mathbf{y}}\langle J^a_{5q}(\mathbf{x},t)J^a_{5q}(\mathbf{y},0)\rangle} \tag{5.18}$$

The ratio, plotted as a function of $t$ should plateau above a value $t \geqslant t_{\text{min}}$. The height of the plateau is $m_{\text{res}}$.

What made domain-wall fermions attractive was the fact that this breaking could be easily reduced by increasing $L_s$. Furthermore, $m_{\text{res}}$ was expected to vanish exponentially fast as $L_s$ was increased. Thus for e.g. a one-loop calculation[56] showed the following dependence[1]

$$am_{\text{res}} \sim \frac{A}{L_s} \mathrm{e}^{-\lambda L_s}, \qquad \text{(perturbative)}$$

where $A$ was a constant.

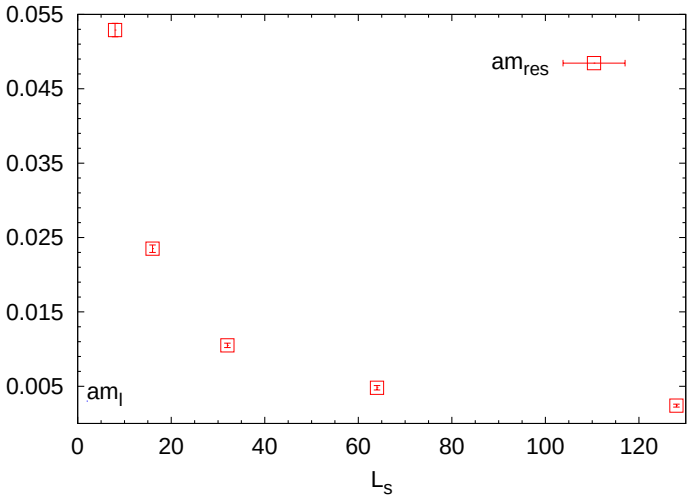


Figure 5.7: $m_{\text{res}}$ as a function of the valence $L_s$ at $\beta = 2.00$.

A different picture emerges at stronger coupling: A study by the Columbia group found that a slower $1/L_s$ falloff also existed in addition to the exponential falloff (fig. 5.7) viz. [58]

$$\begin{aligned} am_{\text{res}} &= am_{\text{res}}^{(\text{pert})} + am_{\text{res}}^{(\text{npert})} \\ &= \frac{A}{L_s} \mathrm{e}^{-\lambda L_s} + \frac{B}{L_s}. \qquad \text{(full)} \end{aligned} \tag{5.19}$$

The origin of this non-perturbative contribution was traced to the appearance or disappearance of zero-modes of the domain-wall operator [58]. By the Banks-Casher relation, these modes are also responsible for spontaneous chiral symmetry breaking. Thus, one ought to see a $1/L_s$-dependence of the chiral-condensate as well. However, note that the chiral condensate also contains a divergent contribution $\sim 1/a^3$. This comes from the eigenvalues at the other

[1] We reinstate the lattice spacing $a$ in this section.

end of the spectrum, $\lambda \sim \mathcal{O}(1/a)$. These eigenvalues are also far more numerous *i.e.* their density equals the phase space density. It is the contribution of these modes that is seen in perturbation theory. Thus, the divergence takes the form

$$\begin{aligned} \langle\overline{\psi}\psi\rangle_{\text{div}} &= C\frac{\mathrm{e}^{-\lambda L_s}/L_s}{a^3} + D\frac{m_f}{a^2}, \\ &\sim D\left\{\frac{m_{\text{res}}^{(\text{pert})} + m_f}{a^2}\right\}. \end{aligned} \tag{5.20}$$

The second term vanishes in the chiral limit. The first term arises because, unlike staggered fermions, domain-wall fermions do not have an exact chiral symmetry at finite $L_s$ (Such a term is seen in Wilson fermion simulations as well). Nonetheless, it vanishes exponentially with $L_s$.

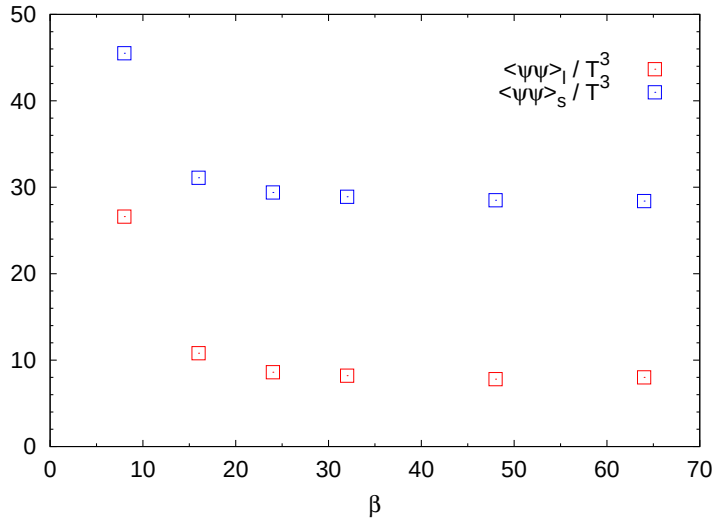


Figure 5.8: The chiral condensate does not change beyond $L_s \simeq 20$, though the residual mass is still changing in this region.

Since the $m_f/a^2$ term dominates over the finite part and is independent of $L_s$, we should expect the unsubtracted condensate to show no $L_s$-dependence. Indeed the condensate does not change beyond $L_s \simeq 20$, as fig. 5.8 shows.

On the other hand, the disconnected chiral susceptibility $\chi_{\text{disc}}$ is a finite quantity that is furthermore sensitive to the mass of the quark. As fig. 5.9 shows, if $L_s$ is increased from 32 to 64, the light quark susceptibility increases as expected. However, if $L_s$ and $m_f$ are varied simultaneously so that $m_f + m_{\text{res}}$ remains constant ($L_s = 96$ curve), the curve does not change at all. This

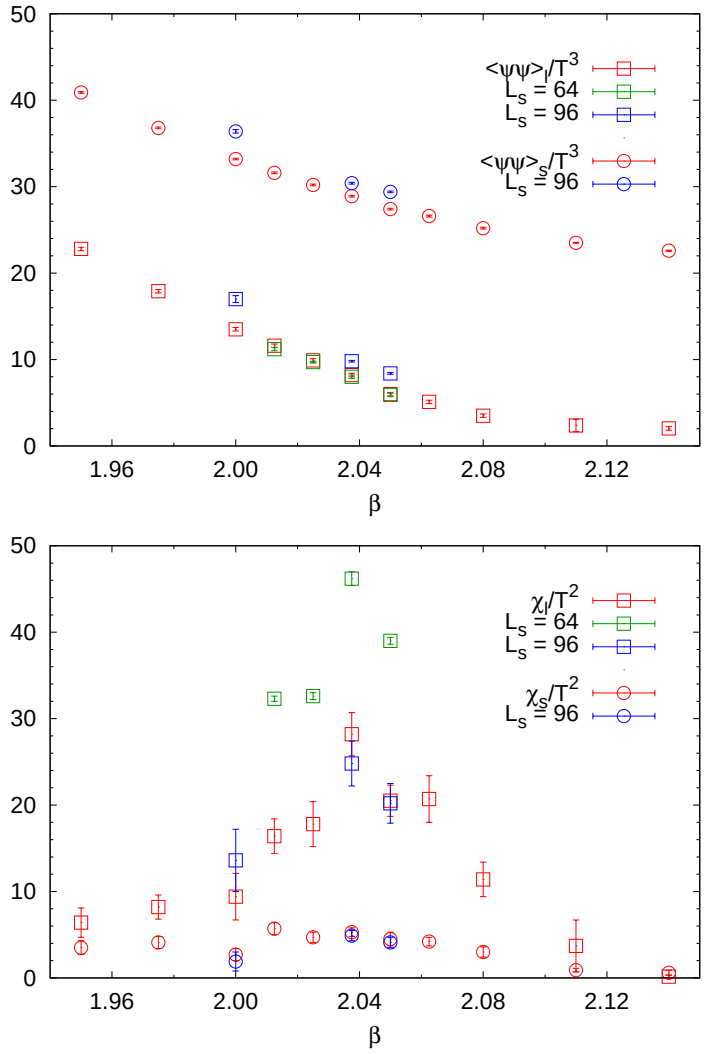


Figure 5.9: Chiral condensate (top) and the disconnected chiral susceptibility (bottom) as a function of $\beta$ and for $L_s = 32,\ 64,\ 96$. If $L_s$ is increased while keeping $m_f$ constant, $\chi_{\text{disc}}$ increases. However, for $L_s = 96$ and $m_f$ varied so as to keep $m_f + m_{\text{res}}$ constant, no shift in the peak is observed.

again proves that the relevant quark mass in the DWF formalism is not $m_f$ but $m_f + m_{\text{res}}$.

Lastly, we see that changing $L_s$ has no effect on the strange quark susceptibility. For that matter, there is no peak in $\chi^s_{\text{disc}}$ either. This is because the $am_s$ is much greater than either $am_l$ or $am_{\text{res}}$.

### 5.3.1 The Challenge of Reducing the Residual Mass

The appearance or disappearance of zero-modes of the domain-wall operator could be related, via the index theorem, to the change in the gauge field topology. On the lattice, topology change proceeds via the occurrence of localized "defects." By using an improved action, one could generate smoother gauge fields which in turn could lead to a reduction in $m_{\text{res}}$.

However, as one moves toward stronger coupling, the lattice gets coarser and it becomes harder to suppress defects. One may expect that, even with improved gauge fields, one sees a rise in $m_{\text{res}}$ with decreasing $\beta$. This is indeed what our study showed, as fig. 5.10 shows.

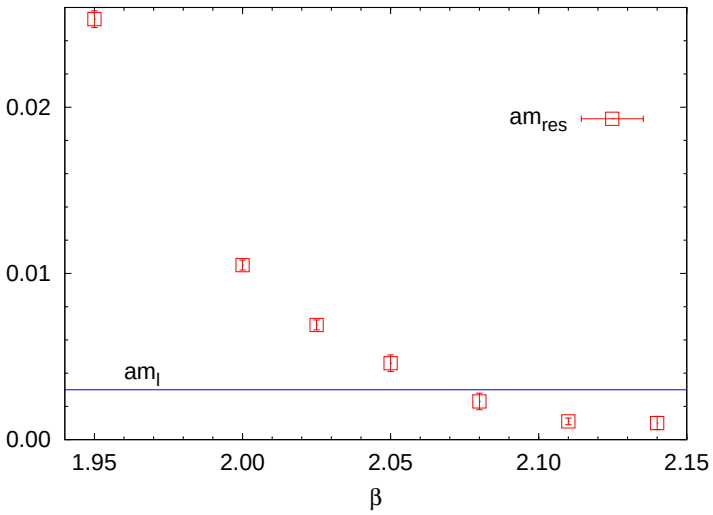


Figure 5.10: $m_{\text{res}}$ grows sharply as we move toward stronger coupling.

A gauge field independent way of suppressing zero-modes was proposed in [68–71]. A zero eigenvalue of the Wilson kernel gave rise to a zero eigenvalue of the DWF operator, although the eigenvectors for the two operators were different. Therefore, one way to suppress zero-modes would be by "weighting" the DWF determinant with the Wilson determinant. Since the latter would go to zero in the presence of a zero-mode, such configurations would have zero weight and would not be generated. This operator has been tested and is currently being used to generate ensembles.

## 5.4 Locating $T_c$

We will now attempt to combine our finite and zero temperature results to determine the pseudo-critical temperature, $T_c$. As discussed in sec. 5.2.1 and shown in fig. 5.2, the chiral susceptibility shows a clear peak whose location gives a value for $\beta_c$. The result for $\beta_c$ is consistent with the region of rapid increase in the Polyakov loop and quark number susceptibilities seen in Figs. 5.4 and 5.6. Even though $\beta_c$ is fairly well resolved, there are still significant uncertainties in extracting a physical value of $T_c$ from our calculation. The most important issues are:

- The distortion in the dependence of the chiral susceptibility on $\beta$ induced by the variation of $m_{\text{res}}$ with $\beta$.
- The uncertainty in determining the lattice scale at the peak location near $\beta_c = 2.0375$ from our calculation of $r_0/a$ at $\beta = 2.025$, performed with light quarks considerably more massive than that those found in nature.
- The absence of chiral and continuum extrapolations.

We address each of these sources of uncertainty in turn.

### 5.4.1 Correcting for $m_{\text{res}}(\beta)$

In Section 5.2.1, we observed that the chiral susceptibility has a peak near $\beta = 2.0375$, which we can identify as the center of the transition region. However, the total light quark mass $m_q = m_l + m_{\text{res}}$ is different for each value of $\beta$ because of the changing residual mass $m_{\text{res}}(\beta)$. This changing quark mass distorts the shape of the chiral susceptibility curve, shifting the location of its peak from what would be seen were we to have held the quark mass $m_q = m_l + m_{\text{res}}$ fixed as $\beta$ was varied.

In order to correct for this effect, we must account for the quark mass dependence of the chiral susceptibility. Our valence measurements at $L_s = 64$ and $L_s = 96$ indicate that the chiral susceptibility is inversely related to the quark mass and depends only on the combination $m_q = m_l + m_{\text{res}}$. Figure 5.11 shows the resulting chiral susceptibility, when one corrects for the known $\beta$ dependence of $m_{\text{res}}(\beta)$ by assuming a power-law dependence of $\chi_l \propto 1/m_q^\alpha$ on the quark mass for various choices of the power $\alpha$ ranging between $\alpha = 0$ and $\alpha = 3/2$. While for $T \leq T_c$ and in the limit of small quark mass the chiral susceptibility is expected to behave as $\propto 1/\sqrt{m_q}$ [12, 59–62] corresponding to $\alpha = 1/2$, our data from the $L_s = 64$ valence measurements

| | Gaussian | | Lorentz | |
|---|---|---|---|---|
| $\alpha$ | $\beta_c$ | $\chi^2$/dof | $\beta_c$ | $\chi^2$/dof |
| 0 | 2.041(2) | 1.7 | 2.041(2) | 2.3 |
| 1/2 | 2.036(3) | 1.7 | 2.035(3) | 1.7 |
| 1 | 2.030(3) | 1.7 | 2.030(3) | 1.8 |
| 3/2 | 2.024(5) | 1.8 | 2.026(3) | 2.0 |

Table 5.7: The corrected peak location ($\beta_c$) in the light chiral susceptibility determined from fits to Lorentzian and Gaussian peak shapes resulting from different assumptions for the light quark mass dependence of $\chi_l$: $\chi_l/T^2 \sim 1/(m_l + m_{res})^\alpha$). All fits include the 7 data points nearest the peak location, *i.e.* $\beta \in [2.00, 2.08]$.

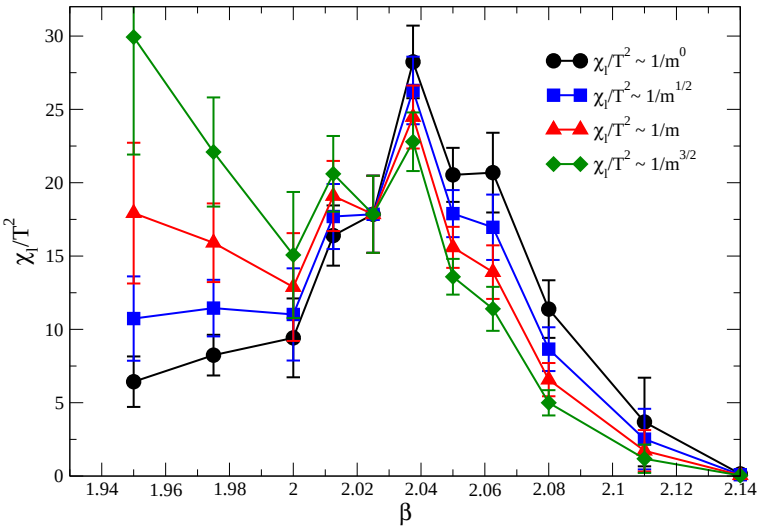


Figure 5.11: The chiral susceptibility corrected for varying $m_{\rm res}$ by assuming $\chi_l \propto 1/m_q^\alpha$ for different choices of $\alpha$.

suggest $\alpha \sim 1.2 - 1.8$, albeit with rather large uncertainty. While $\alpha > 0.5$ is inconsistent with the expected chiral behavior, we conservatively include such larger exponents as a possible behavior over our limited range of non-zero quark mass. Adjusting the chiral susceptibility curve in this manner enhances the chiral susceptibility at stronger coupling, as $m_{\rm res}(\beta)$ is larger on the coarser lattices. This causes a systematic shift in the peak location to stronger coupling when this correction is made.

While a cursory examination of Fig. 5.11 suggests that this correction does not change the peak structure, more careful study reveals that for the extreme $\alpha = 1.5$ case the peak may have disappeared if the two lowest $\beta$ values with large errors are taken seriously. We view this possibility as unlikely but not

absolutely ruled out.

Table 5.7 gives the results of fitting the peak region to Lorentzian and Gaussian peak shapes for various $\alpha$. If we make no adjustment to the raw data ($\alpha = 0$), we obtain $\beta_c = 2.041(2)$. However, with $\alpha = 3/2$, we have $\beta_c = 2.024(5)$ with the Gaussian fit. While $\alpha = 3/2$ seems to be favored by our valence measurements, we would like to emphasize that the quark mass dependence of the chiral susceptibility has large uncertainties. In particular, since we performed valence measurements at only three values of $\beta$, it is unclear if this $\alpha \approx 3/2$ behavior holds over a broader range in $\beta$. Also, we do not know whether the same mass dependence will persist if both the valence and dynamical quark masses are varied.

It should be recognized that if $\chi_l \propto 1/m_q^\alpha$ behavior for $T \leqslant T_c$ persists in the limit of vanishing $m_q$ the peak structure suggested by Fig. 5.11 may take on the appearance of a shoulder as the $\chi_l$ grows for $T < T_c$. Such a singular behavior at small quark mass, for example the $\alpha = 1/2$ case suggested by chiral symmetry, would make $\chi_l$ a poor observable to locate the finite temperature transition [63]. Although our data shows an easily identified peak, unclouded by a large $1/\sqrt{m_q}$ term for $T \leq T_c$, it is possible that such behavior may substantially distort the chiral susceptibility as the light quark mass is decreased from that studied here to its physical value.

With these caveats in mind, we estimate the pseudo-critical coupling to be $\beta_c = 2.03(1)$. The central value corresponds to the peak location if we assume a quark mass dependence of $\chi_l \sim 1/(m_q + m_{\rm res})$. The quoted error reflects the uncertainty in the mass dependence of $\chi_l$, and is chosen to encompass the range of values for $\beta_c$ shown in Table 5.7.

### 5.4.2 Extracting the lattice scale at $\beta_c$

This value of $\beta_c$ differs from that of our zero-temperature ensemble ($\beta = 2.025$) where we have measured the Sommer parameter, $r_0/a$. Thus, in order to determine the lattice scale at $\beta_c$, we need to know the dependence of $r_0/a$ on $\beta$. Fortunately, in addition to our measurements at $\beta = 2.025$, $r_0/a$ has been extensively measured at $\beta = 2.13$ [49].

At $\beta = 2.13$, the value of $r_0/a$ at the quark mass corresponding most closely to the current calculation is $r_0/a = 3.997(22)$. Extrapolation to the chiral limit gives $r_0/a = 4.113(31)$ for $\beta = 2.13$, an approximately 3% increase. A study of finite volume effects in Ref. [49] suggests that, in addition, the value computed on a $16^3 \times 32$ lattice is too low by approximately $1 - 2\%$.

To obtain $r_0/a$ at $\beta_c$, we use an exponential interpolation in $\beta$, giving $r_0/a = 3.12(13)$, which includes the statistical errors for $r_0/a$ and the uncertainty in $\beta_c = 2.03(1)$. To account for chiral extrapolation and finite volume

effects, we add 4% to this central value and also add a 4% error in quadrature, resulting in $r_0/a = 3.25(18)$. This corresponds to $T_c r_0 = 0.406(23)$.

### 5.4.3 Chiral and Continuum Extrapolations

In the end, we wish to obtain a value for the pseudo-critical temperature $T_c$ corresponding to physical quark masses and in the continuum ($a \to 0$) limit. However, our current calculation is performed with a single value for the light quark masses, ($m_l/m_s \approx 0.25$), and a single value for the temporal extent ($N_t = 8$). Thus, we are not at present able to perform a direct chiral or continuum extrapolation.

We can make an estimate of the shift in $T_c$ that might be expected when the light quark mass is reduced to its physical value by examining the dependence of $T_c$ on the light quark mass found in the $N_t = 6$, staggered fermion calculations in Ref. [46]. The quark mass dependence of $T_c$ found in Table IV of that paper, suggests a 3% decrease in $T_c$ when one goes to the limit of physical quark masses.

The effects of finite lattice spacing on our result can be estimated from the scaling errors that have been found in recent zero temperature DWF calculations [64, 65]. Here hadronic masses and decay constants were studied on a physical volume of side roughly 3 fm using two different lattice spacings: $1/a = 1.73$ and 2.32 GeV. The approximate 1-2% differences seen between physically equivalent ratios in this work suggests fractional lattice spacing errors given by $(a\Lambda)^2$ where $\Lambda \approx 260-370$ MeV. If this description applies as well for the $a^{-1} \approx 1.3$ GeV lattice spacing being used here, we expect deviations from the continuum limit of 4-7%.

Thus,to account for the systematic uncertainty in failing to perform chiral and continuum extrapolations, we add a 10% systematic uncertainty to our final value for the pseudo-critical temperature, giving $T_c r_0 = 0.406(23)(41)$. Using $r_0/a = 0.469(7)$ fm, this corresponds to $T_c = 171(10)(17)$ MeV. Here the first error represents the combined statistical and systematic error in determining $T_c r_0$ for our $a^{-1} \approx 1.3$ GeV lattice spacing and light quark mass of $\approx 0.22$ times the strange mass. The second error is an estimate of the systematic error associated with this finite lattice spacing and unphysically large light quark mass.

## 5.5 Status of DWF Thermodynamics

We have carried out a first study of the QCD phase transition using chiral, domain wall quarks on a finite temperature lattice with temporal extent $N_t =$

8. This work represents a advance over earlier domain wall calculations [52, 66] with $N_\tau = 4$ and 6, having significantly smaller residual chiral symmetry breaking and including important tests of the physical interpretation of the resulting residual mass. Most significant is the comparison of the residual mass computed at fixed $\beta = 2.025$ for both zero and finite temperature yielding $m_{\rm res} = 0.0069(5)$ and $0.006647(84)$ respectively. The equality of these two results suggests that $m_{\rm res}$ can indeed be interpreted as a short-distance effect which acts as a small additive mass shift over the range of temperatures which we study.

We found that the chiral susceptibility shows a clear peak around $\beta_c = 2.03(1)$ and suggests a critical region between 155 and 185 MeV. The peak location can be used to estimate a pseudo-critical temperature $T_c r_0 = 0.406(23)(41)$ or $T_c = 171(10)(17)$ MeV. The first error represents the statistical and systematic uncertainties in determining $\beta_c$ and the corresponding physical scale at our larger than physical quark mass ($m_\pi = 308$ MeV) and non-zero lattice spacing, $a^{-1} \approx 1.3$ GeV. The second error is our estimate of the shift that might be expected in $T_c$ as the quark mass is lowered to its physical value and the continuum limit is taken.

The transition region identified from the peak in the chiral susceptibility $\chi_l$ shown in fig. 5.1 agrees nicely with the region of rapid rise of the Polyakov line $L$ shown in Fig. 5.4 and the charge and isospin susceptibilities, $c_2^Q$ and $c_2^I$, shown in Fig. 5.6. This coincidence of the transition region indicated by observables related to vacuum chiral symmetry breaking ($\chi_l$) and those sensitive to the effects of deconfinement ($L$, $c_2^Q$ and $c_2^I$) suggests that these two phenomena are the result of a single crossover transition.

It is of considerable interest to compare this result with those obtained in two recent large-scale studies using staggered fermions [46, 67]. Unfortunately, because of our large uncertainties, our result is consistent with both of these conflicting determinations of $T_c$.

To improve on these measurements, the following two chief sources of systematic error must be brought under control: First and most importantly the size of residual chiral symmetry breaking must be substantially reduced. This could be achieved directly for the calculation described here by simply increasing the size of the fifth dimension. Of course, such an increase in $L_s$ incurs significant computational cost. Never-the-less, a study similar to that reported here is presently being carried out by the HotQCD collaboration using $L_s = 96$. This will provide an improved result for the chiral susceptibility as a function of temperature, giving a new version of Fig. 5.2 in which the total quark mass, $m_f + m_{\rm res}$, remains constant across the transition region.

More promising for large-volume domain wall fermion calculations is the

use of a modified gauge action, carefully constructed to partially suppress the topological tunneling which induces the dominant $1/L_s$ term in Eq. 5.19 [68–71]. This is accomplished by adding the ratio of 4-dimension Wilson determinants for irrelevant, negative mass fermion degrees of freedom to the action. Preliminary results [71] indicate that without increasing $L_s$ beyond 32, this improved gauge action can reduce the residual mass in the $N_t = 8$ critical region by perhaps a factor of 5 below its current value while maintaining an adequate rate of topological tunneling. This improvement, when combined with the next generation of computers should permit a thorough study of the QCD phase transition at a variety of quark masses, approaching the physical value and on larger physical spatial volumes.

The second important source of errors comes from cutoff effects. As we have already seen, these can be unacceptably large: $\sim 20\%$ at $N_\tau = 8$. If we wish to obtain more than just a qualitative understanding of the phase diagram, it is necessary to minimize these errors by improving this action. In the next chapter, we shall describe how we can improve the domain-wall operator and present some preliminary results of simulations with the operator.

# Chapter 6

# The Improved Domain-Wall Operator

We have already seen that improvement is necessary to minimize lattice artifacts on relatively small lattices. In the usual formulation of domain-wall (DW) fermions, the fermion dispersion relation is identical to that for naive fermions. This implies that discretization errors are sizeable even at $N_\tau = 8$. Since DW fermions are quite expensive to simulate, it is a good idea to try and improve the action before going to larger lattices.

In fact, the derivation of the dispersion relation also suggests a way of improving it. Recall that the domain-wall kernel (4-d part) was just the usual unimproved Wilson action. This suggests that if we improve the kernel, we would obtain an improved dispersion relation as well.

## 6.1 Improvement – A Recap

Let us recall that improving an action consists of two parts: First, additional terms are added to an action. These terms vanish in the continuum limit. Next, a criterion is adopted that insures elimination of cutoff errors upto some order and the coupling constants multiplying these terms are tuned so that the criterion is satisfied. What criterion is chosen depends on what sort of simulations one wants to perform with the action.

For example, if one wishes to do spectroscopy, a reasonable criterion is that the lattice propagator be equal to the continuum one upto $\mathcal{O}(a^n)$ for some $n$ and add an appropriate number of terms to the fermion action[1]. In the interacting case, one may even ask that this holds upto $\mathcal{O}(\alpha_s^m)$ for some $m$.

[1]The number of terms to be added grows with $n$. Typically, $n = 4$ is achievable.

Then one adds additional terms to the gauge action too and tunes the coefficients of both gauge and fermion actions. Such tuning is called perturbative improvement as one often calculates these coefficients in perturbation theory.

On the other hand, one may also demand that the low-energy spectrum of the lattice theory ought to resemble the continuum spectrum upto $\mathcal{O}(a^n)$ differences. This is especially important in rooted staggered simulations, where the degeneracy between different tastes is violated by $\mathcal{O}(\alpha_s a^2)$ errors. In this case, one typically "smears" the gauge links to reduce these errors[5]. This is an example of non-perturbative improvement.

In thermodynamics on the other hand, one wishes to calculate quantities such as the pressure, the energy density or various quark number susceptibilities, for example. As we have already seen (sec. 4.3.1), in this case a simple criterion has proved to be very useful. The contribution to these quantities comes from the poles $E(\mathbf{p})$ of the lattice propagator. Thus it is sufficient to ensure that $E(\mathbf{p})$ is $\mathcal{O}(a^n)$-improved. This can be achieved if the propagator is simply rotation-invariant upto that order. This is an important result; it tells us for example why the pressure in the Wilson formulation is $\mathcal{O}(a)$-improved even though the Wilson term is of $\mathcal{O}(a)$. In what follows, we too shall exploit this property: For technical reasons, we shall leave the propagator unimproved but ensure that it is rotation-invariant at $\mathcal{O}(a^2)$.

## 6.2 The (Modified) Hamber-Wu Action

Our starting point is an action first introduced by H. Hamber and C. M. Wu [6] about three decades ago. By adding linear two-link terms to the first and second derivatives and adjusting their coefficients, the authors were able to remove the leading and subleading ($\mathcal{O}(a^2)$ and $\mathcal{O}(a^3)$) corrections to the continuum Dirac operator, $aD_{HW}(m) = a\left(\gamma_\mu \partial_\mu + m\right) + \mathcal{O}(a^4)$[2].

However, the addition of a two-link term is problematic in numerical applications, for e.g. from the point of view of *preconditioning* [73, 74]. Recall that the usual Wilson operator takes the form $1 - \kappa D_{x,x'}$, where $D_{x,x'}$ is non-zero only between sites of different parities (more specifically, between nearest-neighbor sites). This form of the operator makes it easier to invert: First, we separate the components of the field on the even and odd sites viz. $\phi = (\phi_o, \phi_e)^T$. The Wilson matrix $M$ can be written as

$$M = \begin{pmatrix} 1 & -\kappa D_{oe} \\ -\kappa D_{eo} & 1 \end{pmatrix} = I - L - U \ , \tag{6.1}$$

[2]The Hamber-Wu operator has also been used in [72] to improve the overlap operator.

where $U$ and $L$ are is the following upper- and lower-triangular matrices respectively viz.

$$U = \begin{pmatrix} 0 & \kappa D_{oe} \\ 0 & 0 \end{pmatrix}, \qquad L = \begin{pmatrix} 0 & 0 \\ \kappa D_{eo} & 0 \end{pmatrix}. \tag{6.2}$$

Note that the diagonal part of $1 - \kappa D$ is trivial. The matrices $(I - U)^{-1}$ and $(I - L)^{-1}$ are easily found to be

$$(I - U)^{-1} = \begin{pmatrix} 1 & \kappa D_{oe} \\ 0 & 1 \end{pmatrix}, \qquad (I - L)^{-1} = \begin{pmatrix} 1 & 0 \\ \kappa D_{eo} & 1 \end{pmatrix}, \tag{6.3}$$

*i.e.* they can be constructed out of the original Wilson operator itself. Now consider the matrix $\bar{M}$ given by

$$\bar{M} = (I - L)^{-1}\ M\ (I - U)^{-1} = \begin{pmatrix} 1 & 0 \\ 0 & 1 - \kappa^2 D_{eo} D_{oe} \end{pmatrix}. \tag{6.4}$$

The odd sites decouple completely, therefore the size of the matrix to be inverted is reduced by half. The inverse of this matrix is not the same as the earlier one, $M^{-1} = (I - U)\bar{M}^{-1}(I - L)$, and one has to pre- and post-multiply by $(I - U)^{-1}$ and $(I - L)^{-1}$ respectively. However, these are already known and furthermore, multiplication with these is cheap because they are upper- and lower-triangular matrices. The net result is thus a factor-two speedup in inversion.

The above simple preconditioning worked because the diagonal part of the operator was trivial. Had we introduced a two-link term, this would no longer be true. Since domain-wall fermions are quite expensive, it is not a good idea to lose preconditioning. We therefore decided to introduce a three-link term instead of a two-link one.

It is straightforward to implement the program of Hamber and Wu for a three-link term; only the coefficients and the Wilson $\kappa$ term turn out to be different. Below, we outline the steps leading to the final form of the operator.

### 6.2.1 The $\mathcal{O}(a^2)$-Improved Wilson Operator

We start by adding the three-link analogs of the first and second derivative to the usual one-link Wilson Dslash term viz.

$$\begin{aligned} D_{x,x'} = & \sum_{\mu=1}^{4} \frac{\gamma_\mu}{2} \Big\{ \left(\delta_{x',x+\hat{\mu}} - \delta_{x',x-\hat{\mu}}\right) + \alpha \left(\delta_{x',x+3\hat{\mu}} - \delta_{x',x-3\hat{\mu}}\right) \Big\} \\ & - \sum_{\mu=1}^{4} \frac{r}{2} \Big\{ \left(\delta_{x',x+\hat{\mu}} + \delta_{x',x-\hat{\mu}} - 2\delta_{x,x'}\right) + \beta \left(\delta_{x',x+3\hat{\mu}} + \delta_{x',x-3\hat{\mu}} - 2\delta_{x,x'}\right) \Big\}. \end{aligned} \tag{6.5}$$

Next, we have to choose a criterion. The criterion adopted by Hamber and Wu was that the Dirac operator be $\mathcal{O}(a^2)$-improved at tree-level. To see how this fixes the values of $\alpha$ and $\beta$, we first write eq. (6.5) in momentum space viz.

$$\begin{aligned} D_p &= \sum_{\mu=1}^{4} \gamma_\mu \Big\{ i \sin p_\mu + i\alpha \sin 3p_\mu \Big\} - r \sum_{\mu=1}^{4} \Big\{ (\cos p_\mu - 1) + \beta(\cos 3p_\mu - 1) \Big\}, \\ &\to \sum_{\mu} i\gamma_\mu \Big\{ p_\mu(1+3\alpha) - \frac{p_\mu^3}{3!}(1+27\alpha) \Big\} - \frac{rp^2}{2!}(1+9\beta) + \mathcal{O}(p_\mu^4). \end{aligned} \tag{6.6}$$

We have denoted $\sum_\mu p_\mu^2$ by $p^2$ to emphasize that the term is rotation-invariant. Now we see that we can eliminate $\mathcal{O}(a^2)$ and $\mathcal{O}(a^3)$ contributions simply by choosing $\alpha = -1/27$, $\beta = -1/9$ viz.

$$\begin{aligned} D_{x,x'} = & \sum_{\mu=1}^{4} \frac{\gamma_\mu}{2} \Big\{ \left(\delta_{x',x+\hat{\mu}} - \delta_{x',x-\hat{\mu}}\right) - \frac{1}{27} \left(\delta_{x',x+3\hat{\mu}} - \delta_{x',x-3\hat{\mu}}\right) \Big\} \\ & - \sum_{\mu=1}^{4} \frac{r}{2} \Big\{ \left(\delta_{x',x+\hat{\mu}} + \delta_{x',x-\hat{\mu}} - 2\delta_{x,x'}\right) - \frac{1}{9} \left(\delta_{x',x+3\hat{\mu}} + \delta_{x',x-3\hat{\mu}} - 2\delta_{x,x'}\right) \Big\}. \end{aligned} \tag{6.7}$$

### 6.2.2 The Projection Property

The operator derived above is problematic in one respect. To see what that is, let us rewrite eq. (6.5) as follows: Setting $r = 1$ and collecting the one-link

and three-link terms separately, we get

$$\begin{aligned} D_{x,x'} = & -\frac{1}{2}\sum_{\mu=1}^{4}\Big[(1-\gamma_\mu)\delta_{x',x+\hat{\mu}} + (1+\gamma_\mu)\delta_{x',x-\hat{\mu}} - 2\delta_{x,x'}\Big] \\ & - \frac{1}{2}\sum_{\mu=1}^{4}\Big[\left(\beta-\alpha\gamma_\mu\right)\delta_{x',x+3\hat{\mu}} + \left(\beta+\alpha\gamma_\mu\right)\delta_{x',x-3\hat{\mu}} - 2\beta\delta_{x,x'}\Big]. \end{aligned} \tag{6.8}$$

There is an advantage to having a $1 \pm \gamma_\mu$ structure (which the one-link term has but which *a priori* the three-link term doesn't). For example, if we write out the matrices $1+\gamma_\mu$ explicitly viz.

$$1+\gamma_1 = \begin{pmatrix} 1 & 0 & 0 & +i \\ 0 & 1 & +i & 0 \\ 0 & -i & 1 & 0 \\ -i & 0 & 0 & 1 \end{pmatrix}, \quad 1+\gamma_2 = \begin{pmatrix} 1 & 0 & 0 & -1 \\ 0 & 1 & +1 & 0 \\ 0 & +1 & 1 & 0 \\ -1 & 0 & 0 & 1 \end{pmatrix}, \tag{6.9a}$$

$$1+\gamma_3 = \begin{pmatrix} 1 & 0 & +i & 0 \\ 0 & 1 & 0 & -i \\ -i & 0 & 1 & 0 \\ 0 & +i & 0 & 1 \end{pmatrix}, \quad 1+\gamma_4 = \begin{pmatrix} 1 & 0 & +1 & 0 \\ 0 & 1 & 0 & +1 \\ +1 & 0 & 1 & 0 \\ 0 & +1 & 0 & 1 \end{pmatrix}, \tag{6.9b}$$

we see that it is sufficient to know two rows(columns) of the matrices; the other two are obtained by simple multiplication of $\pm 1$ or $\pm$i (Which two rows need to be stored depends on $\mu$)[3]. This property of the matrices carries over to any spinor that they multiply: Given two entries of the spinor, we can obtain the other two by simple multiplication of $\pm 1$, $\pm$i. A similar property also holds for the matrices $1-\gamma_\mu$.

The advantage of this property becomes apparent during the operation of *parallel transport i.e.* the matrix multiplication of a source field by a gauge link $U_\mu(x)$. For example, the Conjugate Gradient (CG) method for inverting the Dirac operator $D$ proceeds by the repeated application of $D$ to a trial solution $\psi$. As is well-known, to be gauge-invariant $D$ cannot contain ordinary derivatives but rather must contain covariant derivatives: $\delta_{x',x+\hat{\mu}} \rightarrow U_\mu(x)\delta_{x',x+\hat{\mu}}$, $\delta_{x',x-\hat{\mu}} \rightarrow U^\dagger_\mu(x)\delta_{x',x-\hat{\mu}}$. The link matrices act on the color indices only; a separate multiplication is required for each spin component. The problem is more acute in the three-link case, where *three* such matrix multiplications are required in each direction. This $\mathcal{O}(N)$ operation (where $N$ is the order of $D$) is the most time-consuming part of the CG algorithm. Projection speeds this up by a factor of two because we need multiply only half the spinor entries.

[3]In the language of linear algebra, the matrices $1 \pm \gamma_\mu$ are rank-two matrices.

The remaining two entries can be determined, after all such multiplications have been done, simply by using eqs. (6.9).

We thus demand that the three-link term preserve the projection property as well. This is possible if we choose $\alpha = \beta$ in eq. (6.8) viz.

$$\begin{aligned} D_{x,x'} = &-\frac{1}{2}\sum_{\mu=1}^{4}\Big[(1-\gamma_\mu)\delta_{x',x+\hat{\mu}} + (1+\gamma_\mu)\delta_{x',x-\hat{\mu}} - 2\delta_{x,x'}\Big] \\ &-\frac{\alpha}{2}\sum_{\mu=1}^{4}\Big[(1-\gamma_\mu)\delta_{x',x+3\hat{\mu}} + (1+\gamma_\mu)\delta_{x',x-3\hat{\mu}} - 2\delta_{x,x'}\Big]. \end{aligned} \tag{6.10}$$

A Taylor expansion in momentum space now yields

$$D_{HW}(p) = \sum_{\mu} i\gamma_\mu\Big\{p_\mu(1+3\alpha) - \frac{p_\mu^3}{3!}(1+27\alpha)\Big\} - \frac{p^2}{2!}(1+9\alpha) + \mathcal{O}(p_\mu^4). \tag{6.11}$$

We have a choice between eliminating the $\mathcal{O}(a^2)$ or the $\mathcal{O}(a^3)$ terms. It might seem that one ought to eliminate the $\mathcal{O}(a^2)$ term; however note that that term is rotation-invariant. We have already seen that rotation-invariant corrections *do not* correct the dispersion relation. Let us therefore choose $\alpha = -1/27$. With this choice, the dispersion relation shall receive corrections at $\mathcal{O}(a^4)$. In fact, we shall see that with this choice of coefficients, the action actually converges faster and more smoothly to the continuum limit. This choice of coefficients also improves the thermodynamics of the domain-wall or overlap operator that uses this kernel, as we shall see.

## Determining $\kappa_{HW}$

So far, we have focused our attention on the kinetic, or "Dslash" part. The full Hamber-Wu operator is actually given by

$$M_{HW}(x,x') = D_{HW}(x,x') + (1+3\alpha)m\delta_{x,x'}, \tag{6.12}$$

with $D_{HW}$ given by eq.(6.5) above. The reason for the $(1+3\alpha)$ factor is clear from eq.(6.6): It is the coefficient of the $\sum_\mu \gamma_\mu p_\mu$ term in the Taylor expansion which is the only term that survives the continuum limit. Since the continuum Dirac operator is $\sum_\mu i\gamma_\mu p_\mu + m$, the mass term must have the same coefficient as the kinetic one.

Putting everything together, we get

$$\begin{aligned} D_{x,x'} =& -\frac{1}{2}\sum_{\mu=1}^{4}\left[(1-\gamma_\mu)\delta_{x',x+\hat{\mu}} + (1+\gamma_\mu)\delta_{x',x-\hat{\mu}} - 2r\delta_{x,x'}\right] \\ &+ \frac{\alpha}{2}\sum_{\mu=1}^{4}\left[(\gamma_\mu - 1)\,\delta_{x',x+3\hat{\mu}} + (\gamma_\mu+1)\,\delta_{x',x-3\hat{\mu}} - 2\delta_{x,x'}\right] \\ &+(1+3\alpha)m\delta_{x,x'} \end{aligned} \tag{6.13}$$

Generally, one rescales the field variables so that the coefficient of $\delta_{x,x'}$ is unity viz.

$$\begin{aligned} M_{x,x'} =& 1 - \kappa_{HW}\left[\sum_{\mu=1}^{4}\left\{(1-\gamma_\mu)\delta_{x',x+\hat{\mu}} + (1+\gamma_\mu)\delta_{x',x-\hat{\mu}}\right\}\right. \\ &\left. -\alpha\sum_{\mu=1}^{4}\left\{(1-\gamma_\mu)\delta_{x',x+3\hat{\mu}} + (1+\gamma_\mu)\delta_{x',x-3\hat{\mu}}\right\}\right], \end{aligned} \tag{6.14a}$$

$$\kappa_{HW} = \frac{0.5}{4\,(1+\alpha) + (1+3\alpha)\,m}. \tag{6.14b}$$

To see how the operator performs, we compute the pressure for massless Hamber-Wu fermions. Fig. 6.1 shows the results. The values are normalized to the continuum value of $P_{SB} = 7\pi^2/180$. It is seen that the rotation-invariant case actually performs better than the improved case. This is reminiscent of the behavior of p4 versus Naik fermions: p4 fermions perform better on coarser lattices even though their Dirac operator has $\mathcal{O}(a^2)$ errors.

From the figure, we also see that the approach to the continuum limit is non-monotonic for the choice $\alpha = -1/27$, $\beta = -1/9$. This makes the choice unreliable for continuum extrapolations in full-fledged simulations.

## 6.3 DWF Thermodynamics with the Hamber-Wu kernel

Next let us consider the domain-wall operator whose 4-d part consists of the Hamber-Wu operator. The formulae that were derived in appendix B for the

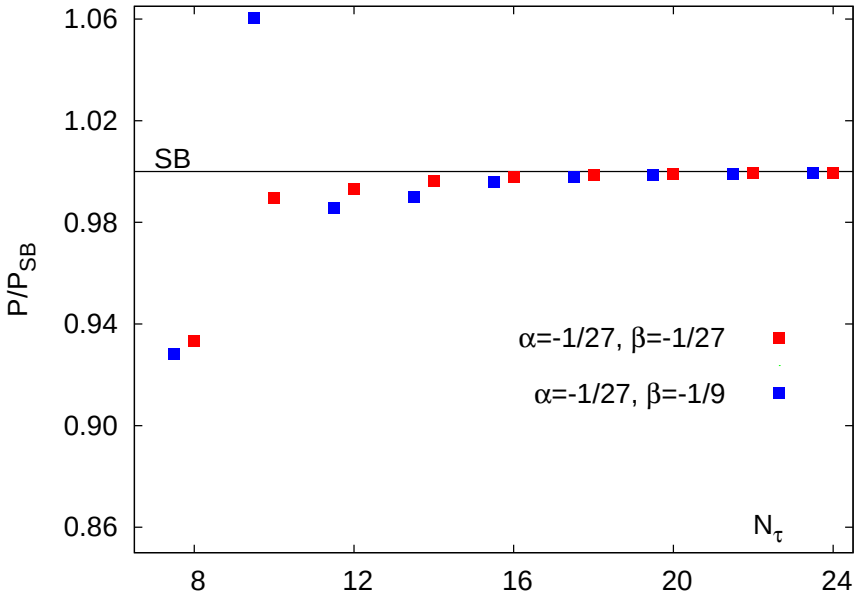


Figure 6.1: The (normalized) pressure of massless Hamber-Wu fermions as a function of $N_\tau$ for two choices of the parameters. The blue points are displaced slightly relative to the red ones for clarity.

propagator and the pressure still hold viz.

$$D^{-1}(p) = 1 + \frac{\mathrm{i}\sum_\mu \gamma_\mu \sin p_\mu}{S^2 + W^2 - 1 + \sqrt{(1+S^2+W^2)^2 - 4W^2}}, \tag{6.15a}$$

$$\frac{P}{T^4} = 2\left(\frac{N_\tau}{N_\sigma}\right)^3 \sum_{\mathbf{p},p_4} \ln\left(1 - \frac{1 - S^2 - W^2}{\sqrt{(1+S^2+W^2)^2 - 4W^2}}\right), \tag{6.15b}$$

except that $W$ and $S^2$ are now given by

$$W = 1 - (1+3\alpha)M_5 + \sum_\mu \Big\{(1-\cos p_\mu) + \alpha(1-\cos 3p_\mu)\Big\}, \tag{6.16a}$$

$$S^2 = \sum_\mu \Big\{\sin p_\mu + \alpha \sin 3p_\mu\Big\}^2. \tag{6.16b}$$

As before, the dispersion relation is given by $S^2 = 0$ subject to the constraint $|W| < 1$. The constraint is satisfied near the origin of the Brillouin zone

provided

$$-1 < 1 - (1+3\alpha)M_5 < 1 \qquad \text{or} \qquad 0 < M_5 < 9/4 \qquad \text{for} \qquad \alpha = -1/27. \tag{6.17}$$

The allowed range of $M_5$ is increased *vis-á-vis* the unimproved case. Next, let us try to solve the dispersion relation for $E = -ip_4$. If we denote $\sum_{i=1}^{3}(\sin p_i + \alpha \sin 3p_i)^2$ by $\omega^2$, then (eq. (6.16b))

$$\begin{aligned} 0 &= (\sin p_4 + \alpha \sin 3p_4)^2 + \omega^2, \\ &= \sin^2 p_4 + \alpha^2 \left(3\sin p_4 - 4\sin^3 p_4\right)^2 \\ &+ 2\alpha \sin p_4 \left(3\sin p_4 - 4\sin^3 p_4\right) + \omega^2, \\ &= 16\alpha^2 \sin^6 p_4 - 8\alpha(1+3\alpha)\sin^4 p_4 - (1+3\alpha)^2 \sin^2 p_4 + \omega^2, \\ \therefore 0 &= \sin^6 p_4 - 2\left(\frac{1+3\alpha}{2\alpha}\right)\sin^4 p_4 - \left(\frac{1+3\alpha}{2\alpha}\right)^2 \sin^2 p_4 + \left(\frac{\omega}{4\alpha}\right)^2. \end{aligned} \tag{6.18}$$

This is a simple cubic equation in $\sin^2 p_4$ which can be solved for $-\mathrm{i}\sinh E = \sin p_4$ (This is in contrast to the Wilson dispersion relation which is a general, sixth-order cubic equation in $\sin(p_4/2)$ and therefore does not admit of a closed-form solution). Here we see yet another advantage to removing the $\mathcal{O}(a^3)$ errors instead of the $\mathcal{O}(a^2)$ one back in eq.(6.11). The $\mathcal{O}(a^2)$ correction comes from the Wilson term which *does not* show up in the domain-wall dispersion relation. The $\mathcal{O}(a^3)$ correction is in fact the leading correction here and it is eliminated by our choice of $\alpha$.

Once we've solved the above equation, we can use the variable $E(\mathbf{p})$ to obtain a series expansion in the lattice spacing $a \equiv 1/N_\tau$ for the pressure viz.

$$\frac{P}{P_{SB}} = 1 - \frac{1143}{980}\left(\frac{\pi}{N_\tau}\right)^4 - \frac{365}{77}\left(\frac{\pi}{N_\tau}\right)^6 + \mathcal{O}(a^8). \tag{6.19}$$

This is the same series as for the Naik equation, but that was to be expected: Unimproved DWF fermions had the same dispersion relation, and thus the same series, as unimproved naive fermions. The addition of a three-link term would make the dispersion relation identical to the Naik one. If we had added bent terms instead of a three-link term, we would have obtained the p4 dispersion relation instead. Fig. 6.2 plots the unimproved and improved pressures as functions of $N_\tau$.

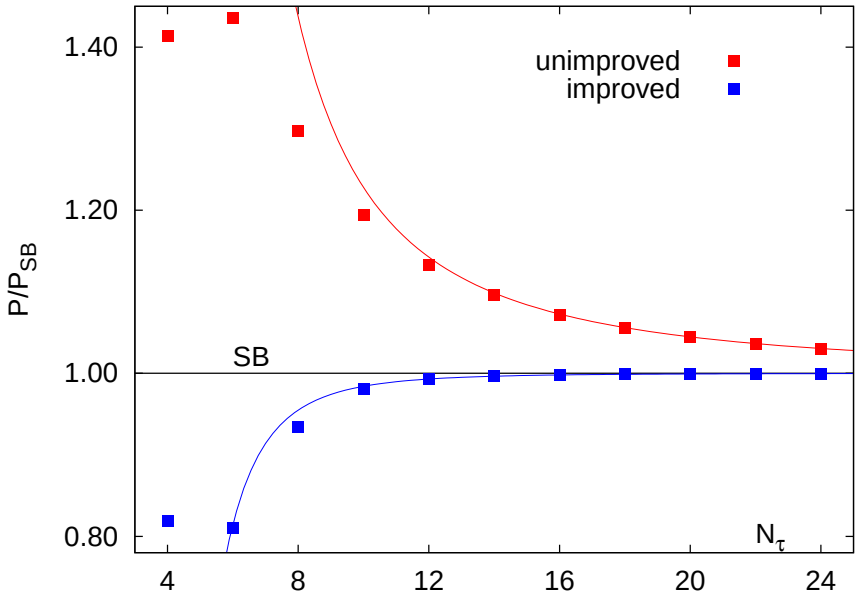


Figure 6.2: $P/P_{SB}$ for improved and unimproved domain-wall fermions ($L_s = \infty$ and $M_5 = 1.0$). The curves plot the corresponding series.

## 6.4 Simulating with the Hamber-Wu Operator

### 6.4.1 Implementation

The next step was to test whether the improvement carried over to the interacting case as well. This involved implementing the Hamber-Wu kernel for the domain-wall operator. Briefly this meant that, given an arbitrary field $\psi(x)$:

- The four-component field was *projected*, by multiplying by $1 \pm \gamma_\mu$, to eight two-component fields, one for each direction.
- The projected fields were parallel-transported: $(1-\gamma_\mu)\psi(x) \longrightarrow U_\mu(x-\hat{\mu})\psi(x)$, etc. Note that the parallel-transported field actually belongs to the site $x - \hat{\mu}$. In effect this moves the lattice by one step, leaving the fields in their original position. The one-link and three-link terms were transported separately.
- The one-and three-link terms *for a given direction* were combined, with the appropriate coefficients $c_{10}$ and $c_{30}$ included.
- These fields were *expanded* back to their four-component analogs.

- The fields along the eight different directions were added together.

The above procedure was implemented twice, since we separated the fields on odd and even sites and transported them separately. Also, along with the kinetic term we needed its derivative with respect to the chemical potential as well. Since the latter only coupled to the fields in the $\hat{4}$-direction, we needed to project/parallel-transport/expand only along two directions. Depending on the order $n$ of the derivative, the backward hop picked up a sign $(-1)^n$, which had to be kept track of.

We tested this operator extensively before employing it in simulations. By placing a unit source at random on a lattice, and using the trivial gauge configuration *i.e.* one in which all links were the unit matrix, we could check that each of the above steps did what was expected of it. We also used a non-trivial gauge configuration to check that the parallel-transporter correctly matched $U_\mu(x)$ with $\psi(x+\hat{\mu})$, etc. (For the unit configuration, all the $U_\mu(x)$ would be identical). We also made sure that the (anti)periodic boundary conditions for the (time)space directions were implemented correctly.

For the more general case of non-trivial source and field, one could only check quantities averaged over the whole lattice. One non-trivial check was to set the coefficient of the three-link term to zero and compare it with the results obtained with the unimproved operator (which we already had). Yet another check was to gauge-transform an arbitrary configuration and check for the invariance of physical observables, such as $\langle\overline{\psi}\psi\rangle$, with respect to it. Lastly, we made some "quick-and-dirty" measurements of quantities such as $\chi_2$ in the free case and checked that the results were within reasonable agreement with the ideal gas values (upto cutoff and finite-volume effects).

### 6.4.2 Partial Quenching

A first test of improvement would be to compute an observable such as $\chi_2$ well above the transition temperature $T_c$ with both the unimproved and improved operators. At temperatures $T \gtrsim 2T_c$, $\chi_2$ attains its ideal gas value of unity. However if cutoff effects are present, these measurements can actually exceed this value by about 10%[4].

The domain-wall ensembles that we had used for our earlier measurements were generated for studying the region around $T_c$, and were consequently at much lower temperatures. We therefore decided to test our operator on the p4 ensembles that had been generated by the RBC-Bielefeld collaboration for its Equation of State studies.

[4]See fig. 4.1 for an example of this artifact in the pressure.

When the action used to measure observables is different from the action used to generate the ensembles, the resulting measurements are referred to as "partially quenched." Partial quenching may be thought of as an intermediate step between totally "quenched" measurements in which fermionic observables are measured on pure gauge ensembles, and "fully dynamical" ensembles in which the valence and sea quarks are identical ("valence" and "sea" refer to the quarks used in making measurements and in generating the ensembles respectively. The latter only show up in virtual quark-antiquark loops, hence the name "sea".).

The use of different actions in the sea and valence sectors implies that the partially quenched theory violates unitarity. Importantly however, unlike the fully quenched case, this violation vanishes in the continuum limit. This may be understood as follows: In the quenched case, the lack of dynamical fermions means that there are no quark-antiquark loops in the theory, irrespective of the spacing. Formally the quenched theory is a theory of infinitely heavy fermions, which explains why they do not propagate — it would cost an infinite amount of energy to create a $q\bar{q}$ pair out of the vacuum. In such a theory, the valence quarks merely act as "test charges." By contrast, in the partially quenched theory one merely has a different fermion action in the sea sector. Since all fermion actions go over to the Dirac action in the continuum, it is reasonable to expect that unitarity-violating effects shall vanish in the continuum.

Of course, this expectation must be verified as rigorously as possible. This has been done within the context of chiral perturbation theory in [75, 77]. A point stressed by these and other authors is that it is not possible to tune the valence and sea quark masses at finite lattice spacing so as to remove all unitarity-violating artifacts [75, 76]. On the other hand, these violations become smaller with smaller spacing and vanish altogether in the continuum limit. Furthermore the chiral and continuum limits commute, so that one may extrapolate in either direction depending on the need. Lastly, the ambiguity in the definition of a quark mass at $a \neq 0$ implies that one is free to use a value appropriate to the task at hand [77, 78].

## 6.5 Measurements

### 6.5.1 The Connected Susceptibility

Our measurements of the susceptibility $\chi_2$ are preliminary, partly because the simulations are still in their early stages, but also because the large size of the p4 lattices viz. $32^3 \times 8$, coupled with our choice of $L_s = 32$, slowed down these measurements. Thus these lattices were eight times larger than the ones we

used for our results in the previous chapter. Lattices of this size have never been employed before in DWF thermodynamics and even with the unimproved action, it took about ten hours to measure $\chi_2$ to sufficient precision at the lowest $\beta$-value.

Another bottleneck obviously was the memory requirement. Since each fermion field consists of 4 spin components times 3 colors = 12 complex, double-precision numbers, we needed $48 \times 16 = 768$ bytes = 0.75 kB of memory per site. Eight such copies are needed (one for each direction) and for the improved operator one needs eight more copies for the three-link terms.

On scalar machines, the improved operator was about four times as slow as the unimproved one. However the latter operator has been optimized over the years for performance on the BlueGene/L machine on which we ran our simulations. On that machine, the improved operator was found to be around ten-fifteen times slower. Clearly, further work is needed so as to bring the operator to its optimum performance level.

Since we were only testing the operator, we used a trial value of $am = 0.01$. Provided the quark mass is small enough that the pion is not too heavy, $\chi_2$ shows no quark mass dependence and should, in principle, attain the Stefan-Boltzmann value of unity. Ideally, one would have liked to make measurements at more than one value of the quark mass and perform an extrapolation of some sort. The fact that these measurements took so long however constrained us to work at one mass value for the time being and defer detailed extrapolations for later.

We have already defined the quark number susceptibilities and listed the traces involved in the lowest-order susceptibilities in eqs. (5.10). Of the three traces that enter in the measurement of $\chi_2$, measuring the square is the hardest. The ensemble average of this quantity is numerically equal to the off-diagonal correlation $\chi_{11}^{ud}$. This quantity, which only receives contributions from disconnected loops, fluctuates a lot from configuration to configuration. Moreover it goes to zero at high temperatures.

| $\beta$ | Unimproved | Improved |
|---|---|---|
| 4.00 | 0.550(7) | 0.483(8) |
| 3.82 | 0.544(4) | 0.486(7) |
| 3.76 | 0.536(8) | |

Table 6.1: The connected susceptibilities for the improved and unimproved DWF operators. The unimproved ones exceed the SB value of 0.5 by about 10%.

If we drop this quantity, the remaining part is called the connected susceptibility. This quantity is much easier to evaluate and furthermore, this

is the part that attains the Stefan-Boltzmann value as $T \to \infty$. Table 6.1 tabulates the quantity $c_2 = 0.5\chi_2$ for the improved and unimproved fermions respectively.

### 6.5.2 The Residual Mass

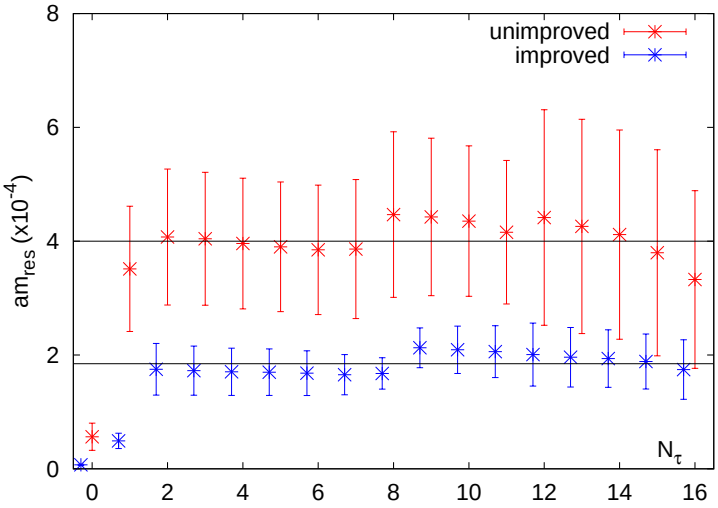


Figure 6.3: The residual mass is seen to decrease by a factor of two in going from the unimproved to the improved case. The above plot is for $\beta = 3.82$.

| $\beta$ | Unimproved | Improved |
|---|---|---|
| 4.00 | $2.42(12) \times 10^{-5}$ | $1.30(9) \times 10^{-5}$ |
| 3.82 | $4.00(8) \times 10^{-4}$ | $1.85(6) \times 10^{-4}$ |

Table 6.2: Values for $m_{\rm res}$ obtained using the unimproved and improved actions on the same (p4) ensembles.

Fig. 6.3 plots the quantity $R(t)$ defined in eq. (5.18) as a function of $t$. We see that it attains a plateau around $t \simeq 2$; the level of the plateau is the residual mass. While the value of the residual mass is small in both cases, it is smaller in the improved case by about a factor of two relative to the unimproved one. Table 6.2 lists the values of $m_{\rm res}$ obtained with the two actions for the different $\beta$-values. In both cases, $m_{\rm res}$ is smaller in the improved case than in the unimproved one. On the other hand, the tendency of $m_{\rm res}$ to increase with the coupling is still present in both cases. It remains to be seen whether the observed reduction in $m_{\rm res}$ persists all the way toward much stronger couplings.

### 6.5.3 Screening Masses

It is characteristic of any plasma that any test charge that is introduced in it is shielded so that its influence falls off exponentially with distance. This falloff is characterized by a length called the *screening length*, whose inverse defines the *screening mass*.

Depending on the type of charge introduced, one may define more than one screening mass. Typically in the case of QCD the test charge is a meson $\overline{\psi}\Gamma\psi$, where $\Gamma$ is one of the sixteen typical combinations of the Dirac matrices. The quantity that is measured is the hadronic correlator viz.

$$C_\Gamma(z) = \sum_{x,y,t} \left\langle \overline{\psi}(\mathbf{x},t)\Gamma\psi(\mathbf{x},t)\ \overline{\psi}(\mathbf{0},0)\Gamma\psi(\mathbf{0},0) \right\rangle. \tag{6.20}$$

The source meson is introduced at the origin, and its influence is measured a distance $z$ away along a spatial axis (in this case, the $z$-axis). $C(z)$ falls off exponentially with $z$. The screening mass for the channel $\Gamma$ is defined as

$$m_\Gamma = \lim_{z\to\infty} \frac{C_\Gamma(z)}{C_\Gamma(z+1)}. \tag{6.21}$$

On a finite lattice, one typically has reflection symmetry with respect to the midplane. Lattice correlators fall off at first as the spacing is increased, then increase again as one nears the opposite end. Thus, the behavior of correlators on the lattice is given by

$$\begin{aligned} C(z) &= A\left(\mathrm{e}^{-m_\Gamma z} + \mathrm{e}^{-m_\Gamma(N_z - z)}\right), \\ &= A\mathrm{e}^{-\frac{m_\Gamma N_z}{2}} \cosh\left(\frac{N_z}{2} - z\right). \end{aligned} \tag{6.22}$$

The Stefan-Boltzmann limit for screening masses is given by $m_\Gamma^{\mathrm{SB}} = 2\pi T$ (where $T$ is the temperature), irrespective of the channel [79]. On our $N_\tau = 8$ lattices therefore, we should expect that $am_\Gamma^{\mathrm{SB}} \to 2\pi/8 = 0.7853\ldots$ at high temperatures.

The correlator for the pseudoscalar channel was measured during our residual mass calculations; fig. 6.4 presents the correlator for $\beta = 4.00$. The fitting function eq. (6.22) was employed, with $N_z = 32$. Only the points from $z = 10$ to $z = 22$ were used for fitting. The error is the total of both the statistical error as well as the systematic error obtained by varying the endpoints of the fit. Similarly, in fig. 6.5, we present our results for the vector correlator at $\beta = 4.00$. Table 6.3 summarizes our results for the pseudoscalar and vector

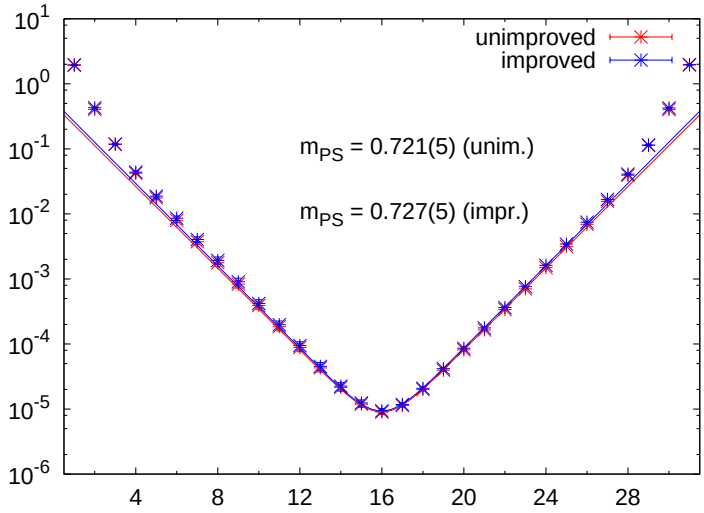


Figure 6.4: The pseudoscalar correlator, measured with both improved and unimproved fermions, at $\beta = 4.00$.

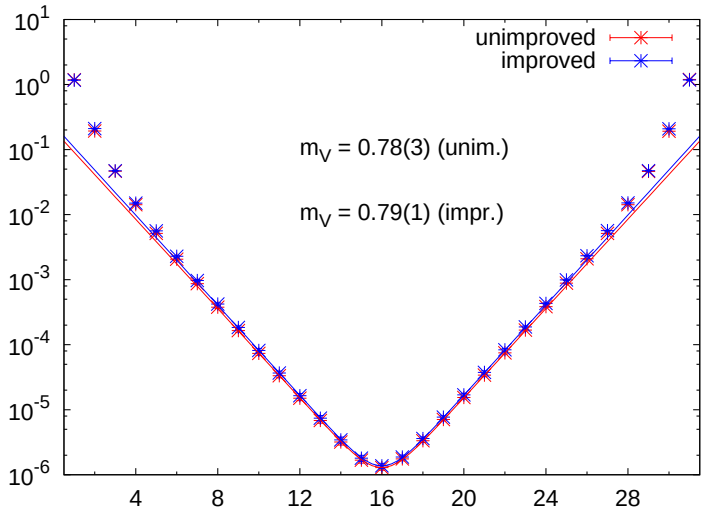


Figure 6.5: The vector correlator measured using both the improved and unimproved operators, at $\beta = 4.00$.

screening masses obtained with the two operators.

From the table, we see that the vector channel attains the Stefan-Boltzmann limit, while the scalar channel lies below it. Actually, a similar behavior has been observed with staggered fermions as well [80]. In figs. 6.6, we superimpose our data on top of results obtained with the p4 action for $N_\tau = 4$, 6 and

| $\beta$ | $T$(MeV) | $M_{PS}$ | $M_V$ | $M_{PS}/M_V$ |
|---|---|---|---|---|
| Unimproved | | | | |
| 4.00 | 475 | 0.721(5) | 0.79(1) | 0.92(1) |
| 3.82 | 351 | 0.70(2) | 0.78(3) | 0.90(4) |
| Improved | | | | |
| 4.00 | 475 | 0.727(5) | 0.79(2) | 0.92(2) |
| 3.82 | 351 | 0.71(3) | 0.76(1) | 0.93(4) |

Table 6.3: Pseudoscalar and vector screening masses for $N_\tau = 8$.

8.

From the figure, we see that cutoff effects are not very pronounced in going from $N_\tau = 4$ to $N_\tau = 8$, which may explain why we observe no difference in our results with the unimproved and improved operators. It is also encouraging to see that the domain-wall results are in agreement with results obtained using a completely different action (*i.e.* the p4 action). Of course, the p4 quark masses have been tuned to their physical values while our choice of quark mass is arbitrary; nevertheless these results show that it is worthwhile to proceed and do a more systematic study of these quantities with domain-wall fermions. Also, we expect that the better chiral symmetry of domain-wall fermions really makes its presence felt close to the transition temperature. At lower temperatures therefore, we may see differences in the two actions. This is something that can be explored in the future.

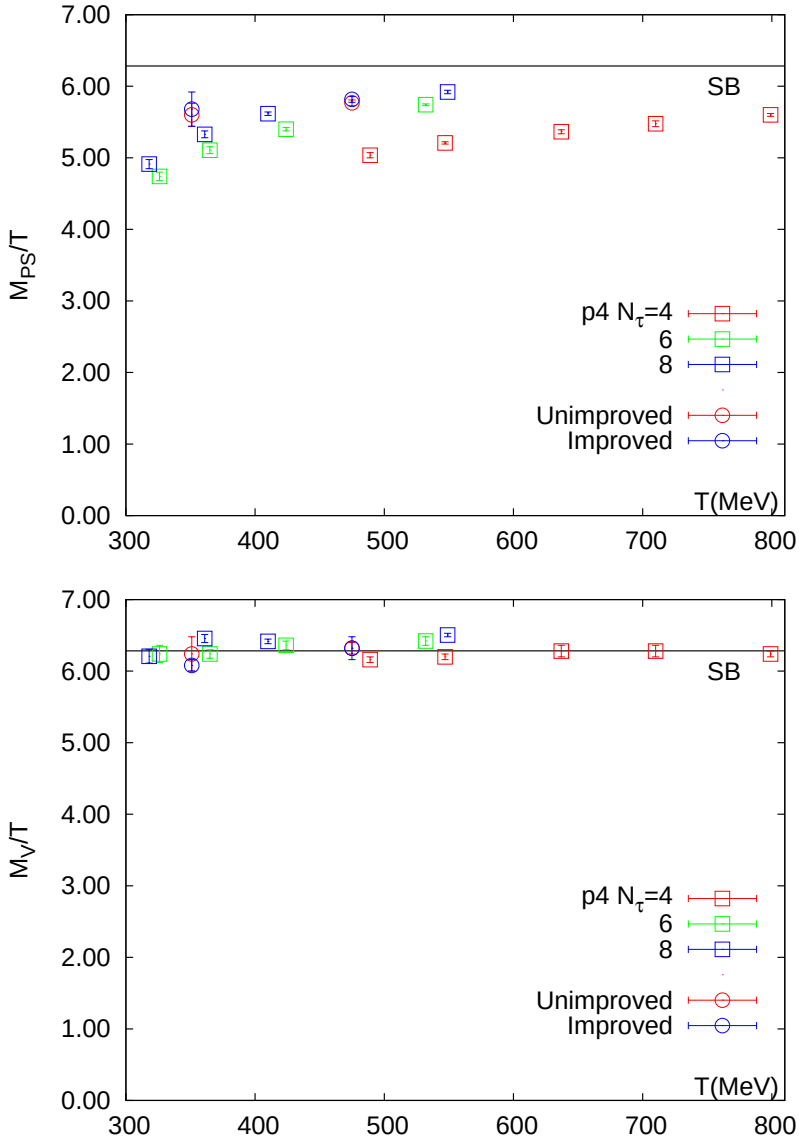


Figure 6.6: p4 screening masses with the DWF results superimposed, for the pseudoscalar and vector channels respectively.

# Chapter 7

# Conclusion

The discovery of chiral fermions gave lattice theorists a handle on chiral symmetry for the first time. Until then, one had to choose between either staggered fermions, which preserved a subgroup of the complete symmetry and also produced doublers, or Wilson fermions which broke chiral symmetry completely at finite lattice spacing. Chiral symmetry is very important as it determines the spectrum of the strong interactions. In thermodynamics too, this symmetry determines the universality class of QCD with respect to its symmetry-restoration transition. The great promise of chiral fermions was that it would be possible to study these questions without messy extrapolations, renormalization or theoretical ambiguities regarding taking the continuum limit.

Unfortunately this advance came at a cost. Even the simplest chiral fermions viz. domain-wall fermions, were about an order of magnitude costlier than staggered fermions. However, through a combination of increased computing power and improved algorithms, the cost barrier is being slowly overcome and we now have several results with chiral fermions (specifically domain-wall fermions) that are in good agreement with staggered or Wilson results.

Of the three known chiral formulations viz. overlap, hypercube and domain-wall, it is the latter that have been studied most extensively and also put to the greatest use. This is because they are the cheapest of the three and also the simplest from the theoretical and implementation points of view. The Riken-Brookhaven-Columbia (RBC) group has been one of the groups to pioneer simulations with these fermions. Our simulations for this thesis were also carried out with these fermions, with the particular implementation used by the RBC group.

In this work we studied the domain-wall operator with an eye on its applications to QCD thermodynamics. As a first step, we calculated the free quark pressure in this formalism analytically. Apart from learning how domain-wall fermions worked, we also got an idea of the discretization errors in the for-

malism. Since these were rather large, we realized that it was necessary to improve the canonical action to avoid these errors on typical lattices used in simulations. A related question involved introducing a chemical potential in this formalism; we verified that the usual way of introducing it produced no divergences and led to the correct pressure in the continuum limit.

Our simulations with the domain-wall operator produced clear evidence of a transition, though our limited statistics prevented us from pinpointing the transition temperature/coupling to sufficient accuracy. However our errors were not merely statistical. The chiral symmetry of domain-wall fermions is only approximate at finite lattice spacing; we found that this breaking worsened very quickly as we moved toward stronger coupling *i.e.* toward coarser lattices. This breaking produces a distortion in quantities sensitive to the quark mass, such as the (disconnected) chiral susceptibility. Since it is this very quantity that is used to determine the transition temperature, to produce an acceptable result we must insure that this breaking remains under control. This is certainly a direction for future work, and in fact the Columbia group has begun preliminary runs with an operator that keeps this breaking down to reasonable levels in simulations.

The other source of errors is of course the discretization errors alluded to earlier. We outlined the steps toward improving this operator and checked that it worked in free-field calculations. We also implemented this operator for numerical work. The ensembles we used for testing were staggered (p4) ensembles with the quark masses very close to their physical values. The use of different actions in the sea and valence sectors is a tricky topic and in this exploratory study we did not study all possible issues. However our results, though preliminary, were very encouraging. In particular, we saw that the improved operator reproduced the correct Stefan-Boltzmann limit for the connected quark susceptibility at high temperatures. Particularly interesting were some preliminary results that suggested that $m_{\rm res}$ (the mass renormalization that parameterizes the chiral symmetry breaking) is smaller in the improved case at the same coupling. Of course, this decrease does not halt the exponential growth of $m_{\rm res}$ with the coupling, but if this suppression holds at stronger coupling it should still be possible to simulate over a larger range of $\beta$ than with the unimproved operator.

Our final results involved screening masses. We measured several correlators using both domain-wall operators. Again, it was encouraging to see that the domain-wall operator reproduced the staggered results. These are possibly the first-ever results for these quantities with the domain-wall operator, and this is certainly something that can be pursued in the future. In particular, various theoretical issues related to the use of two different actions (partial

quenching) need to be settled. It is also necessary to simulate in the region of stronger coupling. These are all possible directions for extending the work described here. We hope that by following these directions we may acquire a better understanding of the chiral phase transition and of the QCD phase diagram in general.

# Bibliography


[1] R. Pisarski and F. Wilczek, Phys. Rev. D **29**, 338 (1984).

[2] P. Chen *et al. Nucl. Phys.* **A663-664**, 31 (2000); G.T. Fleming, Ph.D. thesis (unpublished), hep-lat/0404020 (arXiv).

[3] P. Hasenfratz and F. Karsch, Phys. Lett. B **125**, 308 (1983).

[4] J. Bloch and T. Wettig, Phys. Rev. Lett. 97, 012003 (2006); the derivation of the overlap as the $L_s \to \infty$, $a \to 0$ limit of the domain-wall operator at $\mu \neq 0$ was given in Phys. Rev. D **76**, 114511 (2007).

[5] E. Follana *et al.*, Phys. Rev. D **75**, 054502 (2007).

[6] H. Hamber and C. M. Wu, Phys. Lett. B **133**, 351 (1983).

[7] S. Adler, *Phys. Rev.* **177**, 2426 (1969), J.S. Bell and R. Jackiw, Nuovo Cimento A, Volume 60, Number 1, 47-61 (1969), S. Adler and W. A. Bardeen, *Phys. Rev.* **182**, 1517 (1969).

[8] H.D. Politzer, Phys. Rev. Lett. 30, 1346 (1973); D.J. Gross and F. Wilczek, Phys. Rev. Lett. 30, 1346 (1973).

[9] For example, the mean lifetime of the proton has been determined to be greater than $6.6 \times 10^{33}$ yr (H. Nishino, S. Clark *et al.* Phys. Rev. Lett. 102, 141801 (2009)).

[10] J. Gasser and H. Leutwyler, Phys. Lett. B **125**, 321 (1983).

[11] J.B. Kogut and D.K. Sinclair, Phys. Rev. D **73**, 074512 (2006).

[12] S. Ejiri *et al.*, Phys. Rev. D **80**, 094505 (2009).

[13] C. Morningstar, "The Monte Carlo Method in Quantum Field Theory," hep-lat/0702020 [arXiv].

[14] H. Rothe, "Lattice Gauge Theories: An Introduction (2nd. Ed.)," World Scientific (1997).

[15] T. deGrand and C. deTar, "Lattice Methods for Quantum Chromodynamics," World Scientific (2006).

[16] A discussion of the different algorithms used to generate ensembles in lattice QCD can be found in M. Clark, "The Rational Hybrid Monte Carlo Alogrithm," Ph.D. thesis.

[17] K.G. Wilson, Phys. Rev. D **10**, 2445 (1974).

[18] F.J. Wegner, J. Math. Phys. **12**, 2259 (1971).

[19] "An Introduction to Quantum Field Theory," M. Peskin and D. Schroeder, Westview Press (1995).

[20] K.G. Wilson, *New Phenomena in Subnuclear Physics* (Erice, 1975) ed. A. Zichichi (New York, Plenum 1975).

[21] L. Susskind, Phys. Rev. D **16**, 3031 (1977).

[22] D. Kaplan, arXiv:0912.2560 [hep-lat].

[23] M. Creutz, JHEP 0804, 017 (2008).

[24] L. Karsten and J. Smit, Nucl. Phys. **B183**, 103 (1981).

[25] H. B. Nielsen and M. Ninomiya, Nucl. Phys. **B185**, 20 (1981), Erratum-ibid. **B195**,541(1982), Nucl. Phys. **B193**, 173 (1981), Phys. Lett. B **105**, 219 (1981).

[26] R. Narayanan and H. Neuberger, Phys. Rev. Lett. 71, 3251 (1993); Nucl. Phys. **B443**, 308 (1995); Nucl. Phys. Proc. Suppl. **47**, 591 (1996); Phys. Lett. B **302**, 62 (1998).

[27] H. Neuberger, Phys. Lett. B **417**, 141 (1998); Phys. Lett. B **427**, 353 (1998); Phys. Rev. D **57**, 5417 (1998).

[28] S.A. Frolov and A.A. Slavnov, Phys. Lett. B **309**, 344 (1993).

[29] P. Ginsparg and K. Wilson, Phys. Rev. D **25**, 2649 (1982).

[30] M. Lüscher, Phys. Lett. B **428**, 342 (1998).

[31] M. Lüscher, arXiv: hep-th/0102028.

[32] Y. Shamir, Nucl. Phys. **B406**, 90 (1993); V. Furman and Y. Shamir, Nucl. Phys. **B439**, 54 (1995).

[33] P. Vranas, Nucl. Phys. Proc. Suppl. **53**, 278 (1997); Phys. Rev. D **57**, 1415 (1998).

[34] K. Symanzik, Nucl. Phys. **B226**, 187 (1983) and Nucl. Phys. **B226**, 205 (1983).

[35] B. Beinlich, F. Karsch, E. Laermann and P. Peikert, Eur. Phys. **J6**, 133 (1999).

[36] C. Gattringer and L. Liptak, Phys. Rev. D **76**, 054502 (2007).

[37] P. Hegde, F. Karsch, E. Laermann and S. Shcheredin, Eur. Phys. **J55**, 423 (2008).

[38] K. Originos and D. Toussaint, Phys. Rev. D **59**, 014501 (1999); Nucl. Phys. Proc. Suppl. **99**, 909 (1999); G. P. Lepage, Phys. Rev. D **79**, 074502 (1999); K. Originos, D. Toussaint and R. L. Sugar, Phys. Rev. D **60**, 054503 (1999).

[39] F. Karsch, U. Heller and B. Sturm, Phys. Rev. D **50**, 114502 (1999).

[40] R. Edwards and U. Heller, Phys. Rev. D **63**, 094505 (2001).

[41] G. Aarts and J. Foley [UKQCD Collaboration], JHEP 0702, 062 (2007).

[42] S. Gottlieb *et al.* Phys. Rev. Lett. 59, 2247 (1987); R. V. Gavai, S. Gupta and P. Majumdar, Phys. Rev. D **65**, 054506 (2002); C. Allton *et al.* Phys. Rev. D **71**, 054508 (2005).

[43] R. Hagedorn, Nuovo Cim. Suppl. **3**, 147 (1965).

[44] P. Huovinen and P. Petreczky, arXiv:1005.0324[hep-ph].

[45] A. Bazavov *et al.* Phys. Rev.**D80**, 014504 (2009);arXiv:0903.4379 [hep-lat]

[46] M. Cheng *et al.* Phys. Rev. **D74**, 054507 (2006) [hep-lat/0608013].

[47] C. Bernard *et al.* (MILC), Phys. Rev. **D71**, 034504 (2005) [hep-lat/0405029].

[48] C. Bernard *et al.* Phys. Rev. D **62**, 034503 (2000).

[49] M. Li, PoS LATTICE2006, 183 (2006).

[50] A. Gray *et al.* Phys. Rev. D **72**, 94507 (2005).

[51] Y. Aoki, Z. Fodor, S.D. Katz, and K.K. Szabo, Phys. Lett. **B643**, 46 (2006) [hep-lat/0609068].

[52] P. Chen *et al.* Phys. Rev. **D64**, 014503 (2001) [hep-lat/0006010].

[53] Bornyakov *et al.* arXiv:0910.2392[hep-lat].

[54] M. Cheng *et al.* Phys. Rev. D **77**, 014511 (2008).

[55] Y. Hatta and T. Ikeda, Phys. Rev. D **67**, 014028 (2003).

[56] M. Golterman and Y. Shamir, Phys. Rev. D **68**, 074501 (2003); M. Golterman, Y. Shamir and B. Svetitsky, Phys. Rev. D **71**, 071502 (2005); M. Golterman, Y. Shamir and B. Svetitsky, Phys. Rev. D **72**, 034501 (2005).

[57] D. J. Antonio *et al.* , Phys. Rev. D **75**, 114501 (2007).

[58] T. Blum *et al.* Phys. Rev. D **69**, 074502 (2004); Y. Aoki *et al.* Phys. Rev. D **69**, 074504 (2004).

[59] J. Gasser and H. Leutwyler, Phys. Lett. B **184**, 83 (1987).

[60] P. Hasenfratz and H.Leutwyler, Nucl. Phys. **B343**, 241 (1990).

[61] A.V. Smilga and J. Stern, Phys. Lett. B **318**, 531 (1993).

[62] A.V. Smilga and J.J.M Verbaarschot, Phys. Rev. D **54**, 1087 (1995).

[63] F. Karsch (RBC-Bielefeld), Nucl. Phys. **A820**, 99 (2008).

[64] C. Kelly (RBC and UKQCD), PoS LATTICE2009, 087 (2009).

[65] R. Mawhinney (RBC and UKQCD), PoS LATTICE2009, 081 (2009).

[66] N.H. Christ and L.L. Wu, Nucl. Phys. Proc. Suppl. **106**, 438 (2002).

[67] S. Aoki *et al.* , JHEP 06, 088 (2009).

[68] P.M. Vranas, arXiv:hep-lat/0001006.

[69] P.M. Vranas, Phys. Rev. D **74**, 034512 (2006).

[70] H. Fukaya *et al.* (JLQCD), Phys. Rev. D **74**, 094505 (2006).

[71] D. Renfrew, T. Blum, N. Christ, R. Mawhinney and P. Vranas, arXiv:0902.2587 [hep-lat].

[72] H. Ikeda and S. Hashimoto, PoS LATTICE2009, 082 (2009).

[73] W.H. Press, B.P. Flannery, S.A. Teukolsky and W.T. Wetterling, "Numerical Recipes in C: The Art of Scientific Computing (2nd ed.)," Cambridge University Press (1998).

[74] M. Peardon, hep-lat/0011080; S. Fischer *et al.* Computer Physics Communications, Volume 98, Issues 1-2, 20 (1998); S. Fischer *et al.* Nucl. Phys. B. Proc. Suppl. **53**, 990 (1997).

[75] O. Bär, C. Bernard, G. Rupak and N. Shoresh, Phys. Rev. D **72**, 054502 (2005).

[76] S. Prelovsek, Phys. Rev. D **73**, 014506 (2006).

[77] C. Aubin, J. Laiho and R.S. Van de Water, Phys. Rev. D **75**, 034502 (2007).

[78] C. Aubin, J. Laiho and R.S. Van de Water, Phys. Rev. D **77**, 114501 (2008).

[79] W. Florkowski and B. Friman, Z. Phys. **A347**, 271 (1994).

[80] M. Cheng *et al.* [RBC-Bielefeld], to be submitted.

# Appendix A

# Cutoff Effects at Finite $\mu$

Our starting point is eq. (4.18). Let us denote the fugacity $\mathrm{e}^{\mu/T}$ by $z$. If we switch to radial coordinates and do the angular integrals, we are left with radial ones of the form

$$c_{2n}(z) \propto \int_0^\infty \mathrm{d}q\ q^2 \frac{q^{2n+1}}{z^{-1}\mathrm{e}^q + 1} + \left(z \longrightarrow \frac{1}{z}\right). \tag{A.1}$$

The integral above is well-known; its value is

$$\begin{aligned} \int_0^\infty \mathrm{d}q \frac{q^n}{z^{-1}\mathrm{e}^q + 1} &= -\Gamma(n+1)\mathrm{Li}_{n+1}(-z), \\ \Gamma(n) &= \int_0^\infty \mathrm{d}t\ \mathrm{e}^{-t}\ t^{n-1}, \\ \mathrm{Li}_n(z) &= \sum_{k=1}^\infty \frac{z^k}{k^n}. \end{aligned} \tag{A.2}$$

The function $\mathrm{Li}_n(z)$ is called the polylogarithm function. We see that the $\mathcal{O}(a^2)$ corrections are proportional to $\mathrm{Li}_6(z)$, $\mathcal{O}(a^4)$-corrections to $\mathrm{Li}_8(z)$, etc. The $\mathcal{O}(a^{2n})$-corrections have the generic structure

$$c_{2n}(z) = \frac{c_{2n}(0)}{2\mathrm{Li}_{2n+4}(-1)} \left[\mathrm{Li}_{2n+4}(-z) + \mathrm{Li}_{2n+4}\left(-\frac{1}{z}\right)\right]. \tag{A.3}$$

Note that this is independent of the action; only $c_{2n}(0)$ differs from one action to another. This *universality* is understandable if we recall that $\mu$ actually modifies the gauge part of the action. Since we have not modified the gauge action, we should not be surprised that to find the same $\mu$-dependence for all actions.

Next, we make use of the following remarkable relation between the polylogarithm and the Bernoulli polynomials viz.

$$-\frac{n!}{(2\pi\mathrm{i})^n}\left[\mathrm{Li}_n(z)+(-1)^n\mathrm{Li}_n\left(\frac{1}{z}\right)\right]=B_n\left(\frac{\ln z}{2\pi\mathrm{i}}\right), \tag{A.4}$$

where the Bernoulli polynomials $B_n(x)$ are defined by

$$\frac{te^{tx}}{e^t-1}=\sum_{n=0}^{\infty}\frac{t^n}{n!}B_n(x). \tag{A.5}$$

In our case, $z=e^{\mu/T}$ and we define $\ln(-z)=\ln z+i\pi$. Substituting eq.(A.4) into eq.(A.3), we get

$$c_{2n}\left(\frac{\mu}{T}\right)=-\frac{c_{2n}(0)}{2\mathrm{Li}_{2n+4}(-1)}\,\frac{(2\pi\mathrm{i})^{2n+4}}{(2n+4)!}\,B_{2n+4}\left(\frac{\mu}{2\pi\mathrm{i}T}+\frac{1}{2}\right). \tag{A.6}$$

Equation (A.6) can be used to estimate the corrections for both real and imaginary $\mu$. Our goal is to calculate the Taylor coefficients of an expansion of $P/T^4$ about $\mu/T=0$. These coefficients are known as *Quark Number Susceptibilities* (QNS) $\chi_k(T)$. We can use eq.(A.6) to estimate the error in the $n$th coefficient[1]. Our results are summarized in table 4.1 in chapter 4.

Lastly, let us show that the above method also yields the correct continuum pressure at $N_\tau=\infty$ viz.

$$\begin{aligned}\frac{P}{T^4}&=\frac{2\cdot 4\pi}{8\pi^3}\int_0^\infty \mathrm{d}q\; q^2\ln\left(1+ze^{-q}\right)+\left(z\longrightarrow\frac{1}{z}\right),\\ \frac{\mathrm{d}}{\mathrm{d}z}\frac{P}{T^4}&=\frac{1}{\pi^2}\int_0^\infty\frac{\mathrm{d}q}{z}\frac{q^2}{z^{-1}e^q+1}+\left(z\longrightarrow\frac{1}{z}\right),\\ &=-\frac{2}{\pi^2}\frac{1}{z}\mathrm{Li}_3(-z)+\left(z\longrightarrow\frac{1}{z}\right).\end{aligned} \tag{A.7}$$

Now use the relation

$$\frac{\mathrm{d}}{\mathrm{d}z}\mathrm{Li}_{n+1}(z)=\frac{1}{z}\mathrm{Li}_n(z), \tag{A.8}$$

to get

$$\frac{P}{T^4}=-\frac{2}{\pi^2}\left[\mathrm{Li}_4(-z)+\mathrm{Li}_4\left(-\frac{1}{z}\right)\right]. \tag{A.9}$$

[1]We must remember that the $n$th coefficient is multiplied by $N_\tau^{-n}$.

Again, by using eq.(A.4), we arrive at

$$\begin{aligned}\frac{P}{T^4} &= \frac{2}{\pi^2}\cdot\frac{(2\pi\mathrm{i})^4}{4!}B_4\left(\frac{\mu}{2\pi\mathrm{i}T}+\frac{1}{2}\right),\\ &= \frac{7\pi^2}{180}+\frac{1}{6}\left(\frac{\mu}{T}\right)^2+\frac{1}{12\pi^2}\left(\frac{\mu}{T}\right)^4.\end{aligned} \tag{A.10}$$

which is just the familiar expression for the pressure.

# Appendix B

# The Pressure of Domain-Wall Fermions

Our starting point is the four-dimensional operator derived by Edwards and Heller [40]. The dependence of the fields on the fifth dimension can be integrated out to yield an effective, four-dimensional theory $S = -\sum_{x,x'} \bar{\psi}_x D_{x,x'} \psi_{x'}$, with $D$ given by

$$D(m) = \frac{1+m}{2} + \frac{1-m}{2}\gamma_5 \frac{T^{-L_s}-1}{T^{-L_s}+1}. \tag{B.1}$$

Here $m$, as always, is the mass of the fermion. The matrix $T$ is the transfer matrix along the fifth ($s$-) direction. Its construction is described in the reference cited above; we merely summarize viz.

$$T^{-1} = -Q_-^{-1} Q_+, \tag{B.2a}$$
$$Q_\pm = a_5 H(-M_5) P_\pm \pm 1, \tag{B.2b}$$
$$P_\pm = \frac{1 \pm \gamma_5}{2}, \tag{B.2c}$$
$$H(-M_5) = \gamma_5 D_W(-M_5), \tag{B.2d}$$

and $D_W(-M_5)$ is usually the Wilson operator, but it can be any non-chiral, local, undoubled, four-dimensional lattice operator.

The pressure of this system is given by

$$\frac{P}{T^4} = \frac{N_\tau^3}{N_\sigma^3} \ln \det D(m). \tag{B.3}$$

We need to find the determinant of $D(m)$. We proceed as follows: Since $D(m)$ is diagonal in momentum space, let us switch to a $2 \times 2$ block-matrix notation.

Our $\gamma$-matrices are given by (with $\sigma_\mu = (\boldsymbol{\sigma}, I_{2\times 2})$)

$$\gamma_\mu = \begin{pmatrix} 0 & \sigma_\mu \\ \sigma_\mu^\dagger & 0 \end{pmatrix}, \qquad \gamma_5 = \begin{pmatrix} 1 & 0 \\ 0 & -1 \end{pmatrix}. \tag{B.4}$$

Then the matrices $D_W(-M_5)$ and $H(-M_5)$ become

$$D_W(-M_5) = \begin{pmatrix} B - M_5 & C \\ -C^\dagger & B - M_5 \end{pmatrix}, \; H(-M_5) = \begin{pmatrix} B - M_5 & C \\ C^\dagger & -(B - M_5) \end{pmatrix}, \tag{B.5}$$

with

$$B = \sum_{\mu=1}^{4} (1 - \cos p_\mu), \qquad C = \mathrm{i} \sum_{\mu=1}^{4} \sigma_\mu \sin p_\mu. \tag{B.6}$$

This is the same notation as in [40][1]. The matrices $Q_\pm$ are

$$Q_+ = \begin{pmatrix} B - M_5 + 1 & 0 \\ -C^\dagger & 1 \end{pmatrix}, \qquad Q_- = \begin{pmatrix} -1 & C \\ 0 & -(B - M_5 + 1) \end{pmatrix}. \tag{B.7}$$

We need to determine $T^{-1} = -Q_-^{-1} Q_+$. A straightforward calculation yields

$$T^{-1} = \frac{1}{W} \begin{pmatrix} S^2 + W^2 & C \\ C^\dagger & 1 \end{pmatrix}. \tag{B.8}$$

Here, $W = 1 - M_5 + \sum_\mu (1 - \cos p_\mu)$, while $S^2 = \sum_\mu \sin^2 p_\mu$. The matrix $T^{-1}$ being hermitian, its eigenvalues must be real. Indeed, they are given by

$$\lambda_+ = \frac{(1 + S^2 + W^2) + \sqrt{(1 + S^2 + W^2)^2 - 4W^2}}{2W}, \tag{B.9a}$$

$$\lambda_- = \frac{(1 + S^2 + W^2) - \sqrt{(1 + S^2 + W^2)^2 - 4W^2}}{2W}, \tag{B.9b}$$

$$\lambda_+ = \frac{1}{\lambda_-}, \tag{B.9c}$$

while their reality can be seen from

$$\begin{aligned} (1 + S^2 + W^2)^2 - 4W^2 &= (1 + S^2 + W^2 - 2W)(1 + S^2 + W^2 + 2W), \\ &= (S^2 + (W - 1)^2)(S^2 + (W + 1)^2), \\ &\geqslant 0. \end{aligned} \tag{B.10}$$

[1] We shall suppress the $M_5$-dependence from now on.

The eigenvalues are doubly degenerate. This is because of the following symmetry of $T^{-1}$ viz.

$$\gamma_5 T^{-1}(p)\gamma_5 = T^{-1}(-p). \tag{B.11}$$

This "parity transformation" has the following consequence: If $u_p$ is an eigenvector of $T^{-1}$ with eigenvalue $\lambda_p$, then so is $\gamma_5 u_{-p}$. The eigenvectors of the transfer matrix thus occur in pairs.

More important is the case of the zero-modes $\Psi(x,s)$. The commutator $[T^{-1},\gamma_5]=0$ in the subspace of zero-modes; consequently, the zero-modes of $T^{-1}$ must be chiral, $\gamma_5\Psi(x,s) = \pm\Psi(x,s)$. In fact, they satisfy the lattice Dirac equation for naive fermions viz.

$$\left[\gamma_5, T^{-1}\right] = \frac{2}{W}\begin{pmatrix} 0 & C \\ C^\dagger & 0 \end{pmatrix} = \frac{2}{W}\sum_{\mu=1}^{4} \mathrm{i}\gamma_\mu \sin p_\mu, \tag{B.12}$$

and hence

$$\left[\sum_{\mu=1}^{4} \mathrm{i}\gamma_\mu \sin p_\mu\right]\Psi = \frac{W}{2}\left[\gamma_5, T^{-1}\right]\Psi = 0. \tag{B.13}$$

A unitary matrix that diagonalizes $T^{-1}$ is the following viz.[2]

$$U = \frac{1}{\sqrt{\Gamma^2+S^2}}\begin{pmatrix} \Gamma & C \\ -C^\dagger & \Gamma \end{pmatrix}, \tag{B.14a}$$

$$\Gamma = -\frac{1}{2}\left[(S^2+W^2-1) + \sqrt{(1+S^2+W^2)^2-4W^2}\right]. \tag{B.14b}$$

Let us now assemble the pieces: If $U^\dagger T^{-1} U = \Lambda$, $\Lambda = \mathrm{diag}\,(\lambda_+,\lambda_-)$, then

$$\begin{aligned} \det D(m) &= \det\left[\frac{1+m}{2} + \frac{1-m}{2}\gamma_5 U \frac{\Lambda^{-L_s}-1}{\Lambda^{-L_s}+1}U^\dagger\right], \\ &\xrightarrow[L_s\to\infty]{} \det\left[\frac{1+m}{2} + \frac{1-m}{2}\gamma_5 U\gamma_5 U^\dagger\right], \\ &= \prod_{(\mathbf{p},p_4)} \frac{1}{(\Gamma^2+S^2)^4}\left[\left(\Gamma^2+mS^2\right)^2 + (m-1)^2\Gamma^2 S^2\right]^2. \end{aligned} \tag{B.15}$$

[2]The following derivation was provided to me by Zhongjie Jasper Lin.

For $m = 0$, this can be further simplified to

$$\det D(0) = \prod_{(\mathbf{p},p_4)} \frac{1}{4}\left[1 + \frac{S^2 + W^2 - 1}{\sqrt{(1+S^2+W^2)^2 - 4W^2}}\right]^2, \tag{B.16a}$$

$$\frac{P}{T^4} = 2\left(\frac{N_\tau}{N_\sigma}\right)^3 \sum_{(\mathbf{p},p_4)} \ln\left[1 + \frac{S^2 + W^2 - 1}{\sqrt{(1+S^2+W^2)^2 - 4W^2}}\right]. \tag{B.16b}$$

# Appendix C

# The Pressure of Overlap Fermions

The overlap operator [26, 27] for massless fermions is given by

$$D_{ov}(0) = M_5 \left(1 + \gamma_5 \frac{H}{\sqrt{H^2}}\right) = M_5 \left(1 + \gamma_5\, \epsilon(H)\right). \tag{C.1}$$

$H = \gamma_5 D_W(-M_5)$ is the same as for domain-wall fermions. The second equality *defines* the sign function of a hermitian matrix (Note that $H$ is hermitian at $\mu = 0$).

The steps are mostly the same as before: Let us define $A = W - 1 = -M_5 + \sum_\mu (1 - \cos p_\mu)$. The eigenvalues of $H(-M_5)$ are given by $\lambda_p^\pm = \pm\sqrt{A^2 + S^2}$. A matrix that diagonalizes $H$ is

$$\Delta = A + \sqrt{A^2 + S^2}, \tag{C.2a}$$

$$U = \frac{1}{\sqrt{S^2 + \Delta^2}} \begin{pmatrix} \Delta & C \\ C^\dagger & -\Delta \end{pmatrix} = U^\dagger = U^{-1}. \tag{C.2b}$$

By going through the same steps as before, we end up with

$$D_{ov}(0) = 2M_5 \left[\frac{\Delta}{\Delta^2 + S^2} \begin{pmatrix} \Delta & -C \\ C^\dagger & \Delta \end{pmatrix}\right], \tag{C.3}$$

and hence

$$D_{ov}^{-1}(0) = \frac{1}{2\Delta M_5}\begin{pmatrix} \Delta & C \\ -C^\dagger & \Delta \end{pmatrix}, \\ = \frac{1}{2M_5}\left[1 - \frac{\mathrm{i}\sum_\mu \gamma_\mu \sin p_\mu}{A + \sqrt{A^2+S^2}}\right]. \tag{C.4}$$

while the determinant is given by

$$\det D_{ov}(0) = (2M_5)^4 \prod_{(\mathbf{p},p_4)} \left(1 + \frac{A}{\sqrt{A^2+S^2}}\right)^2, \tag{C.5a}$$

$$\frac{P}{T^4} = 2\left(\frac{N_\tau}{N_\sigma}\right)^3 \sum_{(\mathbf{p},p_4)} \ln\left(1 + \frac{A}{\sqrt{A^2+S^2}}\right). \tag{C.5b}$$